

M.Sc. Dissertation

**Validation of the moderate-resolution satellite burned area products  
across different biomes in South Africa**

**Philemon Lehlohonolo Tsela**

A dissertation submitted in partial fulfilment of the requirements for the degree of  
Master of Science in Geoinformatics.

Department of Geography, Geoinformatics and Meteorology  
University of Pretoria

May 2011

## Declaration of originality

This is to certify that the work is entirely my own and not of any other person, unless explicitly acknowledged (including citation of published and unpublished sources). The work has not previously been submitted in any form to the University of Pretoria or to any other institution for assessment or for any other purpose.

Signed \_\_\_\_\_

Date \_\_\_\_\_

## ACKNOWLEDGMENTS

I would like to express my innermost gratitude to the Almighty, whom I believe this study became possible through Him. This research work was implemented at the Department of Geography, Geoinformatics and Meteorology, University of Pretoria and; Remote Sensing Research Unit (RSRU), Meraka Institute, Council for Scientific and Industrial Research (CSIR), South Africa. Special thanks to these institutions for their firm support with the research facilities needed for the execution of this study.

I am grateful to Prof. Paul van Helden and Prof. Hannes Rautenbach for their incredible support and advice all the way throughout this research work. I would like to thank Dr. Konrad Wessels and Philip Frost for providing me with the opportunity to implement this research project as part of my study, as well as their time and major contributions dedicated to this study. Special thanks to Sally Archibald for her ideas and participation during scientific discussions on various phases of this study. My sincere gratitude also goes to Prof. David Roy for his generous assistance.

Special thanks goes to Joel Botai for his mentorship and encouragement throughout this process until the end. I would like to thank all the researchers at the RSRU Meraka Institute for their hospitableness, explicitly Karen Steenkamp and Derick Swanepoel for their technical assistance.

Last but definitely not least, I would like to express my gratitude to my mom and dad for their endless support and affectionateness during the duration of this research work.

## **PUBLISHED MATERIAL FROM THIS DISSERTATION**

### **PEER-REVIEWED CONFERENCE PROCEEDINGS**

**Tsela, P. L.,** van Helden, P., Frost, P., Wessels, K. and Archibald, S. 2010. Validation of the MODIS Burned-area products across different biomes in South Africa. In: Geoscience and Remote Sensing Society (GRSS), *Proceedings of the 2010 IEEE International Geoscience and Remote Sensing Symposium*. Honolulu, Hawaii, USA, 25-30 July 2010, pp.3652-3655.

Philemon Tsela was the responsible author in the manuscript listed above. This work involved various co-authors who contributed by reviewing the whole paper before it was submitted for publication. This published manuscript provides details on the methodology and preliminary results of this study; and was therefore presented at the 2010 IEEE International Geoscience and Remote Sensing Symposium in Hawaii/USA.

## ABSTRACT

Biomass burning in southern Africa has brought significant challenges to the research society as a fundamental driver of climate and land cover changes. Burned area mapping approaches have been developed that generate large-scale low and moderate resolution products made with different satellite data. This consequently afford the remote sensing community a unique opportunity to support their potential applications in e.g., examining the impact of fire on natural resources, estimating the quantities of burned biomass and gas emissions. Generally, the satellite-derived burned area products produced with dissimilar algorithms provide mapped burned areas at different levels of accuracy, as the environmental and remote sensing factors vary both spatially and temporally. This study focused on the inter-comparison and accuracy evaluation of the 500-meter Moderate Resolution Imaging Spectroradiometer (MODIS) burned area product (MCD45A1) and the Backup MODIS burned area product (hereafter BMBAP) across the main-fire prone South African biomes using reference data independently-derived from multi-temporal 30-meter Landsat 5 Thematic Mapper (TM) imagery distributed over six validation sites. The accuracy of the products was quantified using confusion matrices, linear regression and sub-pixel burned area measures. The results revealed that the highest burned area mapping accuracies were reported in the fynbos and grassland biomes by the MCD45A1 product, following the BMBAP product across the pine forest and savanna biomes, respectively. Further, the MCD45A1 product presented higher sub-pixel detection probabilities for the burned area fractions  $\leq 50\%$  than the BMBAP product, which appeared more reliable in detecting burned area fractions  $> 50\%$  of a MODIS pixel. Finally the results demonstrated that the probability of identifying a burned area within a MODIS pixel is directly related to the proportion of the MODIS pixel burned and thus, highlights the relevance of fractional burned area during classification accuracy assessment of lower resolution remotely-sensed products using data with higher spatial resolution.

**Keywords:** MODIS, Landsat, burned area product, biome

## LIST OF ACRONYMS

ATSR	Along-Track Scanning Radiometer
AVHRR	Advanced Very High Resolution Radiometer
BAI	Burned Area Index
BMBAP	Backup MODIS Burned Area Product
BRDF	Bi-directional Reflectance Distribution Function
CE	Commission Error
ERS	European Remote sensing Satellite
ESA	European Space Agency
ETM+	Enhanced Thematic Mapper Plus
GBA2000	Global Burned Area 2000
GEMI	Global Environmental Monitoring Index
GFED	Global Fire Emissions Database
GOES	Geostationary Operational Environmental Satellite
JRC	Joint Research Centre
MODIS	Moderate Resolution Imaging Spectroradiometer
NASA	National Aeronautics and Space Administration
NDVI	Normalized Difference Vegetation Index
NIR	Near Infrared
NLC2000	National Landcover 2000
NOAA	National Oceanic and Atmospheric Administration
OE	Omission Error
SEVIRI	Spinning Enhanced Visible and Infrared Imager
SPOT	Satellite Pour l'Observation de la Terre
SWIR	Shortwave Infrared
TIR	Thermal Infrared
TM	Thematic Mapper
VIRS	Visible and Infrared Scanner
WAMIS	Wide Area Monitoring Information System
WRS	World Reference System

## TABLE OF CONTENTS

ACKNOWLEDGMENTS .....	iii
PUBLISHED MATERIAL FROM THIS DISSERTATION .....	iv
ABSTRACT .....	v
LIST OF ACRONYMS .....	vi
TABLE OF CONTENTS .....	vii
LIST OF FIGURES .....	ix
LIST OF TABLES.....	xiii
CHAPTER 1.....	1
INTRODUCTION .....	1
1.1: General introduction.....	1
1.2: Problem statement.....	8
1.3: Study aim and objectives.....	9
1.4: Study outline.....	9
CHAPTER 2.....	11
LITERATURE REVIEW.....	11
2.1: The physical processes of biomass burning .....	11
2.2: Monitoring the occurrence and distribution of biomass burning.....	11
2.3: Active fire and burned area mapping .....	12
2.4: Validation of the satellite burned-area products .....	16
2.5: The need for burned area product validation.....	21
2.6 Concluding remarks .....	23
CHAPTER 3.....	25
DATA AND METHODS.....	25
3.1: Introduction .....	25
3.2: Data used and study area .....	26
3.2.1: Landsat 5 TM.....	26
3.2.2: Burned-area reference data .....	30
3.2.3: The moderate-resolution satellite burned area products.....	33

3.2.3.1: The “Backup” MODIS burned area product.....	33
3.2.3.2: The “Official” MODIS burned area product .....	34
3.2.4: Land Cover product.....	35
3.2.5: The MODIS fire product .....	37
3.2.6: TRMM data.....	39
3.2.7: Vegetation map of South Africa, Lesotho and Swaziland.....	42
3.3: Methodology .....	43
3.3.1: Confusion Matrix .....	43
3.3.2: Linear regression analysis.....	48
3.3.3: Sub-MODIS pixel burned area analysis .....	50
3.3.4: Concluding remarks .....	52
CHAPTER 4.....	53
RESULTS AND DISCUSSION.....	53
4.1: Introduction .....	53
4.2: Classification error assessment.....	53
4.2.1: Analysis of the response of Oe to variations in burned area sizes.....	55
4.2.2: Comparison of product performance.....	60
4.2.2.1: Savanna.....	60
4.2.2.2: Grassland .....	65
4.2.2.3: Pine Forest .....	67
4.2.2.4: Fynbos.....	72
4.3: Influence of fractional burned area on detection accuracy.....	74
4.4: Analysis of burned area estimations .....	79
4.5: Analysis of sub-MODIS pixel burned area .....	88
4.6: Concluding remarks .....	92
CHAPTER 5.....	96
CONCLUSION .....	96
5.1: Conclusions .....	96
5.2: Recommendations and future work .....	99
REFERENCES .....	100



## LIST OF FIGURES

a) Figure 3.1: Methodological framework showing the three important phases addressed in this research study.....	25
b) Figure 3.2: An example of a dual display using TM date 1 (15 July 2007) and TM date 2 (16 August 2007) false colour images of Thabazimbi in ENVI software version 4.3, which simplified GCP collection for image to image registration. ....	28
c) Figure 3.3: Illustration of the computed statistics in ENVI for the 20 collected GCPs. The estimated RMS error for each GCP (highlighted in blue for legibility) was kept below an RMS error threshold of 0.5 pixels. ....	29
d) Figure 3.4: In the first row is the acquired TM scene pair in Kruger. Second row depicts the computed burn-sensitive vegetation index (VI) on the TM pair to identify burned areas. Third row depicts the elevated burned areas between the multi-temporal TM indices and their interpretation. ....	31
e) Figure 3.5: Zoomed in example of a VI difference image (A) showing high spectral contrast of the burned areas (A) and the interpreted burned areas delineated by red polygons (B). ....	32
f) Figure 3.6: The manager-mapped plantation boundaries showing the approximate spatial location of the commercial pine forest in Sabie according to the 2000 NLC product. ....	36
g) Figure 3.7: The MODIS active fire locations showing a comprehensive spatial representation of burning activity in South Africa for the year 2007. The Landsat TM acquisitions are superimposed on the fire locations to indicate the main prone areas.....	38
h) Figure 3.8: TRMM Mean Annual Rainfall (MAR) of southern Africa calculated from the monthly data from 1998 – 2007 in mm per year.....	40
i) Figure 3.9: The biome map showing the Landsat TM acquisitions distributed across the main fire prone biome types in South Africa. ....	42

j) Figure 3.10: Comparison of Landsat (interpreted) burned-area reference data and the MCD45A1 product to derive the Ce and Oe by use of a confusion matrix.....	45
k) Figure 3.11: The 500 m MODIS reference grids used to compute fractional burned areas corresponding to Landsat TM interpreted burns. ....	51
l) Figure 4.1: Burned areas mapped with Landsat within 500 m MODIS pixels identified as burned by the BMBAP product in the Free State (Grassland biome).....	54
m) Figure 4.2: Changes in the Oe relative to the burned area sizes of the MCD45A1 and BMBAP products in Free State (grassland). The Oe was derived for the MODIS burned areas corresponding to the individual Landsat burned areas).....	57
n) Figure 4.3: Changes in the Oe relative to the burned area sizes of the MCD45A1 and BMBAP products in Thabazimbi (savanna). The Oe was derived for the MODIS burned areas corresponding to the individual Landsat burned areas).....	58
o) Figure 4.4: Changes in the Oe relative to the burned area sizes of the MCD45A1 and BMBAP products in Western Cape (fynbos). The Oe was derived for the MODIS burned areas corresponding to the individual Landsat burned areas).....	58
p) Figure 4.5: Changes in the Oe relative to the burned area sizes of the MCD45A1 and BMBAP products in Sabie (pine forest). The Oe was derived for the MODIS burned areas corresponding to the individual Landsat burned areas). ....	59
q) Figure 4.6: A measure of variability of Oe due to changes in burned area size for the MCD45A1 and BMBAP product.....	59
r) Figure 4.7: Illustration of the burned areas in southern Kruger reveals strong spectral contrast (i.e. appear dark) and complex shapes. ....	61
s) Figure 4.8: Ce in the MCD45A1 product over southern Kruger National Park in the absence of any burns.....	61

t) Figure 4.9: Illustration of the mapping performance of the products in Thabazimbi reveals similar performance by corresponding to most of the Landsat burned areas.....	63
u) Figure 4.10: Illustration of <i>O<sub>e</sub></i> in the MODIS products over spectrally distinct burned areas in Thabazimbi.....	64
v) Figure 4.11: MODIS-based burned area mapping in Middelburg with the MCD45A1 product showing higher burned area classification relative to the BMBAP product. ....	65
w) Figure 4.12: The burned area mapping performance of the MODIS products in the Free State.....	66
x) Figure 4.13: A spatial representation of the burned area mapping performance of the products in the Sabie region, which depicts effective performance of the BMBAP product than the MCD45A1 product.....	69
y) Figure 4.14: Landsat TM data acquired 15 June (first row) and 18 August (second row), 2007, in the Sabie region along with unmapped areas (third row) showing the interpretation process.....	71
z) Figure 4.15: A spatial representation of the burned area products in the Western Cape showing their overall mapping performance.....	72
aa) Figure 4.16: Illustrations of Landsat burned areas (A – D) superimposed on the TM difference VI image not identified by the burned area products in Western Cape.....	73
bb) Figure 4.17: Changes in <i>O<sub>e</sub></i> and <i>C<sub>e</sub></i> (presented in Table 4.1) for the 500 m MODIS burned area products based on Landsat 30 m pixels. The symbols F, S, K, M, T and W represents the Free State, Sabie, Kruger, Middelburg, Thabazimbi and Western Cape sites respectively.....	76
cc) Figure 4.18: Changes in <i>O<sub>e</sub></i> and <i>C<sub>e</sub></i> (presented in Table 4.3) for the burned area products based on 500 m MODIS pixels that are $\geq 50\%$ burned according to Landsat data. The symbols F, S, K, M, T and W represents the Free State, Sabie, Kruger, Middelburg, Thabazimbi and Western Cape sites respectively. ....	77
dd) Figure 4.20: Scatter plots of the burned area proportions derived from the two MODIS burned area products (y-axis) and multitemporal Landsat data (x-	

axis) across the 2.5 x 2.5 km grid cells for the Western Cape encompassing the fynbos biome. Only grid cells containing proportions tagged as burned in the Landsat and the MODIS burned area products were considered. ....81

ee) Figure 4.21: Scatter plots of the burned area proportions derived from the two MODIS burned area products (y-axis) and multitemporal Landsat data (x-axis) across the 2.5 x 2.5 km grid cells for Sabie. Only grid cells containing proportions tagged as burned in the Landsat and MODIS burned area products were considered. ....81

ff) Figure 4.22: Scatter plots of the burned area proportions derived from the two MODIS burned area products (y-axis) and multitemporal Landsat data (x-axis) across the 2.5 x 2.5 km grid cells for the Free State encompassing the grassland biome. Only grid cells containing proportions tagged as burned in the Landsat and MODIS burned area products were considered.....82

gg) Figure 4.23: Scatter plots of the burned area proportions derived from the two MODIS burned area products (y-axis) and multitemporal Landsat data (x-axis) across the 2.5 x 2.5 km grid cells for Middelburg encompassing the grassland biome. Only grid cells containing proportions tagged as burned in the Landsat and MODIS burned area products were considered.....83

hh) Figure 4.24: Scatter plots of the burned area proportions derived from the two MODIS burned area products (y-axis) and multitemporal Landsat data (x-axis) across the 2.5 x 2.5 km grid cells for Thabazimbi encompassing the savanna biome. Only grid cells containing proportions tagged as burned in the Landsat and the MODIS burned area products were considered. ....85

ii) Figure 4.25: Scatter plots of the burned area proportions derived from the two MODIS burned area products (y-axis) and multitemporal Landsat data (x-axis) across the 2.5 x 2.5 km grid cells for southern Kruger encompassing the savanna biome. Only grid cells containing proportions tagged as burned in the Landsat and the MODIS burned area products were considered. ....85

jj) Figure 4.26: Spatial coherence of the burned area patterns interpreted and produced from multitemporal Landsat TM data over the three validation sites. ....86

kk) Figure 4.27: Spatial coherence of the burned area patterns interpreted and produced from multitemporal Landsat TM data over the three validation sites. ....87

ll) Figure 4.28: Histograms of sub-MODIS pixel burned area analysis used to depict the relationship between burned area proportions according to Landsat and the probability of detection by the products in Kruger, Thabazimbi and Western Cape.....89

mm)..... F

Figure 4.29: Histograms of sub-MODIS pixel burned area analysis used to depict the relationship between burned area proportions according to Landsat TM and the probability of detection by the products in Middelburg, Free State and Sabie.....90

## LIST OF TABLES

a) Table 3.1: The spectral and spatial characteristics of the Landsat 5 Thematic Mapper (TM) multispectral scanner (<http://landsat.usgs.gov>).....26

b) Table 3.2: Landsat 5 TM scene pairs used to produce high-resolution burned-area independent (validation) reference datasets. ....27

c) Table 3.3: The TRMM Mean Annual Rainfall estimates derived from the monthly data spanning the period 1998 – 2007 in mm. ....41

d) Table 3.4: Characteristics of a typical confusion matrix for a remotely-sensed product.....43

e) Table 3.5: Classification accuracy assessment of the MODIS burned area products based on 500 m MODIS pixels that are at least 50% and 75% burned according to Landsat.....46

f) Table 4.1: Classification error assessment validation results based on the Official MODIS burned area product (MCD45A1) (highlighted in grey to aid interpretation) and the Backup MODIS burned area product (BMBAP) compared with Landsat TM burned area at 30 m resolution. 54

- g) Table 4.2: Inter-quartile range used to measure the sensitivity of  $O_e$  in the products to the variations in burned area sizes. A rate of change of  $O_e$  to the burned area size is computed based on the inter-quartile range. ....57
- h) Table 4.3: Classification accuracy assessment of the Official MODIS burned area product (MCD45A1) and the Backup MODIS burned area product (BMBAP) based on 500 m MODIS pixels which are  $\geq 50\%$  and  $\geq 75\%$  burned according to Landsat.....75
- i) Table 4.4: Coefficient of determination and regression coefficients of the comparison between the burned area proportions derived from the two MODIS products and multi-temporal Landsat interpreted burned area in 2.5 x 2.5 km grid cells.....79

# CHAPTER 1

## INTRODUCTION

### 1.1: General introduction

Biomass burning is a major global ecological disturbance that occurs every year throughout the world. This phenomenon is a major cause of land surface changes with multi-spatial and multi-temporal impacts on the climate system, vegetated ecosystems and chemical composition of the atmosphere (Loboda and Csiszar, 2004; Tansey, et al., 2004; Roy, et al., 2005a). The extent and severity of biomass burning effects have regional variations that depend on the amount of available biomass fuel, climatic conditions, and the type of vegetation that burns (Pereira, et al., 1997; Roy, et al., 1999). Dwyer, et al. (2000) reported that, approximately 70% of global biomass burning occur in tropical regions where there is often sufficient biomass fuel to produce fires with large amounts of trace gases and aerosol particulate emissions that significantly influence the regions atmospheric chemistry and climate.

The frequency of occurrence and distribution of fires in the African continent is considered to be remarkably high in long-term historical perspective (Delmas, et al., 1991; Andreae, 1997; Bird and Cali, 1998; Giglio, et al., 2010a). The majority of burning events in the continent are as a result of human activity, particularly for land management practices (Bond,1997) while the minority are lightning-induced fires associated with thunderstorm activity (van Wilgen and Scholes, 1997). In southern Africa, biomass burning during the dry season (from approximately May to October) is distributed over a considerable extent particularly when a large portion of vegetation cover is covered with dried material, thus increasing the biomass fuel load that can be sufficient to produce large and more intense fires.

The frequency of occurrence, distribution, extent and severity of biomass burning has raised concerns over recent years among scientific communities, policymakers, and resource managers with regard to the provision of reliable fire information that includes the location, timing, and the spatial extent of burning at

local, regional and global scale (Crutzen and Goldammer, 1993; Levine, 1996; Frost, 1999). Although fire information exists for localized areas such as commercial forests, nature reserves and conservation areas, this may not provide a comprehensive spatial representation of biomass burning activity over extensive regions.

Satellite remote sensing has proven to be a valuable method that provides consistent and extensive monitoring of biomass burning at regional to global scale. For more than two decades, orbital satellite sensor technology has been widely used to systematically observe and assess the occurrence and distribution of fire over large areas. Satellite algorithms such as the hotspot detection algorithms have been developed for large-scale fire monitoring and operate on satellite data produced by different low and moderate resolution sensors such as the Geostationary Operational Environmental Satellite (GOES) Imager (Prins and Menzel, 1992), European Space Agency (ESA) Along Track Scanning Radiometer (ATSR) (Arino and Rosaz, 1999), National Oceanic and Atmospheric Administration (NOAA) Advanced Very High Resolution Radiometer (AVHRR) (Dozier, 1981; Giglio, et al., 1999), and the National Aeronautic Space Administration (NASA) Moderate Resolution Imaging Spectroradiometer (MODIS) (Justice, et al., 2002a).

Satellite active fire mapping is typically a daily activity that capitalizes on the enhanced radiance signal emitted by hot fires in the thermal infrared spectral region, and it can be measured as the most suitable and comprehensive method to determine the differences in the seasonal pattern and spatial details of burning. However, cloud obscuration, smoke, and the satellite overpass frequency may constrain active fire mapping and consequently, the satellite-derived hot-spot data may not provide reliable information on the location, timing and spatial extent of burning (Justice, et al., 2002b). On the other hand, given that the surface fire effects are temporally persistent, burned area mapping algorithms that use multi-temporal satellite data are less subject to the limitations of active fire mapping.

Burned area mapping has extensively been studied for the last twenty years with a variety of low and moderate resolution satellite sensors. The burned areas are computed by algorithms that utilize the temporal persistence of the burned area spectral signature to provide an approximate measure of the timing, location, and



spatial extent of area burned (Eva and Lambin, 1998a; Barbosa, et al., 1999; Fraser, et al., 2000; Roy, et al., 2002; Tansey, et al., 2004). In this study, *burned area* (also referred to as *burnt areas*, *fire affected areas*, *burn scars*, and *fire scars*) is used as the term that denotes the land surface changes induced by fire. Burned areas are contrasted by the cumulation of black carbonaceous material; particularly char and mineral ash, change of vegetation formation and the removal of vegetation cover bringing forth the underlying soil surface. These changes are spatially and temporally dependent upon various biophysical parameters such as, the type of vegetation that burns, combustion completeness, post-burn vegetation re-growth, precipitation amount and the wind velocity (Roy, et al., 1999).

Previous attempts to systematically map the location and timing of burned areas using low (~1-5 km) and moderate (~250-500 m) resolution satellite data in various spheres of the African continent have been successfully demonstrated and showed potential for extensive regional applications, in particular the estimation of burned biomass, pyrogenic gases and aerosols. Eva and Lambin (1998a), for instance, used the remotely sensed 1 km resolution ATSR data to map fire-affected areas in central Africa during the 1994-95 dry seasons, by determining the enhanced burned and unburned spectral separability between the short-wave infrared (SWIR) (1.2  $\mu\text{m}$ ) and thermal-infrared (TIR) reflectances. Barbosa and Grégoire (1999) used multi-temporal 5 km resolution AVHRR data to map burned areas in the African continent based on numerous thresholds on the surface brightness temperature contained in TIR channels, and the burned and unburned spectral signatures derived from vegetation indices. Moreover, Silva, et al. (2005) applied a method of “classification tree” on reflectances in the Visible-Infrared (VIR) bands and vegetation indices to identify burned areas in sub-Saharan Africa based on 1 km resolution SPOT-VEGETATION (VGT) imagery. Furthermore, Roy, et al. (2002, 2005a) utilized the 500 m MODIS time series data to map the location and timing of burned areas in southern Africa during the 2000 dry season based on a predictive bi-directional reflectance modelling change detection approach.

These burned area mapping approaches generate large-scale low and moderate resolution products made with different satellite data. Consequently, this afford the remote sensing community a unique opportunity to support their potential

applications, including resource management and ecological assessment activities particularly in extensive regions, for example, in identifying the main fire prone areas, formulating regional fire management strategies to minimize fire spread, examining the impact of fire on natural resources, estimating the quantities of burned biomass and gases emitted into the atmosphere. Although these satellite burned-area data products provide useful information to a range of multi-disciplinary users, their potential use in various applications could raise uncertainties about their accuracy (Trigg, et al., 2007). Burned area product accuracy could possibly be affected by: i) differences between burned and unburned spectral reflectances, ii) similar spectral changes not caused by fire and ii) size distribution of the burned areas. For the three identified land cover features an abstract review for each is provided below.

The spectral response of burned areas may vary as a function of the combustion completeness, type of vegetation that burned, swiftness of vegetation re-growth and, the amount of available charcoal and mineral ash (Eva and Lambin, 1998a; Roy, et al., 1999). As a result, the spectral signal of burned areas has different reflectance properties at different wavelengths (Eva and Lambin, 1998a) and this could necessitate the appropriate use of spectral constraints and thresholding techniques on the reflected signatures within the selected bands in order to provide a good discrimination of burned and unburned areas. Several studies (e.g., Barbosa, et al., 1999; Roy, et al., 2002; Roy, et al., 2005a; Roy and Landmann, 2005c) conducted in southern Africa using temporal spectral profiles have demonstrated that post-fire effects typically cause a drop in infrared reflectance. In addition, stronger burned area discrimination was correlated to the abrupt decrease in the near-infrared (NIR) (0.8  $\mu\text{m}$ ) and SWIR spectral signatures which are less influenced by smoke aerosols (Eva and Lambin, 1998a; Roy, et al., 2002). During post-fire activity, the surface brightness temperature increases followed by a decrease in evapotranspiration caused by a significant absorption of the incident solar radiation. Therefore, the TIR spectral band may be used as an additional parameter concurrently with other infrared bands such as SWIR, to optimally indicate the persistence of the burned area spectral signature as well as to provide an enhanced spectral separability between burned and unburned areas. Conversely, the infrared spectral signature emitted from moist vegetation and water bodies lowers reflectance in the SWIR band and provide similar

non-fire induced spectral changes, which may consequently lead to spectral confusion (Roy, et al., 2005a). Similarly, the transformation of green vegetation to unburned dry material shows a low reflectance in the NIR band due to its sensitivity for healthy green vegetation. The spectral aliasing arising from band reflectances of interest may be complex to eradicate, but their impact could be significantly minimized by use of, for example, ratio spectral indices (Roy, et al., 1999) and/or a thematic map of active-fire observations coupled with statistical thresholds (Giglio, et al., 2006).

The size distribution of the burned areas has an influence on the accuracy of moderate resolution burned-area products. For example, small and scattered burned areas may remain unobserved in the product primarily due to the limitations arising from the inherent spatial resolution of the satellite sensor. In addition, the complex structures of fire-affected areas may also not be well represented in the product, resulting in proportions of unburned areas being classified as burned. Burned area product accuracy increases when large contiguous burned areas dominate the landscape, and decreases as the patch size reduces (Smith, et al., 2003). Similarly, burned areas across different vegetation types with varying levels of available biomass fuel and climatic conditions could have spatial and temporal differences, which affect product accuracy. Generally, burned areas are small and scattered in dense humid forests with prolonged moist conditions (Roy, et al., 2005b), whereas in semi-arid regions burned areas are large and more contiguous, particularly in the grassland and savanna biomes (Bond, 1997). Recent estimates of burned area by vegetation type in Africa reported by Roy, et al. (2008) depict that the impact of biomass burning is greatest in savanna and grassland vegetation in contrast to forests for the July 2001 – June 2002 period. Therefore, variations in burned area patterns across a range of biomes present a sample of conditions that influence product accuracy.

The MODIS onboard the NASA's Terra (~10:30 a.m. equatorial crossing time) and Aqua (~1:30 p.m. equatorial crossing time) satellites has specific lineaments for reliable long-term observations of biomass burning at regional, continental and global scale. MODIS has been used to systematically generate a collection of global land cover products at a range of spatial scales (Justice, et al.,

2002c) such as, a daily 1 km resolution active-fire product (Kaufman, et al., 1998; Giglio and Justice, 2003) and a monthly 500 m resolution burned area product (Roy, et al., 2002; Giglio, et al., 2006). In the present study, we evaluate the accuracy of the reported burned area in the moderate resolution burned-area products recently generated using the 500 m MODIS time series data, namely the official MODIS burned area product (MCD45A1) (Roy, et al., 2008) and the Backup MODIS burned area product (hereafter BMBAP) (Giglio, et al., 2009). Each product is briefly summarized below, followed by the protocol on evaluating satellite product accuracy in subsequent paragraphs.

The change detection algorithm used to define the MCD45A1 product maps the location and approximate Julian day (1-366) of burning at 500 m spatial resolution. The algorithm locates the occurrence of persistent post-fire changes in the MODIS daily surface reflectance time-series data (Vermote and Justice, 2002) using a predictive bi-directional reflectance modelling approach (Roy, et al., 2002; Roy, et al., 2005a). Basically seven MODIS 500 m land surface reflectance bands are pre-processed to provide more accurate observations of the terrain, by removal of cloud and aerosol contaminated, non-geolocated, high view zenith and high solar zenith MODIS data. The primary assumption of the algorithm is that the surface state remains constant on subsequent days. Consequently, a bi-directional reflectance model described by the Bi-directional Reflectance Distribution Function (BRDF) (Roujean, et al., 1992; Lucht, et al., 2000) is applied to the seven observed surface reflectances sensed within a minimum of 16 days to predict reflectance on a subsequent day. The model also accounts for directional effects induced by varying viewing and solar sensor angles in the satellite time series reflectance observations. The algorithm further employs a statistical threshold to quantify the discrepancies in change probability between the model predicted reflectance and observed reflectance values, and in addition, provides a robust statistical framework for normalizing the amount of noise in the observed reflectance. The temporal discrepancies that are spectrally similar to persistent fire-induced changes, such as cloud shadows are discriminated by use of a temporal consistency constraint to minimize the occurrence of false burn detections (Roy, et al., 2005a).

On the other hand, the algorithm used to define the BMBAP product detects burned areas at 500 m spatial resolution coupled with data derived from the 1 km MODIS active fire product (Justice, et al., 2002b). The algorithm observes spectrally persistent post-burn changes reflected in the daily vegetation-index (VI) time series data derived from the independently selected MODIS band 5 (1.2  $\mu\text{m}$ ) and band 7 (2.1  $\mu\text{m}$ ) surface reflectances (Roy and Landmann, 2005c; Giglio, et al., 2006). Generally, the algorithm assumes that the reflectance in VI time series data will decrease shortly after the occurrence of fire, which provides an enhanced burned area spectral signal. The identified burned area changes are aggregated to generate composite imagery accompanied by the cumulative active fire map of the same specified time period. A series of threshold tests are applied on the available spectral persistence information for the selection of burned and unburned training pixels in the composite active fire map. This is further refined through comparison of the pixel-derived statistical distributions to produce a complementary mask of training pixels (Giglio, et al., 2009). The mask is used to guide the generation of conditional probability density functions (PDFs) as well as the selection of the appropriate classification procedures suitable for classifying the scene into burned and unburned pixels. A minimum of approximately 10 valid surface reflectance observations sensed before and after the specified period are required as prerequisites for burned area mapping (Giglio, et al., 2009). This is to allow sufficient number of MODIS observations that are free from cloud cover and coverage gaps to be available for the change detection process and hence, avoids potentially large errors of omission in the final product.

In general, the satellite-derived burned area products produced with dissimilar analysis procedures using time-series data provide mapped burned areas at different levels of accuracy, as the environmental and remote sensing conditions vary both spatially and temporally. The use of these moderate resolution products by multi-disciplinary users in a range of different applications, reinforce the need to objectively characterize their accuracy, differences and limitations in order to guide users in product utilization, and to identify possible refinements for consideration by product producers (Silva, et al., 2005; Morissette, et al., 2006; Strahler, et al., 2006). To allow validation of the lower resolution burned area products, the independent

high spatial resolution reference data must be derived, preferably over a sufficient set of locations and time periods (Roy, et al., 2008), to extract accurate information from the products. The validation of lower spatial resolution burned area products in different hemispheres of Africa, particularly in southern Africa, using independently-derived reference data from high spatial resolution satellite imagery, such as Landsat, has been extensively studied (Eva and Lambin, 1998a; Barbosa, et al., 1999; Korontzi, et al., 2003; Silva, et al., 2005; Boschetti, et al., 2006; Sa, et al., 2007; Roy and Boschetti, 2009; Giglio, et al., 2009). The differences as well as the possible reasons for the observed discrepancies in the derived accuracy information of the low and moderate spatial resolution burned area products, such as those generated using 5 km AVHRR, 1 km SPOT-VGT, 1 km ATSR and 500 m MODIS data, have been vastly provided including the conditions and factors that influence their accuracy. Nonetheless, the mapping accuracy of burned area products may vary not only spatially as a function of available biomass fuel, climate and, the type and condition of vegetation; but also temporally depending on the rate of post-fire vegetation recovery and persistence time of the char and mineral ash (Roy, et al., 2008). Therefore, validation exercises performed using a finite set of reference data may not comprehensively characterize a range of error associated with a particular burned area product. However, the derived accuracy information could be made more useful if the product's accuracy is assessed over a widespread set of locations and durable time periods, which encompass different vegetation types and weather seasons.

## **1.2: Problem statement**

Recently, regional southern Africa burned-area products have been produced using 500 m MODIS time-series data, which includes the MCD45A1 (Roy, et al., 2008) as well as the BMBAP (Giglio, et al., 2009). Previous research that has been undertaken to validate the MCD45A1 (Roy and Boschetti, 2009) and BMBAP (Giglio, et al., 2009) burned area products in South Africa only used ETM+ reference data located around the southern Kruger National Park (KNP), which encompassed the savanna biome. The goal of the current research is to expand validation of the MCD45A1 and BMBAP burned area products across the main fire prone biomes in South Africa. This research contributes some answers to the following specific questions:

- i) what is the performance of the two burned area products across the selected biomes?
- ii) are there notable differences in the accuracy of the burned area products across the biomes? and
- iii) to what extent does sub-MODIS pixel burned area affect burned area detection accuracy?.

### **1.3: Study aim and objectives**

The objectives of this study were to i) quantify the commission and omission errors in the MCD45A1 and BMBAP products; ii) compare the burned area proportion estimates derived from the MCD45A1 and BMBAP products to that of Landsat TM reference data for the 2007 burn season; and iii) to quantify the influence of the extend of sub-MODIS pixel burned area on the probability of detection by each burned area product.

These objectives directly affect the accuracy of moderate-resolution burned area mapping, and were analysed keeping in mind the type of biome, spectral characteristics and the size distribution of the burned areas. Therefore, the execution of these objectives intends to extend on the validation exercise of the MCD45A1 and BMBAP products in South Africa, by applying similar analysis methods to Roy and Boschetti (2009). Furthermore, an additional analysis of sub-MODIS pixel burned area that was not considered during previous validation of the MCD45A1 (Roy and Boschetti, 2009) and BMBAP (Giglio, et al., 2009) products is performed.

### **1.4: Study outline**

Five important phases were addressed in this research study. The first phase (presented in Chapter 1), discussed the biomass burning phenomenon, the significance and heritage of satellite fire remote sensing, and characteristics of burned area mapping. In the second phase (Chapter 2) we studied, the difference between active fire and burned area mapping, heritage of satellite burned area products and their validation, significance of validating the satellite burned area products, and methodologies used to evaluate product accuracy. The third phase describes the criteria adopted to guide selection of the validation sites, and applies

the internationally recognized burned-area satellite validation protocol (described in Chapter 3) to a series of Landsat 5 TM data to generate high-resolution burned-area validation reference data. The fourth phase (Chapter 4) concentrated on the validation results of MODIS burned area products and observed differences in the derived accuracy metrics in the products over each biome type. In addition, a quantitative analysis of fractional burned area of a MODIS-pixel on the probability of detection by each product was conducted, in order to understand the inherent error in the products due to the limitations arising from the moderate spatial resolution of the MODIS sensor. Lastly, concluding remarks, recommendations and future perspectives are briefly presented in Chapter 5.



## CHAPTER 2

### LITERATURE REVIEW

#### **2.1: The physical processes of biomass burning**

Biomass burning is a significant ecological disturbance phenomenon that is distributed over a considerable extent and its occurrence depends on seasonal changes and other diverse environmental variables such as vegetation type and condition, the available biomass fuel load, land use and climate (Dwyer, et al., 2000). The frequency of occurrence, distribution and severity of biomass burning has brought serious challenges to the research society as a fundamental driver of global climate and land cover change. For instance, about 70 - 80% of the terrestrial biomass is burned every year (Greenburg, et al., 1984; Andreae, et al., 1991) and has been thought to constitute approximately 40% of the annual carbon emissions (Levine, et al., 1996; Andreae and Merlet, 2001; Kasischke and Bruhwiler, 2003) that strongly affects the atmospheric chemistry and climatic processes (Justice, et al., 2006). Although these estimates could present varying magnitudes of uncertainty due to, for example climatic variations; the global satellite observations of biomass burning reveal that Africa has by far the highest occurrence of vegetation fires (Dwyer, et al., 2000) and thus, the most extensive biomass burning world-wide (Giglio, et al., 2010a). The current fire frequency in the African continent is closely related to human activity (Bond, 1997), especially for land management practices (e.g. pest control, preparation of agricultural fields and land clearance), and is accountable to the overwhelming majority of burning particularly in the grassland and savanna biomes (Hao, et al., 1990; Archibald, et al., 2010)

#### **2.2: Monitoring the occurrence and distribution of biomass burning**

There is a growing demand amongst the scientific community, policymakers, ecologists and resource managers for the provision of a comprehensive view of the frequency of occurrence, geographic extent and timing of biomass burning. Large

scale assessment of burned biomass is considered as an important parameter in, for example deriving quantitative estimates of the amount of biomass consumed by fire, greenhouse gas emissions and, for analysing the interaction between natural and anthropogenic contributions to biomass burning (Roy, et al., 1999; Giglio, et al., 2006; Archibald, et al., 2010). Previously, large scale assessments of burned biomass have been primarily founded on localized fire records (especially for some protected areas with specific fire management policies) (Frost, 1999) or use of national geostatistical data (Tansey, et al., 2004), that may not be adequate for a robust assessment of fire distribution across diverse environments.

In recent times, several research efforts have been successfully executed to investigate suitable Earth observation data and methods for the mapping of burned areas at different spatial scales (regional, continental and global) (Fernández, et al., 1997; Eva and Lambin, 1998a; Barbosa, et al., 1999; Silva, et al., 2005; Roy, et al., 2005a; Giglio, et al., 2009) and producing global estimates of the total burned surface using satellite data (Tansey, et al., 2004; Giglio, et al., 2006; Roy, et al., 2008). Large archives of data derived from the low (~1-5 km) and moderate (~250-500 m) resolution satellite sensors (such as ATSR, AVHRR, SPOT-VGT and MODIS) have been utilized for extensive monitoring and estimation of burned areas. Their spatial, spectral, temporal resolutions and varying spatial coverage (e.g., ~512-3000 km) make the satellite-derived data apt for use in large-scale applications in particular, the mapping and estimation of burned biomass. Two significantly distinct satellite-based methods have been vastly developed to aid the above-mentioned process, namely, active fire and burned area mapping algorithms. In the present study, burned area mapping and the validation thereof is the major focus, whereas active fire mapping is considered simply to highlight the differences between the two methods.

### **2.3: Active fire and burned area mapping**

Active fire mapping is primarily based on the detection of the surface radiant temperature released by fires (Dozier, 1981). Active fire mapping is a daily activity that can be regarded as the most convenient and valuable method to determine the seasonality, location, timing and spatio-temporal variability of fires over a large

spatial extent (Roy, et al., 2005b; Miettinen, 2007). For more than twenty years, numerous active fire mapping approaches have been widely developed for different satellite sensors and they operate on lower spatial resolution satellite data, arranged in chronological order were the AVHRR (Dozier, 1981; Matson and Dozier, 1981), GOES (Prins and Menzel, 1992), Defense Meteorological Satellite Program (DMSP) Operational Linescan System (OLS) (Elvidge, et al., 1996), ATSR (Arino and Rosaz, 1999), the Visible and Infrared Scanner (VIRS) (Giglio, et al., 2000), MODIS (Justice, et al., 2002a), and the Spinning Enhanced Visible and Infrared Imager (SEVIRI) (Roberts, et al., 2005).

However, active fire mapping has several limitations, which hinder reliable capturing of the location and timing of actively burning fires across various regions in multiple biomes. The limitations include, fixed fly-over times of the satellites, obscuration by optically thick clouds, heavy smoke or overstorey vegetation (Robinson, 1991; Giglio, et al., 2003; Giglio, 2007). In addition, regions susceptible to persistent cloud cover could result in significant under-mapping (large omission errors) of the fires (Justice, et al., 2002b; Roy, et al., 2006), particularly in humid tropical regions (Eva and Lambin, 2000). While active fire mapping provides useful information on the location, spatial distribution and time of burning, it may not reliably cover the actual area affected by fire. Giglio, et al. (2009) for example, reported that the least possible mapping size of an active fire is up to approximately 1000 times smaller than that of a burned area. In addition, since the burning duration of fires last only a few hours, only a fraction of the actively burning fires during satellite overpass would be detected (Eva and Lambin, 1998b). Consequently, this could probably lead to great uncertainty concerning the estimates of burned area derived using active fire maps. While underscoring these limitations, the growing demand for the spatio-temporal explicit estimates of burned area as well as the scarcity of long-term burned area data has led to numerous varying successful attempts in the exploitation of active fire maps as a surrogate to produce regional and global estimates of burned area (e.g., Scholes, et al., 1996; Giglio, et al., 2006; Ellicott, et al., 2009; Giglio, et al., 2009; Giglio, et al., 2010a).

In contrast to active fire mapping, burned area mapping is primarily based on the detection and delineation of the enhanced spectral changes of the fire-affected

areas (Roy, et al., 2005a). This has an importance to the research community, for instance, the derived quantitative estimates of burned area (this are the proportions of the land surface consumed by fire), and possible integration with other sources of data (e.g., land cover, fire maps, and climatic data) could be used to improve our understanding of the impacts of biomass burning on the Earth's environment and its troposphere. Fire-affected areas on the other hand, have lengthy existence lasting up to several days through months (depending on the type of vegetation that burns, wind and rainfall activity) (Roy, et al., 1999) and as a result, their mapping is insensitive to fixed satellite fly-over times and less affected by non-persistent obscuration of cloud and smoke occurrence.

In the last few years, several global burned-area thematic maps (products) derived from low to moderate resolution satellite data have been made publicly available. Initially, Tansey, et al. (2004) developed the GBA2000 global burned area product that provided monthly estimates of area burned for the year 2000. This product was produced using nine distinct regional burned area algorithms (Tansey, et al., 2002), which were applied to the 1 km resolution SPOT-VGT daily surface reflectance data. Additionally, Simon, et al. (2004) produced the GLOBSCAR global burned area for the year 2000 using monthly 1 km resolution European Remote Sensing 2 satellite (ERS-2) ATSR-2 data. Two algorithms were used to detect the burned areas. The first algorithm (Piccolini, 1998) took advantage of the reflectance changes in the NIR and TIR spectral bands associated with the burned-unburned vegetation status and land surface radiant temperature. Consequently, the enhanced burned-area changes were further calibrated by the second algorithm that performed fixed-threshold trials on the ATSR-2 visible-infrared bands for the final burned-unburned classification (Simon, et al., 2004). The above mentioned products were single-year ESA projects undertaken to demonstrate global estimates of area burned and as a result had limited assurance of continuity and consistency in the estimated burned area statistics. As a consequence, Plummer, et al. (2006) developed the GLOBCARBON global monthly burned-area product (promoted by the ESA) for the period April 1998 to December 2007, which provided more consistent and long temporal sequence of the product. The GLOBCARBON product was derived from the 1 km satellite data of SPOT-VGT, ATSR-2 and the Advanced ATSR (AATSR)

using a combination the GBA2000 and GLOBSCAR regional mapping algorithms (Simon, et al., 2004). Recently, Tansey, et al. (2008) developed the L3JRC multi-annual global burned area product from the 1 km SPOT-VGT reflectance data using a revised version of the GBA2000 algorithm developed by the International Forest Institute (IFI) (Ershov, et al., 2004). A composite image of the global atmospherically corrected reflectance observations is compiled across the daily moving window. Later on, the algorithm computes a temporal index using the NIR spectral band for all valid observations including the mean and standard deviation to characterize change between the newly acquired observation and the previous observations (composite image) over a 200 x 200 km window (Tansey, et al., 2008). Consequently, a pixel is considered as burned if its index value is below the mean value minus two standard deviations, taking into account the spectral trials based on the 0.83  $\mu\text{m}$  and 1.66  $\mu\text{m}$  reflectance values to provide the final burned classification. Roy, et al. (2008) developed the first global MODIS burned area product (also known as MCD45A1) as part of the recent generation of the moderate-resolution Collection 5 product suite. The MCD45A1 is expected to achieve higher burned-area mapping accuracies over the above-mentioned global burned-area products (particularly in regions dominated by small and scattered burned areas) due to the use of the moderate spatial resolution of the MODIS time-series data (Roy and Boschetti, 2009). Additionally, rather than using spectral indices, empirically-derived thresholds or training data, the global MODIS burned area algorithm (Roy, et al., 2002; Roy, et al., 2005a) systematically applies a bi-directional reflectance model on a time-series of 500 m land surface reflectance data. The algorithm accounts for surface state variations thus, employing a robust statistical comparison to detect change in reflectance from a previously observed state. The MCD45A1 is available as a monthly product and describes the location and approximate date of burning at 500 m resolution (Roy, et al., 2008). Most recently, Giglio, et al. (2010a) introduced the Global Fire Emissions Database (GFED3) 500 m monthly burned-area product (which is also similar to the BMBAP product) currently spanning July 1996 through mid-2009. The GFED3 was created from large archive of MODIS 500 m burned-area reference maps for the period mid-2000 through 2009, which were produced using the recently published Giglio, et al. (2009) MODIS burned-area mapping algorithm.

During the period July 1996 through mid-2000, the direct estimates of daily burned-area training data were unavailable to obtain monthly area burned (Giglio, et al., 2010a). As a consequence, local and regional regression trees were merged (see for example in Giglio, et al., 2006; Giglio, et al., 2010a) in order to express monthly area burned from the MODIS active-fire counts aggregated to 500 m spatial resolution. As with the MCD45A1, GFED3 describes the spatial extent and approximate Julian date of burning on a monthly basis.

## **2.4: Validation of the satellite burned-area products**

Recognizing the availability of the lower-resolution burned-area products; their practical use in different environmental assessment activities has provided useful information regarding the areas consumed by the occurrence of fire. In the literature, recent comparison results of the burned area products (Roy and Boschetti, 2009; Giglio, et al., 2010a) indicated significant spatio-temporal differences and similarities between the products (these are often generated using dissimilar algorithms) in areal estimates. As a result, the provision of product accuracy information at different spatial scales, (because the mapping accuracy of the satellite burned area products changes with climatic, environmental, and remote sensing factors that also vary both spatially and temporally (Roy, et al., 1999; Roy, et al., 2005b; Roy and Landmann, 2005c)) is important. The accuracy assessment of lower-resolution satellite burned-area products require gathering independent reference data (assumed as ground truth information) over a sufficient number of locations and time periods (Roy, et al., 2008) in order to obtain a representative sample encompassing the conditions and factors affecting product mapping accuracy.

The independent reference data are expected to be spatially explicit maps that have higher accuracy than the satellite product to be assessed, hence describing the actual burned areas, their mapping time period, and the areas that could not be mapped due to for example, cloud obscuration (Roy, et al., 2005b). Using independent reference data acquired by means of ground-based measurements may not provide sufficient spatial coverage in a timely manner, and could complicate reliable identification of the pre- and post-burn dates during validation of the satellite burned area products. Recognizing these limitations, previous studies have

demonstrated that ground-based measurements could be used as an additional parameter to ascertain the quality of the reference data (Eva and Lambin 1998b; Roy and Landmann, 2005c). Conversely, satellite data can be acquired to independently derive the reference data over a comprehensive spatial view, provided that the data must have higher spatial resolution (e.g., <60 m) than that of the product to be evaluated including, sufficient spectral resolution for the explicit identification of burned areas. Numerous studies have acquired archives of Landsat data to generate high-resolution (30 m) independent reference data for the validation of low-moderate resolution burned area products in an attempt to: a) quantitatively analyse the relationship between the spectral reflectance of the burned areas and product detection accuracy, b) quantify the burned area detection and areal estimation accuracies in the product and, c) quantify the influence of sub-pixel burned area on the detection accuracy of the product. Below we provide a summary of the successful attempts by various authors that dealt with the three inter-related aspects stated above, whereas the current study focuses on the latter two upshots.

Razafimpanilo, et al. (1995) for example, compared the detection accuracy of two approaches that attempt to estimate the proportion of a pixel burned from the coarse resolution AVHRR data. The first approach was expressed as a near-linear correlation between the burned pixel proportion and the atmospherically-corrected AVHRR band 2 reflectance data; and the second approach as a non-linear correlation between pre- and post-fire NDVI data derived from the AVHRR band 1 and 2 reflectance. Comparison results for both approaches revealed accurate burned-area estimates for pixels spanning uniform background variations with high spectral contrasts. On the other hand, for pixels characterized by low spectral reflectance (e.g., as a result of partially burned overstorey vegetation or water), influenced the estimation accuracy of the two approaches. Eva and Lambin (1998a) used the TM reference data to validate the 1 km ATSR regional burned area maps in Central Africa during the 1994-95 burning season. In their work, they compared the burned area proportions derived from the TM and ATSR data across the 9 x 9 km grids through linear regression for the sensitivity of ATSR burned area maps, and produced with different SWIR and TIR thresholds. Their findings revealed that the coarse-resolution ATSR-based maps underestimated the true burned area particularly

across small and spatially fragmented burned areas. On the other hand, over landscapes dominated by large and compact burned areas, the coarse resolution maps overestimated true area burned. Furthermore, they concluded that the burned area pattern and background spectral variations affect the performance of coarse resolution burned area mapping. Chuvieco, et al. (2002) assessed the enhanced burned land changes provided by the Normalized Difference Vegetation Index (NDVI), Soil Adjusted Vegetation Index (SAVI), Global Environmental Monitoring Index (GEMI) and Burned Area Index (BAI) spectral indices in the red-NIR spectral region using the AVHRR and Landsat TM data sets for different post-fire periods. Their findings revealed that while BAI attained the highest burned-area discrimination; water bodies and cloud shadows were primarily reported as potential sources of spectrally confusing phenomena for the indices. Landmann (2003) compared the burned area sizes derived from Landsat ETM+ reference data with those mapped on the 500 m MODIS data using simple linear regression in Kruger National Park, South Africa across the savanna biome for the September 2001 burning period. While a significant correlation measure ( $R^2 = 0.98$ ) was discovered between the two variables, MODIS was reported to have missed 7% of the true burned area which was classified in the Landsat product and, hardly detected burned area sizes below approximately 2 km<sup>2</sup> due to small burned areas and spectral aliasing (from e.g., rapid post-fire re-vegetation, recently ploughed fields and understorey low intensity fires).

Loboda and Csiszar (2004) generated 20 ETM+ independent reference data sets to validate burned areas mapped from the coarse resolution MODIS and AVHRR data on the Russian boreal forests during the 2002 fire season. Furthermore, they applied the widely-used error matrix (Congalton, et al., 1983) and linear regression analysis to evaluate the geospatial detection accuracy of burned areas along with the estimation accuracy of the detected burned areas. Their derived accuracy results indicated trade-offs for the MODIS and AVHRR products and consequently, the authors identified possible sources of error in the observed discrepancies between the products. These errors were related to either the lower spatial resolution of the satellite sensor, burned area heterogeneity, omitted burns and false detections, or geolocation accuracy of the products. Varfeidis and Drake (2005)



evaluated the use of burned pixel identification and sub-pixel burned area estimation approaches to reliably estimate the extent of burned area on a time series of AVHRR data using ground reference data provided by the Greek National Forest Service in Greece during the summer of 1998. In the first approach, burned or unburned changes were classified using spectral indices while in the second approach, the identified burned changes are considered for the estimation of sub-pixel burned area. Their results demonstrated large overestimation of true burned area when the approaches were applied independently. Furthermore, their integrated use revealed significant agreements ( $R^2$  values  $> 0.9$ ) and much lower errors of commission and omission (below 5% for individual burned areas). However, they concluded that the differences in the derived accuracy measures are dependent on the degree of spectral separability and size of the burned areas. This finding closely corroborates the analysis executed by Pereira, et al. (1999), who demonstrated that the combined use of the two approaches stated above could be less prone to commission and omission errors and further lead to better estimation results of total burned area extent.

Silva, et al. (2005) compared the 1 km VGT burned area product with 13 ETM+ independently derived reference maps distributed widely across the African continent for the year 2000 using a linear regression approach. Their findings demonstrated the influence of vegetation type and spatial patterns of the burned area (which includes the shape, size, spatial distribution and spectral contrast) on the accuracy of burned area estimations present in the VGT product. They concluded that, burned areas characterized by small sizes, complex shapes, or low spectral contrasts lead to less estimation accuracy of burned areas mapped at coarse resolution. Boschetti, et al. (2006) assessed the estimation accuracy of the GBA2000 burned area product in the Africa continent with widely distributed high-resolution ETM+ reference data sets for the year 2000 and, applied a regression estimator between the computed burned-unburned proportions in grid cell sizes of 25, 50 and 100 km respectively. The comparison suggested moderately-sufficient correlations with  $R^2$  values between 0.579-0.630. There were however, slight differences in areal estimates with higher slope values and furthermore, the author reported that the statistical measures increased as the grid cell size enlarged due to the effect of spatial aggregation. Sa, et al. (2007) quantitatively studied the relationship between the

burned area spatial patterns and their spectral detectability. In this study the burned area fractional estimates derived from the 500 m MODIS imagery and 6 ETM+ independent reference data sets across the 15 km<sup>2</sup> grids, in southern Africa, were compared during the fire season of year 2000. They found a negative linear trend implying a decline in spectral detectability as the fraction of burned area increased, particularly as a result of dominant, cumulated small burned area patches. They concluded that small and scattered burned areas could be hardly mapped at 500 m spatial resolution. Furthermore, reasonable detection could only be observed for fractional burned area threshold of at least 0.5 due to unification of burned area patches, and thus decreasing areal mixed pixels.

Recently, Roy and Boschetti (2009) validated the MCD45A1, L3JRC and GlobCarbon burned area products with multi-temporal ETM+ independent reference data in southern Africa for the 2001 burning season by means of error matrices and linear regression statistical measures. Their findings revealed that at local scales, all three burned area products had lower false detections (low commission errors) but missed a significant proportion of the burned areas (high omission errors). Furthermore, for regional applications the MCD45A1 achieved the highest estimated true burned area of 75%, followed by GlobCarbon at 60% and 14% for the L3JRC burned area product. They concluded that small and fragmented, coupled with the relatively weak spectral signature and, the adopted minimum-mapping threshold of the burned areas largely influenced the observed discrepancies in the derived accuracy measures for the products. The independent reference data used for validation by Roy and Boschetti, (2009) were derived using the recently published international global burned-area product validation protocol (Roy, et al., 2005b). This protocol requires the acquisition of multi-date high spatial resolution data coupled with intensive visual inspection and on-screen digitizing practices, to more carefully interpret the burned areas and non-burned spectrally confusing phenomena arising from, for example cloud and relief shadows. This protocol seeks to enhance the quality of the high-resolution independent reference data than the typically used supervised and/or unsupervised classification approaches (e.g., ISODATA) which have been applied in previous validation studies to produce the independent

reference data (e.g., Eva and Lambin, 1998a; Chuvieco, et al., 2002; Silva, et al., 2005; Boschetti, et al., 2006; Smith, et al., 2007; Sa, et al., 2007).

Furthermore, Giglio, et al. (2009) validated the 500 m MODIS burned area maps using multi-temporal ETM+ data sets spanning a variety of biomes in Central Siberia, United States and southern Africa, respectively. The moderate-resolution burned area maps were produced using the recently published Backup MODIS burned-area detection algorithm (Giglio, et al., 2009; Giglio, et al., 2006). The Backup MODIS burned-area detection algorithm, generally creates burned area maps by taking advantage of the spatial and temporal information provided by active fire observations and the summarized persistent post-fire changes in the MODIS cloud-free surface reflectance observations. The accuracy of the burned area maps was evaluated by means of an error matrix and linear regression procedures. The assessment results revealed very high overall mapping accuracies and significant Pearson's correlation coefficients in all sites, but underestimated of true burned area by 14% (over low tree canopy) and 41% (over high tree canopy) in southern Africa. Furthermore, the burned area maps overestimated ~12% of true area burned in the United States primarily spanning grassland, shrubland, woodland, and forested fires. Lastly, the assessment revealed slight underestimation of ~8% true burned area in Central Siberia with the reference maps densely distributed across the evergreen and deciduous needle leaf forests, sparse and mixed larch forests and open woodlands. They concluded that obscuration by tree canopy, persistent cloud cover, lower combustion completeness of the biomass, and the inherent moderate-resolution of MODIS could influence the reliability of detection of the burned areas, thus amplifying the errors of omission. On the other hand, regions characterized by recently clear-felled unburned forests could raise spectral uncertainty between unburned forest patches with true burned areas, and thus may result in commission errors due to spectrally similar reflectance changes (Giglio, et al., 2009).

## **2.5: The need for burned area product validation**

The validation studies highlighted above, pointed out that the detection accuracy of lower spatial resolution satellite burned-area products could have regional variations that dependent on the algorithm procedures, remotely-sensed data, biome type, and

weather conditions. As a result, accuracy assessments executed using a finite selection of reference data and time periods may not characterize comprehensively the errors accompanying a particular product (Roy, et al., 2006). This strengthens the need for rigorous validation of the products (particularly those defined using dissimilar algorithms) (Roy and Boschetti, 2009), spanning a sufficient range of space and durable time periods. This validation is necessary to quantitatively express the discrepancies across the products and determine possible reasons for the observed product differences. Furthermore, describing product discrepancies pertaining to biome type and fire season could make product accuracy information more user-friendly (Roy, et al., 2006). This would thus act as a guide for choosing the most suitable product to supervise the spatial and temporal distribution of burning in particular regions.

Previous research that validated the MCD45A1 (Roy and Boschetti, 2009) and BMBAP (Giglio, et al., 2009) products in South Africa was limited to ETM+ reference data sets located around the southern Kruger region, which encompassed the savanna biome. The current research intends to expand validation of both the MODIS burned area products across six sites encompassing a variety of biomes (such as grassland, fynbos, pine forest, and savanna) and different climatic conditions in South Africa by applying the widely known accuracy reporting methods (these are based on the error matrix and simple linear regression). However, as an additional analysis during validation not considered by Roy and Boschetti (2009) and Giglio, et al. (2009) sub-MODIS pixel burned area analysis is done for both products. Generally, the analysis attempts to quantify the influence of extent of sub-MODIS pixel burned area on the probability of detection by each burned area product. Other than extending validation of the MODIS burned area products using traditional methods (e.g., error matrix), the additional sub-pixel analysis seeks to provide a graphical representation of the impact of fractional burned-area within a 500 m MODIS pixel on the detection accuracy of both MCD45A1 and BMBAP products.

It has been widely reported that statistical measures derived by means of an error matrix alone (during comparison of low-moderate resolution burned area products with high-resolution reference data), may not provide reliable error

measurements for a particular product (Foody, 1996; Binaghi, et al., 1999). This is because the typical application of an error matrix assumes that the data being compared are all at the same spatial resolution, which often does not hold true when validating low-moderate resolution remotely-sensed products (Boschetti, et al., 2004). Such additional sub-pixel analysis mentioned above could reveal useful information that allows comprehension of possible classification biases as a result of inherent differences in the spatial resolutions of the satellite data being compared.

## **2.6 Concluding remarks**

Previous accuracy assessment of the MCD45A1 product involved the acquisition of 22 multitemporal Landsat ETM+ data sets distributed across southern Africa (including Namibia, Botswana, Zimbabwe, Mozambique, Malawi and South Africa) to encompass regional variations in temperature, rainfall and vegetation type (e.g., ranging from evergreen broadleaf forest, grasslands, savannas, croplands and open shrublands) (Roy, et al., 2005b; Roy and Boschetti, 2009). The high-resolution burned area reference data were produced following a protocol implemented to validate the burned area product derived from the MODIS 500 m multi-temporal data (Roy, et al., 2005b). Validation results of the MCD45A1 product in southern Africa (Roy and Boschetti, 2009) revealed that at local scale, the product had lower false detections (~35% in overall) but missed a significant fraction of the burned areas (~60% in overall), particularly over small and spatially fragmented burned areas. Furthermore, for regional applications the MCD45A1 achieved a high estimated true burned area of 75%. On the other hand, Giglio, et al. (2009) validated the 500 m Backup MODIS burned area product using multi-temporal ETM+ data sets spanning a variety of biomes in Central Siberia, United States and southern Africa, respectively. The assessment results revealed very high overall mapping accuracies and significant Pearson's correlation coefficients in all sites, but underestimated true burned area by 14% (over low tree canopy) and 41% (over high tree canopy) in southern Africa.

Previous research that has been undertaken to validate the MCD45A1 (Roy and Boschetti, 2009) and BMBAP (Giglio, et al., 2009) products in South Africa used ETM+ scenes (these include two scenes for MCD45A1 and only one scene for

BMBAP) located around the Kruger National Park, which encompassed the savanna biome. The research presented here focuses on an extension to the quantitative accuracy assessment of the MODIS burned area products across in South Africa. The accuracy assessment is carried out by adopting previously used accuracy reporting measures but further introduces an additional quantitative analysis of sub-MODIS pixel burned area. This analysis takes cognisance of biases present in the derived product accuracy measures, as a result of the inherent difference in the spatial resolutions of the satellite burned area product and the independent reference data (derived from Landsat) during comparison. Furthermore, inter-comparison and continuous evaluation of the MODIS burned area products undertaken in this study, attempts to provide a spatial and temporal analysis on how these products perform across the different South African biomes and, to improve understanding of a range of errors and error sources present in the burned area products.

## CHAPTER 3

### DATA AND METHODS

#### 3.1: Introduction

This section gives a brief introduction of the methodology and data used in the study. The primary goal of this research study is to extend validation of the moderate resolution satellite-derived burned area products over additional fire-prone biomes in South Africa. Figure 3.1 depicts the schematic flowchart of the methodology adopted. The schematic view demonstrates that validation of the moderate resolution burned area products required the interpretation of multitemporal Landsat TM images to produce high-resolution independent reference data. This was then used for accuracy assessment through confusion matrices, fractional burned area assessment and linear regression analysis.

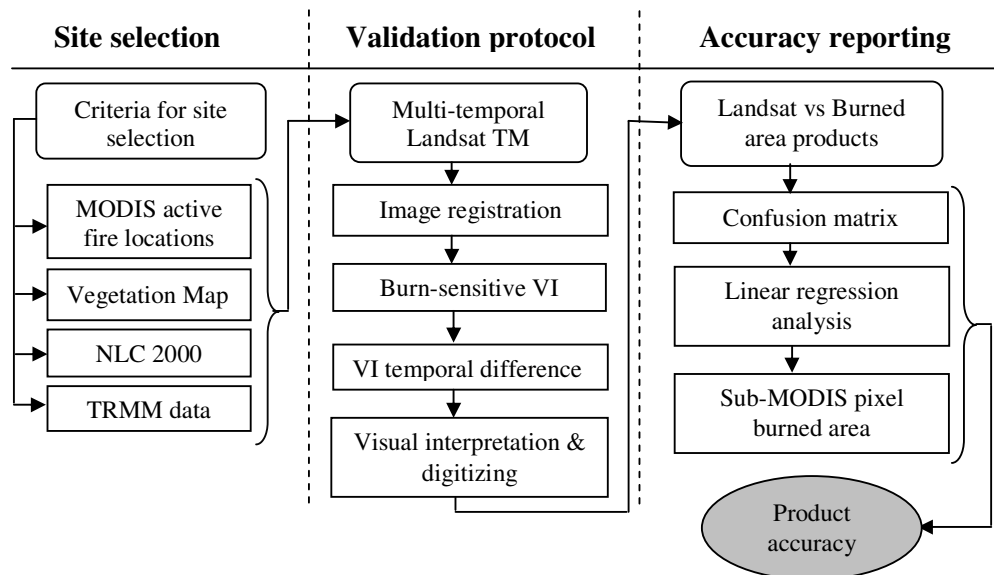


Figure 3.1: Methodological framework showing the three important phases addressed in this research study.

## 3.2: Data used and study area

### 3.2.1: Landsat 5 TM

The TM onboard the Landsat 5 satellite is a multispectral scanner which has been observing the earth's surface since 1984. The TM has a repeat cycle of 16 days and provides remotely sensed data from seven spectral bands (Table 3.1) at a spatial resolution of 30 m for the visible, near and middle infrared (bands 1-5 and 7) and a resolution of 120 m for the thermal infrared (band 6). Each TM scene covers an area of approximately 185 x172 km defined in the Universal Transverse Mercator (UTM) coordinate system. Landsat 5 data are identified using path and row coordinates defined by the World Reference System-2 (WRS-2), which allows efficient search and retrieval of the requested imagery for any fractional surface of the Earth (<http://landsat.usgs.gov>).

Table 3.1: The spectral and spatial characteristics of the Landsat 5 Thematic Mapper (TM) multispectral scanner (<http://landsat.usgs.gov>)

<b>Landsat 5 (TM sensor)</b>	<b>Wavelength (micrometers)</b>	<b>Spatial resolution (meters)</b>
Band 1: red	0.45-0.52	30
Band 2: green	0.52-0.60	30
Band 3: blue	0.63-0.69	30
Band 4: near-infrared	0.76-0.90	30
Band 5: middle-infrared	1.55-1.75	30
Band 6: thermal-infrared	10.40-12.50	120
Band 7: middle-infrared	2.08 -2.35	30

Two Landsat TM data sets were obtained for each of the six study sites during the fire season of 2007 in eastern and south-western regions of South Africa (this corresponds to the summer and winter rainfall respectively). The multi-temporal TM data sets were provided by the CSIR's (Council for Scientific and Industrial Research) SAC (Satellite Application Centre) in tiff format processed to a Level 1T (terrain and precision corrected). The temporal differences of the acquired TM data



pairs shown in Table 3.2 had different time intervals ranging from 16 days - 64 days. The TM data pairs that display shorter time intervals, for example of 16 - 32 days are highly preferable for producing burned-area reference data (Roy, et al., 2005b). This is because during change detection, the post-fire reflectance changes reveal a stronger burned area signal that can be unambiguously identified (Roy, et al., 2005b). However, not all multi-temporal TM data sets acquired in this study had shorter time intervals; this was because of the limitation arising from the lack of cloud free TM images for our period of study, especially in the Western Cape and Sabie regions.

Table 3.2: Landsat 5 TM scene pairs used to produce high-resolution burned-area independent (validation) reference datasets.

Biome	Site, Landsat path/row	TM acquisition dates 2007	Temporal difference between TM dates	Study region between the TM dates
Savanna	Southern Kruger 168/077	11 Aug 07 27 Aug 07	16 days	1271190.47 ha
Grassland	Middelburg 169/078	18 Aug 07 3 Sep 07	16 days	1018192.47 ha
Fynbos	Western Cape 175/083	17 Feb 07 6 Apr 07	48 days	608950.7 ha
Pine forest	Sabie 169/077	15 Jun 07 18 Aug 07	64 days	71936.46 ha
Savanna	Thabazimbi 171/077	15 Jul 07 16 Aug 07	32 days	1698936.14 ha
Grassland	Free State 169/080	18 Aug 07 3 Sep 07	16 days	1066678.36 ha

Although all Landsat TM acquisitions have been geometrically corrected, an image to image registration was crucial for conducting rigorous change detection of the burned areas that occurred between the two TM acquisitions of each scene. The registration process ensures perfect co-registration or high sub-pixel accuracy among the TM acquisition pairs (Jensen, et al., 1993; Phinn and Rowland, 2001). This significantly minimizes spurious reflectance changes such as, high contrast non-burn related changes that may occur along the feature edges (Roy, et al., 2000). At least 16

ground control points (GCPs) were selected uniformly throughout both TM images of each scene by identifying salient and distinctive features that are considered likely to remain stable over time at fixed positions (such as, road crossings, lakes, water streams, building edges, and agricultural fields) (Figure 3.2). To simplify GCP selection, the GCPs on each TM acquisition pair (TM date 1 and TM date 2) were located using an enhanced false colour display provided by TM band 5 (1.75  $\mu\text{m}$ ), 4 (0.90  $\mu\text{m}$ ), 3 (0.69  $\mu\text{m}$ ) (mid-infrared, near-infrared and red correspondingly) combination.

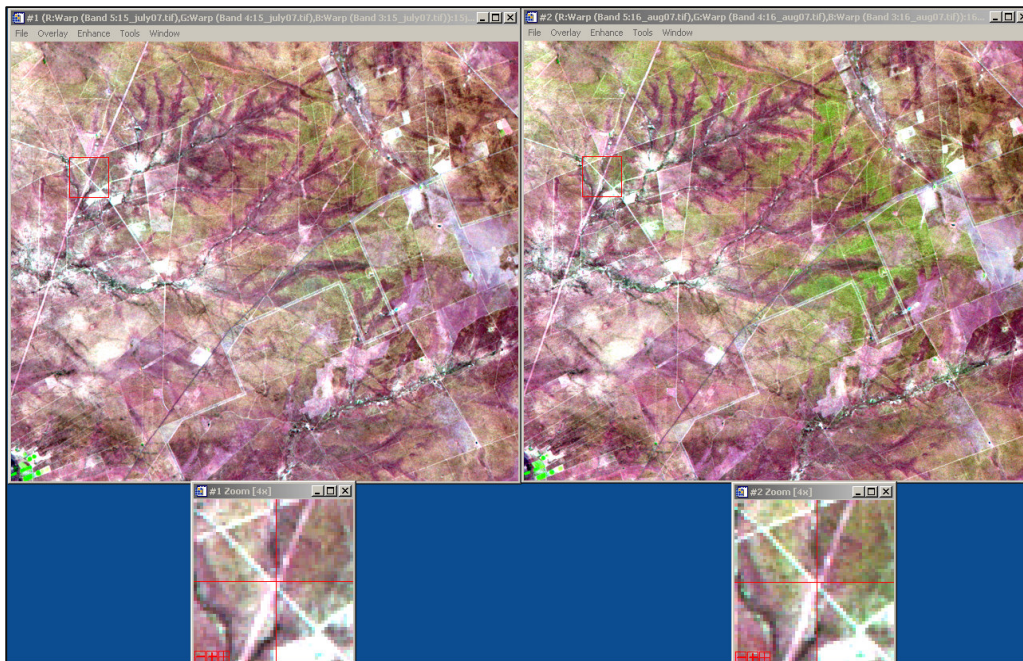
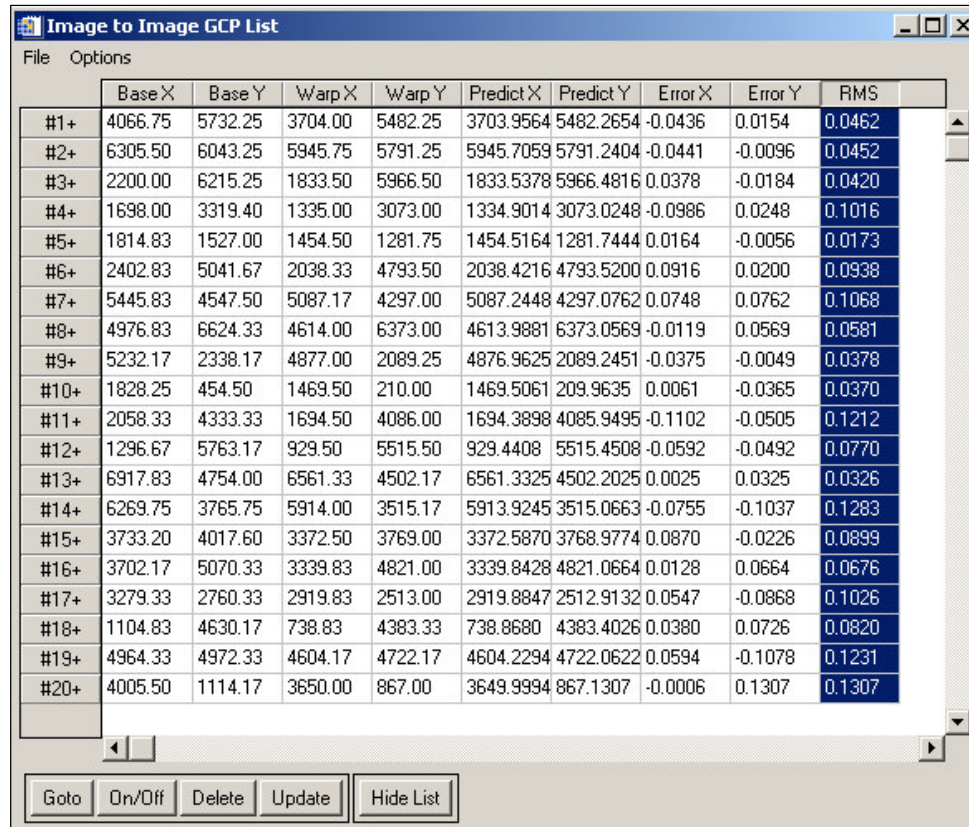


Figure 3.2: An example of a dual display using TM date 1 (15 July 2007) and TM date 2 (16 August 2007) false colour images of Thabazimbi in ENVI software version 4.3, which simplified GCP collection for image to image registration.

Numerous studies on change detection have proposed varying threshold values of acceptable root mean square (RMS) error for co-registration accuracy. Wedderburn-Bishop, et al. (2002) for example, suggested an acceptable RMS error threshold of < 0.70 pixels, whereas Jensen (1996) suggested an RMS error threshold of < 0.50 pixels. In addition, Townshend, et al. (1992) proposed varying magnitudes of

adequate RMS error thresholds based on land cover, where for regions characterized by dense vegetation a RMS error of  $< 0.2$  pixels was essential, and for regions marked by sparse vegetation a RMS error of between 0.5 and 1 pixel was required. Generally, a RMS error is considered acceptable if it is  $< 1.0$  pixel for every GCP and/or when the total RMS error from all GCPs is  $< 1.0$  pixels.



	Base X	Base Y	Warp X	Warp Y	Predict X	Predict Y	Error X	Error Y	RMS
#1+	4066.75	5732.25	3704.00	5482.25	3703.9564	5482.2654	-0.0436	0.0154	0.0462
#2+	6305.50	6043.25	5945.75	5791.25	5945.7059	5791.2404	-0.0441	-0.0096	0.0452
#3+	2200.00	6215.25	1833.50	5966.50	1833.5378	5966.4816	0.0378	-0.0184	0.0420
#4+	1698.00	3319.40	1335.00	3073.00	1334.9014	3073.0248	-0.0986	0.0248	0.1016
#5+	1814.83	1527.00	1454.50	1281.75	1454.5164	1281.7444	0.0164	-0.0056	0.0173
#6+	2402.83	5041.67	2038.33	4793.50	2038.4216	4793.5200	0.0916	0.0200	0.0938
#7+	5445.83	4547.50	5087.17	4297.00	5087.2448	4297.0762	0.0748	0.0762	0.1068
#8+	4976.83	6624.33	4614.00	6373.00	4613.9881	6373.0569	-0.0119	0.0569	0.0581
#9+	5232.17	2338.17	4877.00	2089.25	4876.9625	2089.2451	-0.0375	-0.0049	0.0378
#10+	1828.25	454.50	1469.50	210.00	1469.5061	209.9635	0.0061	-0.0365	0.0370
#11+	2058.33	4333.33	1694.50	4086.00	1694.3898	4085.9495	-0.1102	-0.0505	0.1212
#12+	1296.67	5763.17	929.50	5515.50	929.4408	5515.4508	-0.0592	-0.0492	0.0770
#13+	6917.83	4754.00	6561.33	4502.17	6561.3325	4502.2025	0.0025	0.0325	0.0326
#14+	6269.75	3765.75	5914.00	3515.17	5913.9245	3515.0663	-0.0755	-0.1037	0.1283
#15+	3733.20	4017.60	3372.50	3769.00	3372.5870	3768.9774	0.0870	-0.0226	0.0899
#16+	3702.17	5070.33	3339.83	4821.00	3339.8428	4821.0664	0.0128	0.0664	0.0676
#17+	3279.33	2760.33	2919.83	2513.00	2919.8847	2512.9132	0.0547	-0.0868	0.1026
#18+	1104.83	4630.17	738.83	4383.33	738.8680	4383.4026	0.0380	0.0726	0.0820
#19+	4964.33	4972.33	4604.17	4722.17	4604.2294	4722.0622	0.0594	-0.1078	0.1231
#20+	4005.50	1114.17	3650.00	867.00	3649.9994	867.1307	-0.0006	0.1307	0.1307

Figure 3.3: Illustration of the computed statistics in ENVI for the 20 collected GCPs. The estimated RMS error for each GCP (highlighted in blue for legibility) was kept below an RMS error threshold of 0.5 pixels.

In the present study, considerable effort was taken to ensure that the RMS error was kept at minimum for the located features identified in both images (Figure 3.3). We adopted total RMS error threshold of  $< 0.5$  pixels associated with the GCPs and a first order polynomial function to tolerate translation, rotation, and a scaling

correction in both axes of the TM images. Consequently, the collected GCPs were used to warp one TM image (date 1) into co-registration with the other (date 2).

### 3.2.2: Burned-area reference data

The high-resolution burned-area reference data were generated based on the satellite burned-area product validation protocol described by Roy, et al. (2005b). This protocol requires visual interpretation and on-screen digitizing of the enhanced post-fire reflectance changes highlighted between the TM acquisition dates. These changes, as demonstrated in Figure 3.4 and Figure 3.5 had low spectral reflectance and were easier to identify as they appeared dark due to a burn-sensitive vegetation index (VI) that was computed for the TM acquisition pairs ( $VI_{\text{date 1}}$  and  $VI_{\text{date 2}}$ ) using the TM smoke-insensitive middle-infrared bands 5 (1.75  $\mu\text{m}$ ) and 7 (2.35  $\mu\text{m}$ ) (Kaufman and Remer, 1994; Roy, et al., 2005b). The VI was computed from Equation (1):

$$VI_i = \frac{b_{5,i} - b_{7,i}}{b_{5,i} + b_{7,i}} \quad (1)$$

Where  $i$  represent the date of the acquired TM data, and  $b$  represent the corresponding bands 5 and 7 (Roy, et al., 2005b). Further, a temporal difference of the spectral indices ( $VI_{\text{date 2}} - VI_{\text{date 1}}$ ) was derived in order to identify the burned areas that occurred between the two dates. During interpretation of the burned areas, some non-fire induced changes were evident, such as those caused by cloud shadows, and they appeared to be spectrally similar to the actual burned areas. To aid interpretation in these instances, the false-colour TM imagery based on the red, green and blue (RGB) band 5, 4, and 3 combinations were used. This was augmented by the TM thermal-infrared band 6 (12.50  $\mu\text{m}$ ) in order to clearly distinguish burned areas from the clouds, shadows, and water bodies (Roy, et al., 2005b). As a result, the high-resolution independent reference data sets generated comprised of digitized polygons with the following information:

- a) mapped regions outlining the selected study sites covered by the acquired TM scene pairs;

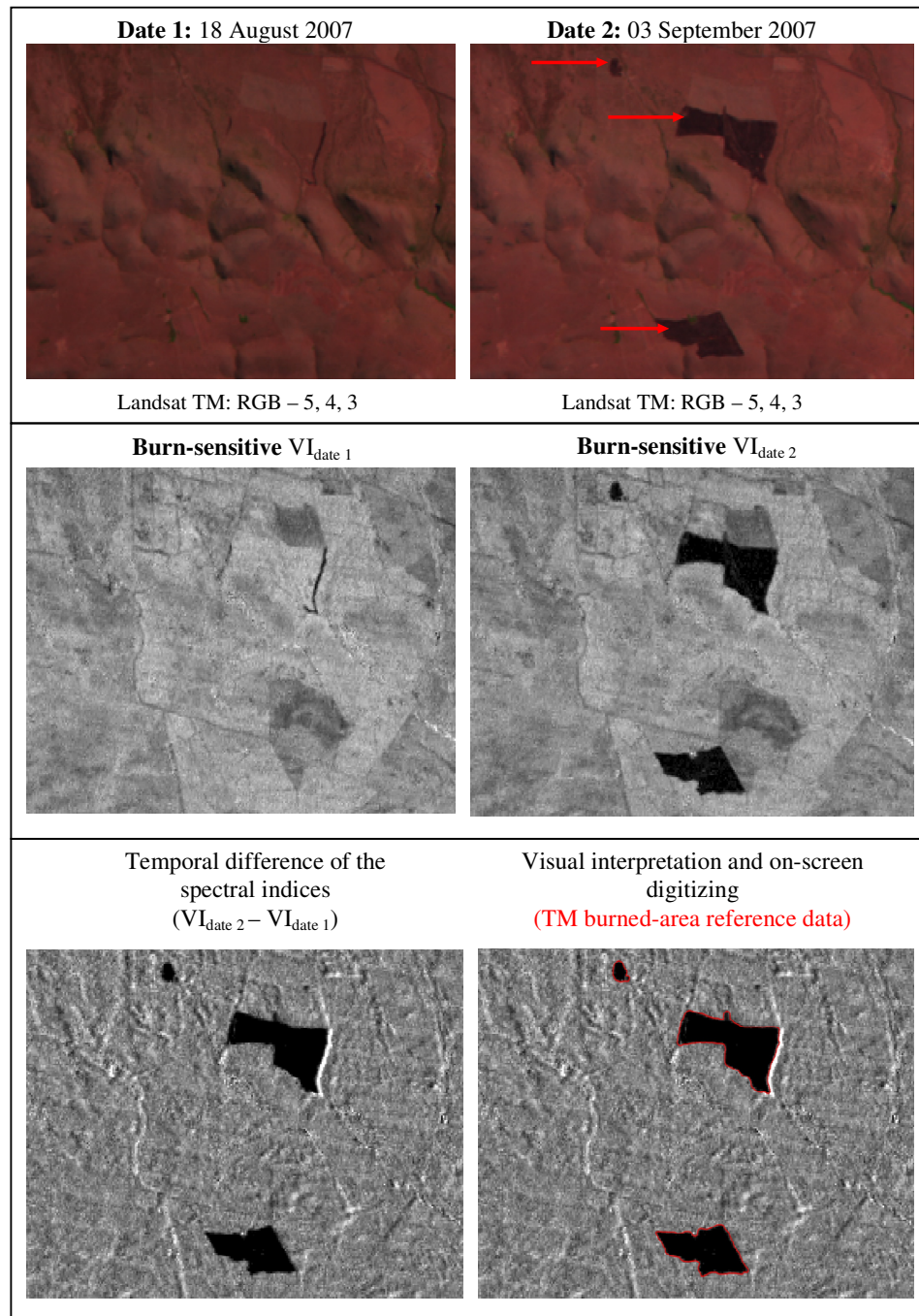


Figure 3.4: In the first row is the acquired TM scene pair in Kruger. Second row depicts the computed burn-sensitive vegetation index (VI) on the TM pair to identify burned areas. Third row depicts the elevated burned areas between the multi-temporal TM indices and their interpretation.

- b) identified and interpreted burned areas that occurred between date 1 and date 2 of the TM acquisitions and;
- c) unmapped areas which include clouds, cloud shadows and ambiguous spectral features within the study sites that could not be interpreted as either burned or unburned.

Categorising the reference data into interpreted burned areas and unmapped areas as shown above, avoids taking into account areas that could not be interpreted, as either burned or unburned during the evaluation phase (comparing reference data with the moderate-resolution burned area products).

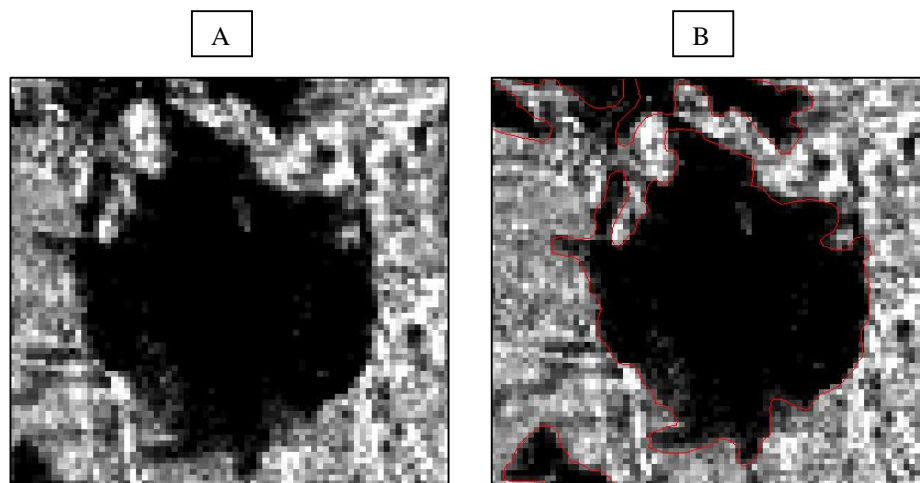


Figure 3.5: Zoomed in example of a VI difference image (A) showing high spectral contrast of the burned areas (A) and the interpreted burned areas delineated by red polygons (B).

In order to help minimize the mapping effort during on-screen digitising when producing the independent reference data, only burned areas that correspond to at least 4 pixels (at Landsat 30 m resolution) were considered (Roy, et al., 2005b). This threshold is equivalent to approximately 2 % of fractional burned area within a 500 m MODIS pixel, which due to the lower resolution of the MODIS sensor, such burns may remain undetected. Despite this challenge, in the present study we also applied the above stated threshold to provide comparability of the MODIS burned area validation results with those reported by Roy and Boschetti (2009). We also

acknowledge the importance and use of supervised and/or unsupervised classification techniques (such as Maximum Likelihood or ISODATA) to generate high-resolution burned area reference data. However, challenges imposed by variable post-fire reflectance changes, such as the spectrally confusing changes not caused by burning, coupled with the presence of small and spatially fragmented burned areas (Roy, et al., 2006; Roy, et al., 2008), could necessitate human interpretation and manual mapping efforts to enhance the accuracy of the independent reference data generated from high spatial resolution satellite data (Roy, et al., 2005b).

### *3.2.3: The moderate-resolution satellite burned area products*

#### *3.2.3.1: The “Backup” MODIS burned area product*

The monthly BMBAP product covering South Africa was provided by the CSIR, Meraka Institute spanning time periods of 1 January to 30 April 2007 (generally summer season) and 1 June to 30 September 2007 (generally dry season). This product is publicly made available on the CSIR, Meraka Institute’s Wide Area Monitoring Information System (WAMIS) website (<http://afis.meraka.org.za/wamis>) in Tagged Image File Format (tiff) defined in Geographic projection and World Geodetic System 1984 (WGS84) datum. The BMBAP product is defined by the recently developed “active-fire based burned area mapping algorithm” (Giglio, et al., 2009). The algorithm uses the 500 m MODIS surface reflectance time-series data (Vermote, et al., 2002) sensed within a temporal window of 20 days to select the daily atmospherically-corrected MODIS band 5 (1.2  $\mu\text{m}$ ) and band 7 (2.1  $\mu\text{m}$ ) reflectances. These bands are used in the algorithm to compute a spectral index suitable for identifying the persistent post-fire changes as well as to minimize other similar changes not associated with burning, such as cloud shadows and water bodies.

The identified post-fire reflectance changes are then matched with 1 km MODIS active fire maps to guide the statistical selection (based on the mean, standard deviation and temporal separability tests) of burned and unburned training pixels during the time period being processed. Having discovered the training areas, dynamic thresholds based on conditional PDFs are derived and a series of quartile

tests are performed which are suitable for classifying approximately 80% of pixels in the scene as either burned or unburned. It is important to note that the active fire data used within the algorithm may not represent regions dominated by small and spatially fragmented burns well. This is because the minimum detectable size of an active fire is up to approximately 1000 times less than that of a burned area and therefore, regions characterized by these conditions will usually result in large omission errors (Giglio, et al., 2006).

The algorithm completes the classification by use of iterated conditional modes (ICM) reported by Besag (1986) which uses a Markov Random Field (MRF) to model the spatial behaviour of the remaining unclassified pixels in the scene by considering their proximity to pixels which have already been classified as either burned-unburned. Ultimately, the algorithm maps the location and approximate Julian date of burning at 500 m spatial resolution globally. The BMBAP product was re-projected to match the Landsat UTM projection of each scene while retaining the product output pixel-dimension at 500 m spatial resolution using nearest neighbour re-sampling.

#### *3.2.3.2: The “Official” MODIS burned area product*

The MCD45A1 product over South Africa was downloaded from the NASA website (<http://wist.echo.nasa.gov>) covering the dates 1 January to 30 April 2007 and 1 June to 30 September 2007 (which are the same dates as the acquired BMBAP product in section 3.2.3.1). The MCD45A1 product was received in Hierarchical Data Format (hdf) defined in Sinusoidal equal area projection. The global algorithm used to generate the MCD45A1 uses as input data, the 500 m MODIS cloud-free surface reflectance time-series data sensed at smaller view-zenith angles below 45° (Roy, et al., 2005a). The algorithm then applies a bi-directional reflectance change detection method based on a Bi-directional Reflectance Distribution Function (BRDF) model to a minimum of 7 observations sensed within a temporal window of at least 16 days, to compute predicted reflectances reference to the previously sensed ( $m \geq 7$ ) reflectance observations (Roy, et al., 2002; Roy, et al., 2005a) as well as to account for the angular variations and noise found within the MODIS data. Furthermore, the algorithm employs a statistical threshold to quantify the discrepancies in change



probability between the model-predicted and observed reflectance values. Large discrepancies between the observed and model-predicted reflectance values are attributed to possible post-fire changes (Roy, et al., 2005a), and consistency constraints are used to monitor the temporal persistence of these changes to differentiate between non-fire spectrally confusing (e.g., cloud shadows) and actual fire-induced changes. In addition, the identification of the burn date is often problematic due to the thresholding of the view zenith geometry information during the selection of MODIS surface reflectance observations. This could lead to the lack of sufficient valid MODIS observations required by the BRDF model (data gaps in the model) to compute predicted reflectances. Consequently, the algorithm is executed to report the date of burning with an eight-day precision (Justice et al., 2002b; Roy, et al., 2005a).

Eventually, this BRDF model-based change detection algorithm defines the collection 5 MCD45A1 product which maps the location and approximate date of burned areas at 500 m spatial resolution (Roy, et al., 2005a; Roy, et al., 2008). Furthermore, the product describes information on snow and water events or missing MODIS observations as part of summary quality assessment information. The MCD45A1 product was re-projected to correspond with the Landsat UTM projection of each scene, and the product output pixel-dimension was retained at 500 m spatial resolution using nearest neighbour re-sampling.

#### *3.2.4: Land Cover product*

The recently completed national land cover (NLC) product was developed through joint research collaboration between CISR and the Agricultural Research Council (ARC). The NLC product was officially released to the public domain in October 2000 (hereafter 2000 NLC) and it was designed to encompass standardized baseline information on the current land cover for the whole of South Africa, Lesotho and Swaziland (Thompson, 1996; Fairbanks, et al., 2000). The data used to produce the 2000 NLC product were primarily based on geo-rectified single-date Landsat 5 TM imagery from the CSIR SAC acquired during the period 1994 to 1996 in order to classify land cover types that can be identified in a consistent and repetitive manner from the imagery (Thompson, 1996). Manual photo-interpretation techniques

coupled with expert knowledge of the geographic region being mapped were considered to aid interpretation of the land cover classification results derived from TM satellite imagery, which may include the temporal effects such as, burned vegetation, shadows imposed by clouds or relief and spectral similarities between land cover types.

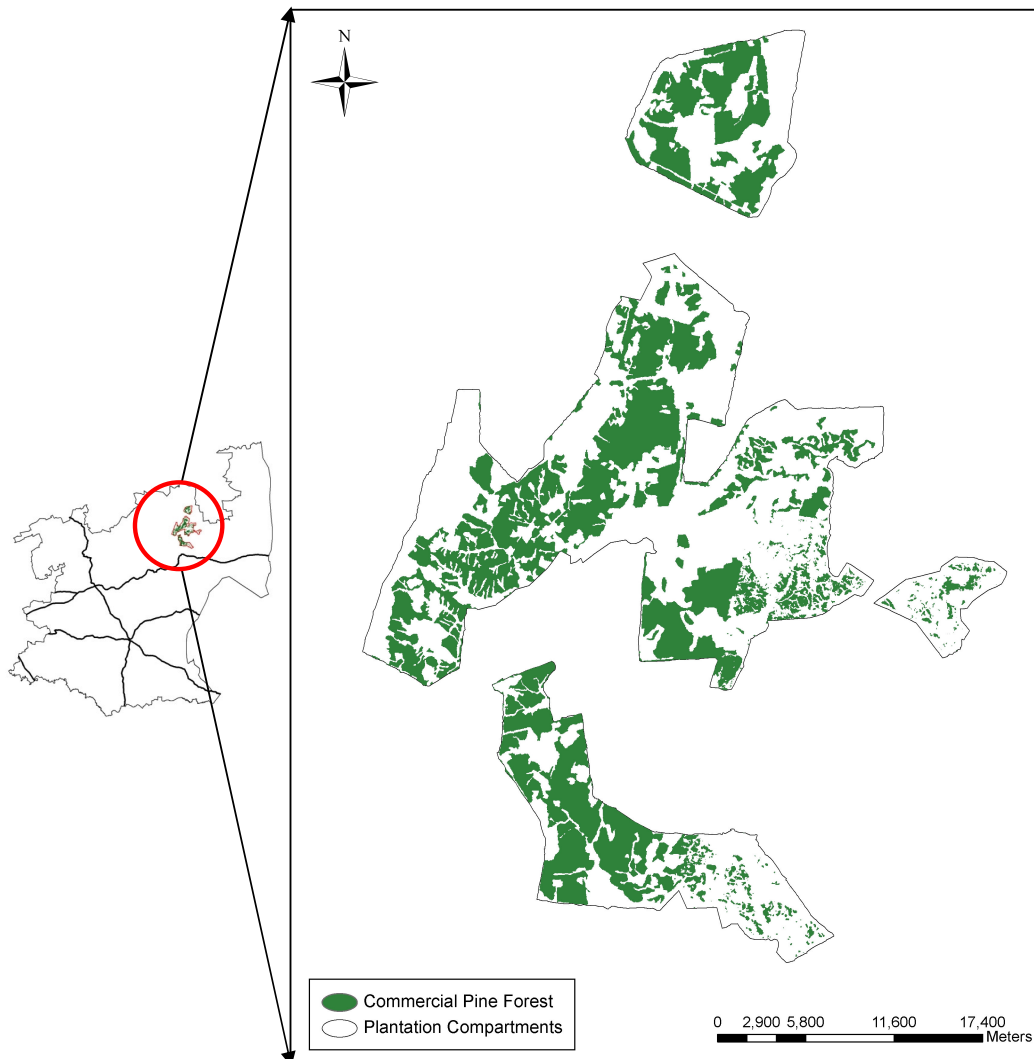


Figure 3.6: The manager-mapped plantation boundaries showing the approximate spatial location of the commercial pine forest in Sabie according to the 2000 NLC product.

The 2000 NLC product has a legend with 49 classes and adopts a standard physiognomic classification scheme (Edwards, 1983; Thompson, 1996) that uses clear, unambiguous terminology to ensure data standardization and comparability with national, continental or international classification systems such as those proposed by Edwards (Edwards, 1983), Food and Agriculture Organization (FAO) Africover (White, 1983; Anon, 1993) and, the United States Geological Survey (USGS) (Lindgren, 1985) land cover classification systems. Generally, the 2000 NLC product has an overall mapping accuracy of approximately 80%.

The 30 m spatial resolution 2000 NLC product defined in Geographic coordinates in tiff format was collected from the ARC and then, re-projected into registration with the UTM projection of the Sabie scene. This product facilitated the search for the commercial pine forest that is being used for timber production in the Sabie region. Figure 3.6 illustrate a spatial representation of the manager-mapped plantation boundaries provided by EnviroGIS and, were used to indicate the precise location of the commercial forest plantations investigated in this study. In particular, only the evergreen needle-leaf or pine forest class in the 2000 NLC product was considered when validating the MODIS burned area products in the Sabie region. While the overall commercial plantations cover an area totalling 71936.46 ha as reported by the manager-mapped plantation boundaries, only 28756.17 ha constitutes the commercial pine forest according the pine forest class in the 2000 NLC product.

### *3.2.5: The MODIS fire product*

The MODIS active fire product identifies, at 1 km spatial resolution one or more actively burning fires, including their approximate location and timing, at different spatio-temporal scales. Essentially, the product is defined by a contextual algorithm (Giglio, et al., 2003) that uses surface radiant temperatures derived from the MODIS thermal infrared spectral bands 21 (4.0  $\mu\text{m}$ ), 22 (4.0  $\mu\text{m}$ ), 31 (11.0  $\mu\text{m}$ ) and 32 (12.0  $\mu\text{m}$ ) for active fire detection and cloud masking, augmented by the red (0.65  $\mu\text{m}$ ), near (0.86  $\mu\text{m}$ ) and middle (2.1  $\mu\text{m}$ ) infrared MODIS bands to eliminate the occurrence of false detections. The algorithm examines individual pixels of the MODIS orbital swath width to identify potential fire pixels including pixels lacking valid data, and immediately classifies them as fire, non-fire, missing data, cloud,

water or unknown (Giglio, 2010b; Justice, et al., 2006). Processing continues on the MODIS swath to eliminate all unambiguous non-fire related pixels, while retaining potential fire pixels for a series of threshold trials. As a result, geo-located cloud-free neighbouring pixels in an expansible window are identified using an optimized nearest-neighbour search and used to estimate the radiometric signal of the potential fire pixel in the absence of fire and a background value (Giglio, et al., 2003). If background characterization is successful, the algorithm employs contextual threshold trials (Giglio, et al., 2003) to look for significant changes of interest in the radiation emitted at combustion temperatures compared to those of the non-fire background in order to perform relative fire detection. Furthermore, conditional steps are used to reject the errors of commission triggered by sun glint, desert boundaries, and errors in the water mask while retaining candidate fire pixels in the process to be assigned a class of fire (Giglio, et al., 2003). If the number of neighbouring pixels within the background window is inadequate, i.e. below a threshold of eight, background characterization will not succeed and as a result, those pixels are assigned a class of unknown.

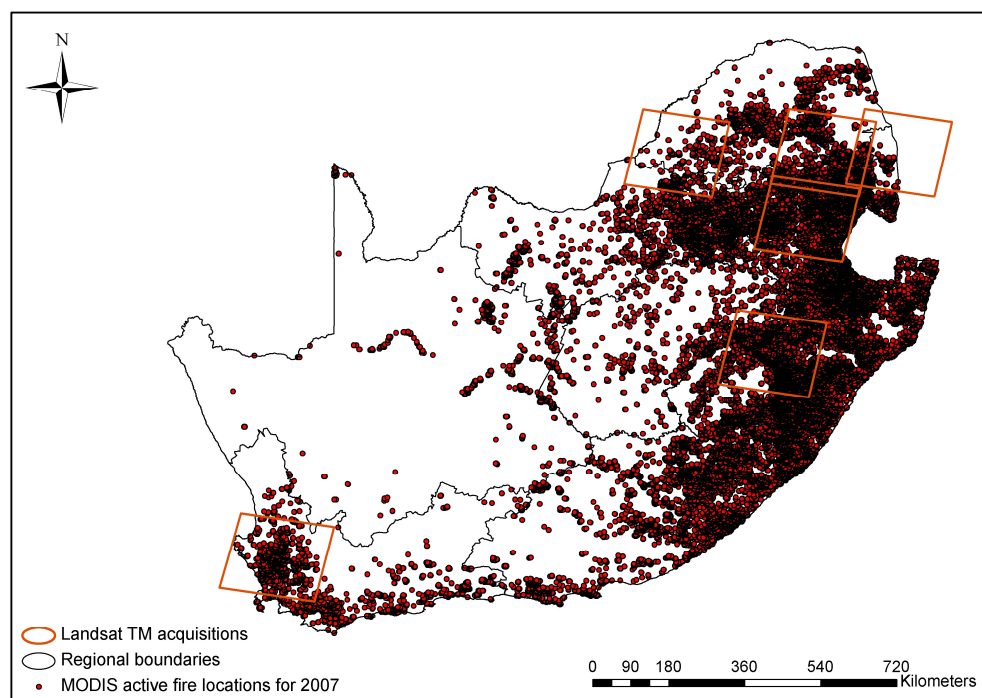


Figure 3.7: The MODIS active fire locations showing a comprehensive spatial representation of burning activity in South Africa for the year 2007. The Landsat TM acquisitions are superimposed on the fire locations to indicate the main prone

The algorithm can be expected to reliably detect both flaming and smoldering fires with coverage of approximately 50 m<sup>2</sup> (Giglio, 2010b, Justice, et al., 2003) but under relatively good satellite observing conditions. However, significant errors of omission may occur since the algorithm will only detect active fires at the time of satellite overpass, that are free from cloud or smoke obscuration, and on moderate homogenous land surfaces. In this study we used the MODIS fire pixel locations for the year 2007 downloaded from the MODIS Global Fire Web Mapping Services website (<http://maps.geog.umd.edu/firms>). These fire pixel locations were displayed on the map to provide a comprehensive spatial representation of burning activity in South Africa (Figure 3.7), and more important to guide the selection of the main fire prone areas across a variety of biomes. Each pixel location includes information about the band, fire radiative power (FRP), date, time, MODIS satellite, and the confidence value. However, information about cloud cover or missing data was not included but since these fire pixel locations were used for displaying purposes over a longer time interval (i.e., year 2007) they were considered more appropriate to use other than gridded fire products.

### *3.2.6: TRMM data*

The Tropical Rainfall Measuring Mission (TRMM) satellite has been measuring space-based rain estimates since November 1997 and provides worldwide distribution and variability of precipitation over the tropical and subtropical regions, where more than two-thirds of global precipitation occurs (Kummerow, et al., 1998; Kummerow, et al., 2000). The TRMM satellite improves on previous rainfall estimation techniques, such as climate prediction models and rain gauges. It aggregates rainfall information derived from the passive and active microwave sensors, together with sensors operating in the visible-infrared spectral region (Simpson, et al., 1988; Huffman, et al., 1995). TRMM has a low orbital inclination of 35° at an altitude of 402.5 km and visits each sampling area in the tropics about 15 times per day every 92.5 minutes (Kummerow, et al., 1998; Kummerow, et al., 2000). The low altitude of the TRMM satellite allows for the necessary horizontal resolution in the microwave observations whereas, the low inclination permits detection and documentation of the daily rainfall variation. There are three primary

rainfall sensors onboard the TRMM spacecraft that operate both separately and in conjunction to observe and obtain quantitative precipitation measurements.

These sensors include the TRMM Microwave Imager (TMI), the Precipitation Radar (PR) and, the Visible-Infrared Radiometer System (VIRS) (Kummerow, et al., 1998). Measurements made by the active PR instrument indicate a three dimensional structure of the vertical distribution and intensity of precipitation over the earth's surface encompassing a swath between 35° north and south latitudes.

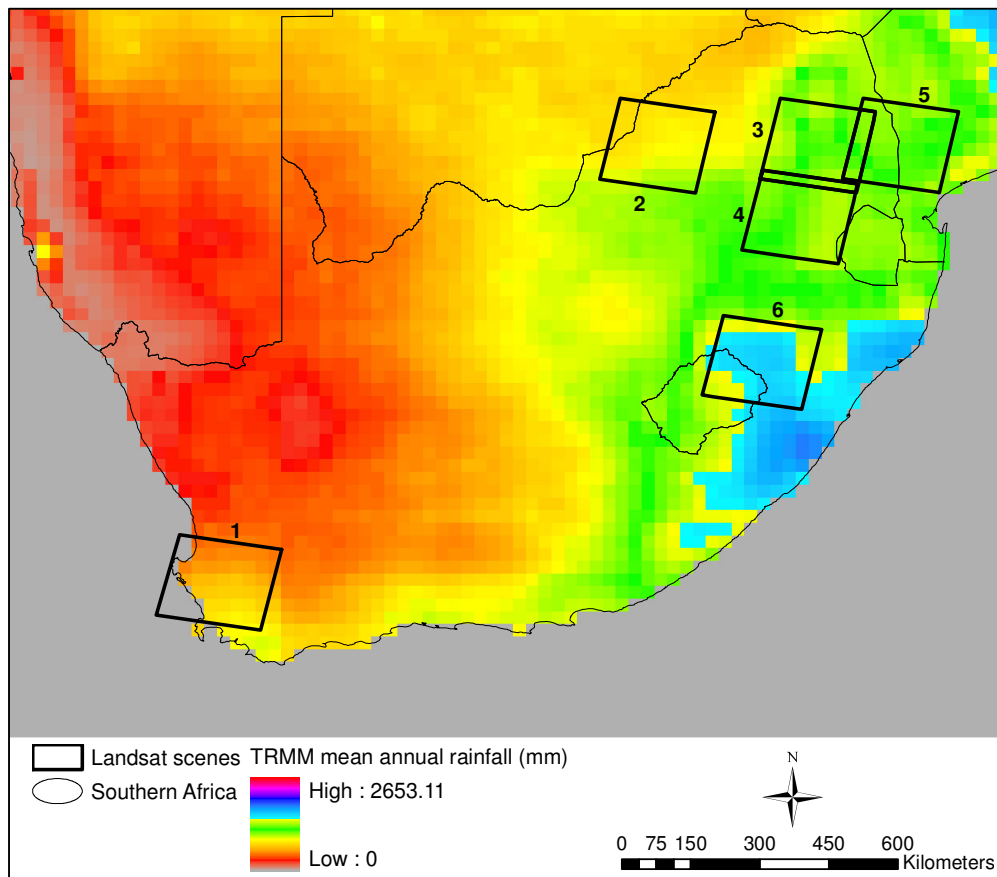


Figure 3.8: TRMM Mean Annual Rainfall (MAR) of southern Africa calculated from the monthly data from 1998 – 2007 in mm per year.

Table 3.3: The TRMM Mean Annual Rainfall estimates derived from the monthly data spanning the period 1998 – 2007 in mm.

#	Location	TM path/row	Mean Annual Rainfall estimates (mm)
1.	Western Cape	175/083	259.89 - 503.50
2.	Thabazimbi	171/077	458.15 - 623.51
3.	Sabie	169/077	568.67 - 810.11
4.	Middelburg	169/078	608.52 - 811.87
5.	Kruger	168/077	609.47 - 858.48
6.	Free State	169/080	814.32 - 974.81

Data gathered by passive TMI instrument are quantitative measurements of water vapour, cloud and water intensity including the extreme rates of tropical precipitation at a higher resolution. Both the PR and TMI are used as complementary sensors that can ameliorate the overall TRMM rainfall estimation accuracy (Kummerow, et al., 1998). On the other hand, the TRMM VIRS provides a connection between the TMI and PR rainfall estimates (Kummerow, et al., 1998). It estimates cloud-top temperature information for use in predicting the probability of rainfall. The combination of all three instruments provides improved space-based precipitation measurements throughout the Tropics.

The acquired TRMM gridded data set for southern Africa has a low spatial resolution of 0.25° and is defined in Geographic coordinates based on the WGS 1984 datum. This data set was considered to provide a spatio-temporal view of the mean annual rainfall distribution in South Africa spanning the period 1998 through 2007. More important, was to ensure that the distribution of TM scenes encompass regional climatic variations, which have an effect on the vegetation structure, rate of vegetation re-growth, canopy cover and moisture content (Figure 3.8 and the corresponding rainfall estimates in Table 3.3). Consequently, these present conditions that could constrain and/ or intensify the spread of fires particularly during the burning season, thus producing burned areas with different spatial patterns, which may influence the mapping accuracy of the moderate-resolution burned area products (Roy, et al., 2005b).

### 3.2.7: Vegetation map of South Africa, Lesotho and Swaziland

The 2006 Vegetation Map of South Africa, Lesotho and Swaziland (Mucina and Rutherford, 2006; Van der Merwe and Van Niekerk, 2007) was published by the South African National Biodiversity Institute (SANBI) and comprises the map produced at a scale of 1: 1,000,000 that encompasses the whole of South Africa, Lesotho and Swaziland including the Prince Edward islands.

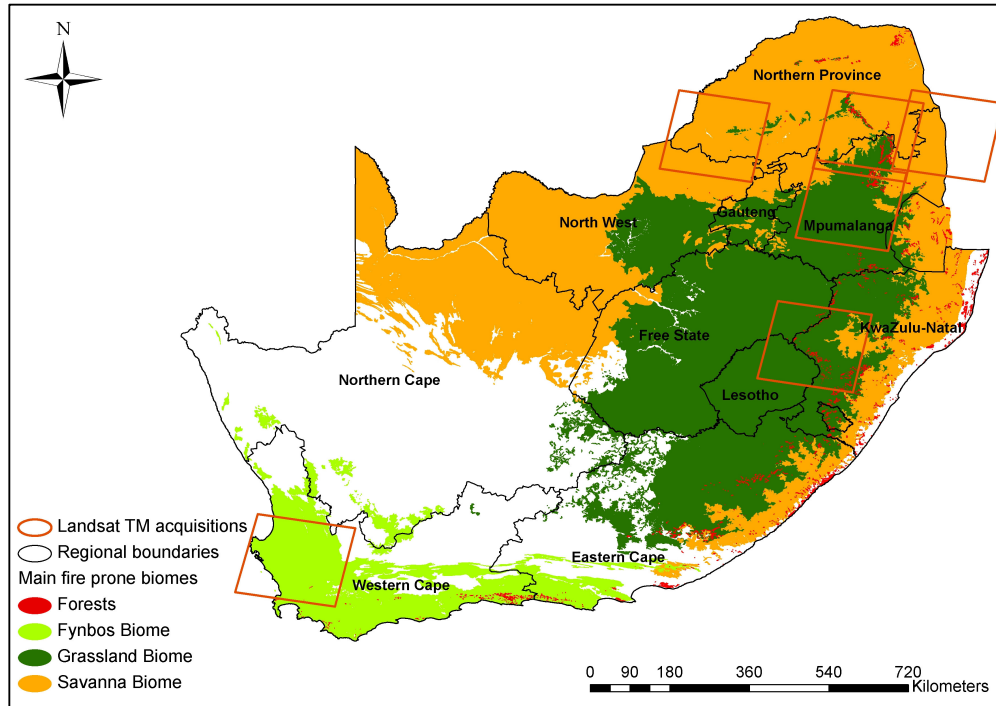


Figure 3.9: The biome map showing the Landsat TM acquisitions distributed across the main fire prone biome types in South Africa.

Compilation of the vegetation map was a joint mission between various organisations and scientists in capturing and delineating the region's vegetation and biome types. The map has a database with approximately 17, 796 digitized polygons and a legend describing 435 vegetation types (Van der Merwe and Van Niekerk, 2007). The legend adopts a floristic or habitat-based classification scheme (Acocks, 1988; Rutherford, 1997) that adequately differentiates the region's vegetation types. The map is defined in an Alber's equal area projection, based on the Hartebeesthoek '94



datum, to ensure positional accuracy (Van der Merwe and Van Niekerk, 2007). This map was considered in this study to provide a comprehensive and spatial detail of the region's biome types (Figure 3.9) and therefore, was used to guide selection of the main fire prone biomes in South Africa, namely, grassland, savanna, fynbos and pine forest.

### 3.3: Methodology

#### 3.3.1: Confusion Matrix

A classification error (pixel-level accuracy) assessment was conducted by using a confusion matrix to compute the Commission and Omission errors (hereafter  $C_e$  and  $O_e$ , respectively) present in the MODIS satellite-derived burned area products. This assessment is intended to describe the per-pixel detection accuracy of the burned area products particularly for local scale applications (Roy, et al., 2006; Roy, et al., 2009). A confusion matrix (sometimes also referred to as a contingency table or error matrix) provides the basis on which to both describe classification accuracy and characterize errors in a remotely-sensed product by comparison with the independent reference data (Congalton, et al., 1991; Stehman, et al., 1997). Table 3.4 shows an example of a typical confusion matrix, of which the column represents the independently-derived reference data ( $x_r$ ) and the row represents the remotely-sensed classification product ( $x_p$ ).

Table 3.4: Characteristics of a typical confusion matrix for a remotely-sensed product

Remotely-sensed product	Independent reference data	
	$x_p$	$x_r$
$x_p$	$x_{p,p}$	$x_{p,r}$
$x_r$	$x_{r,x_p}$	$x_{r,r}$

In this study, the remotely-sensed classification product represents the MODIS satellite-derived burned area products, namely MCD45A1 and BMBAP. On the matrix, the  $Ce$  in the evaluated product will be considered as the probability of a burned pixel detected by the product, but not present in the reference data which is denoted as  $x_{p,r}$ . Conversely, the  $Oe$  will be considered as the probability of a burned pixel present in the reference data, and not detected by the evaluated product which is denoted as  $x_{r,p}$ . The diagonal of the matrix (for example:  $x_{p,p}$  and  $x_{r,r}$ ) represent those pixels, which have been included in both the product and the reference data (also referred to as the correctly classified pixels). Therefore, the  $Ce$  and  $Oe$  are derived using the following expressions:

$$1 - Ce = \frac{x_{p,p}}{x_{p,p} + x_{p,r}} \quad (2)$$

$$1 - Oe = \frac{x_{r,r}}{x_{r,r} + x_{r,p}} \quad (3)$$

The expressions shown in (2) and (3) were derived for each study site and summarized in the cells of the confusion matrix by comparing the 500 m MODIS burned area products (MCD45A1 and BMBAP, respectively) with 30 m Landsat TM independently-derived reference data. Additionally, the unmapped areas or areas that could not be interpreted (which included cloud cover, shadows imposed by relief or clouds, and ambiguous spectral features) were also statistically reported in order to minimize biases in the summarized burned area statistics (Roy, et al., 2008). Consequently, the more concise notation is adopted for legibility of the expressions shown in (2) and (3) during classification accuracy assessment of the MCD45A1 and BMBAP satellite products as follows:

$$1 - Ce = \frac{I_{Modis} + I_{Landsat}}{I_{All\_Modis}} \quad (4)$$

$$1 - Oe = \frac{I_{Modis} + I_{Landsat}}{I_{All\_Landsat}} \quad (5)$$

where  $I_{\text{Modis}} + I_{\text{Landsat}}$  represents the intersection of MODIS and Landsat burned area at 30 m resolution,  $I_{\text{All\_Modis}}$  are the pixels at 30 m resolution of MODIS burned area and,  $I_{\text{All\_Landsat}}$  are the pixels at 30 m resolution of Landsat burned area.

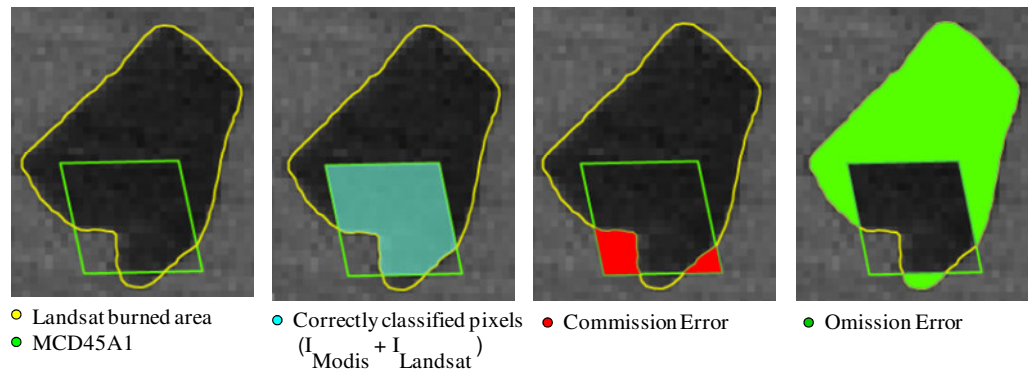


Figure 3.10: Comparison of Landsat (interpreted) burned-area reference data and the MCD45A1 product to derive the  $Ce$  and  $Oe$  by use of a confusion matrix.

This accuracy assessment evaluates entirely the 500 m MODIS pixels at a spatial resolution of 30 m as either burned or unburned. Figure 3.10 illustrates the pixel-level accuracy assessment used to derive the  $Ce$  and  $Oe$  in the burned area products using Landsat interpreted burned-area reference data, while taking the MCD45A1 product as an example. The reference data and product being evaluated are both in vector format superimposed on a Landsat grey-scale temporal difference image of a particular area in the Western Cape region. As a result, when the burned area product does not map the same extent of area burned as the reference data (Landsat interpreted burned area), a  $Ce$  and/or  $Oe$  is introduced in the product being evaluated. This is because, the typical use of a confusion matrix assumes that the data being compared (reference data and the classified product) have the same spatial resolution. Consequently, this is often not the case especially when evaluating low and moderate spatial resolution data remotely-sensed by, for example MODIS, NOAA-AVHRR, or SPOT-VGT (Boschetti, et al., 2004).

Additionally, there are small burns covering a fraction of the MODIS-pixel according to the reference data, as well as complex burn shapes having little unburned gaps between the shapes. Often this leads to numerous inclusions of the unburned land surface (Landsat 30 m pixels) and therefore, contributes to the  $C_e$  in the product. On the other hand, there could be small (i.e. burns that correspond to approximately 10% or less of a MODIS-pixel) and low combustion completeness burns (Roy and Landmann, 2005c; Sa, et al., 2007), which may not be reliably identified in the evaluated product. This could be due to limitations arising from the inherent difference in the spatial resolutions of the remotely-sensed MODIS data and/or possible misclassifications during several phases of the classification algorithm. The confusion matrix does not take cognisance of any of such issues mentioned above and therefore, the accuracy measures derived from this assessment alone may not adequately describe classification errors (Foody, 1996; Binaghi, et al., 1999; Boschetti, et al., 2004) in the evaluated MODIS burned area products.

Table 3.5: Classification accuracy assessment of the MODIS burned area products based on 500 m MODIS pixels that are at least 50% and 75% burned according to Landsat.

		MODIS product	
		Burned	Unburned
Reference data	Burned	TP	FN
	Unburned	FP	TN

Supplementary to this matter, Table 3.5 present a classification accuracy assessment of the burned area products based on 500 m MODIS pixels that are  $\geq 50\%$  and  $\geq 75\%$  burned (according to Landsat interpreted burned area). In Table 3.5 TP and FN represent the true positives and false negatives furthermore; FP and TN represent the false positives and true negatives accordingly (Boschetti, et al., 2004). Note the terms positive and negative in this study denote burned and

unburned, correspondingly. In order to derive the accuracy indices, the table was interpreted as follows:

- i. TP cognises the proportion of truly burned pixels that were correctly classified as burned (flagged “1”) in the product simply expressed as TP / (TP + FN), and describe the producer’s accuracy;
- ii. FN cognises the proportion of truly burned pixels that were incorrectly classified as unburned (flagged “0”) in the product expressed as FN / (FN + TP) and represent *Oe*, whereas;
- iii. TN cognises the proportion of truly unburned pixels that were classified correctly as unburned (flagged “0”) in the product expressed as TN / (TN + FP), and describe the user’s accuracy and;
- iv. FP cognises the proportion of truly unburned pixels that were incorrectly classified as burned (flagged “1”) in the product and represent *Ce*.

Moreover, these expressions can be formulated as follows (for MODIS pixels with fractional burned areas  $\geq 50\%$  or  $\geq 75\%$ ):

$$Prod's_{Acc} = \frac{MODIS\_product\_pixels\_ \geq 50 / 75\% \_ burned \_ (flagged \_ "1" )}{MODIS\_reference\_pixels\_ \geq 50 / 75\% \_ burned \_ according \_ to \_ Landsat} \quad (6)$$

$$Oe = \frac{MODIS\_product\_pixels\_ \geq 50 / 75\% \_ burned \_ (flagged \_ "0" )}{MODIS\_reference\_pixels\_ \geq 50 / 75\% \_ burned \_ according \_ to \_ Landsat} \quad (7)$$

$$User's_{Acc} = \frac{MODIS\_product\_pixels\_ < 50 / 75\% \_ burned \_ (flagged \_ "0" )}{MODIS\_reference\_pixels\_ < 50 / 75\% \_ burned \_ according \_ to \_ Landsat} \quad (8)$$

$$Ce = \frac{MODIS\_product\_pixels\_ < 50 / 75\% \_ burned \_ (flagged \_ "1" )}{MODIS\_reference\_pixels\_ < 50 / 75\% \_ burned \_ according \_ to \_ Landsat} \quad (9)$$

This implies a MODIS pixel is considered as burned only if  $\geq 50\%/75\%$  of the pixel is burned (according to Landsat interpreted burned area). Consequently, this is expected to minimize the inherent biases in the accuracy indices derived for both products by means of the confusion matrix (i.e. see equations (4) and (5)) as, the moderate-resolution burned area products could be expected to reliably detect burned

areas that correspond to at least 50% (~13 ha) of a 500 m MODIS pixel (e.g. Giglio, et al., 2009). However, this may vary across vegetation types and the degree of burned area spectral reflectance, as for some sub-pixel burned area sizes <20% of a 500 m MODIS pixel may be reasonably detected (Eva and Lambin, 1998b). Such burns (below our specified threshold of 50%/75%) are recorded as unburned during the assessment based on MODIS pixels.

### 3.3.2: *Linear regression analysis*

Regression analysis is a very useful statistical technique that is widely and frequently utilized for describing the relationships between two or more variables (that assume linear dependence) (Montgomery and Runger, 2007). In this study, a bivariate regression technique was used, which considers a single independent variable  $x$  and a dependent variable  $Y$ . The usual assumption is that a true relationship between  $Y$  and  $x$  is a straight line and that the observation of  $Y$  at each level of  $x$  is a random variable. Therefore the expected value of  $Y$  for each value of  $x$  is described using the linear regression model as follows:

$$Y = \beta_0 + \beta_1 x \quad (10)$$

The intercept  $\beta_0$  and the slope  $\beta_1$  shown in (10) are unknown regression coefficients that must be estimated from sample data (Montgomery and Runger, 2007). The intercept,  $\beta_0$ , can be interpreted as the estimated value of  $Y$  where the regression line cuts the vertical axis whereas, the estimated slope,  $\beta_1$ , of the regression line can be interpreted as the amount that  $Y$  changes as  $x$  changes by a unit (Walford, 1995; Montgomery and Runger, 2007). Usually, when analysing real-world problems a perfect linear correlation between the measured variables is unlikely to occur however, the challenge is to find the best possible fit of the regression line between the scattered points. Therefore, the variability of the observed values of  $Y$  for a given value of  $x$  must be ascertained, including the extent to which the straight line approximates to a scatter of data points. In this instance, it is necessary to consider the standard error of the estimate described using Equation (11) which represents the standard deviation of the vertical differences of the scattered data points from the regression line, as a result of variability in  $Y$  (Walford, 1995).

$$\sigma_{x,y} = \sqrt{\frac{\sum Y^2 - \beta_0 \sum Y - \beta_1 \sum x \sum Y}{n-2}} \quad (11)$$

The resulting statistic  $\sigma_{x,y}$  summarizes the discrepancies in the samples to be compared, with respect to the extent to which their points are distributed about the regression line (Walford, 1995) such that, a small value of  $\sigma$  would suggest that the observed values of Y lie close to the regression line. Conversely, a large value of  $\sigma$  denotes deviation of the observed values of Y from the regression line.

In this study, simple linear regression approach was used to assess the linkage between burned area proportion estimates derived from the MODIS burned area products and Landsat TM. Generally, this analysis is intended for users who are interested in regional scale applications (or at scales larger than the product pixel size) such as, calculation of gas and aerosol emissions and the quantities of biomass burned (Korontzi, et al., 2003; Tansey, et al., 2004; Roy and Boschetti, 2009).

A continuous grid of 2.5 km x 2.5 km was selected and overlaid onto each study site. Initially a 5 km grid was envisaged for this analysis. The aim of such specification was to provide comparability of burned area estimates from the MODIS burned area product, particularly the MCD45A1, with those reported by Roy and Boschetti (2009). While Roy and Boschetti (2009) considered the entire Landsat scene as their mapped region, in the study reported here, a fraction of the extent of the entire Landsat image size area was considered as the mapped region. Therefore, using a 5 km grid in this study was thought to be substantially larger and could as a result; lessen the number of grids containing burned area proportions in both the product and Landsat reference data. This would result to a few observations around the regression line and thereby yielding an inflated Pearson's correlation coefficient ( $R^2$ ) (Openshaw, 1984; Boschetti, et al., 2006).

Generally, in addition to grid cell size, the scale (regional, continental or global) at which the study is conducted and the spatial pattern of the burned areas could affect statistical analysis results of the landscape (Sa, et al., 2007). Consequently, a 2.5 km quadrant size (containing estimated area burned in both the MODIS burned area product and Landsat data) was considered. The selected quadrants were then used to compute the proportions of estimated area burned by the

product and the proportions of estimated area burned by the Landsat interpreted burned area.

### 3.3.3: *Sub-MODIS pixel burned area analysis*

The influence of fractional burned area within a MODIS pixel on the probability of detection by each product was assessed quantitatively. In the polygon-based analysis considered here, a 500 m MODIS reference grid was created and overlaid onto the Landsat interpreted burned areas (Figure 3.11). These grids were then utilized to compute proportions of burned area within each 500 m grid cell according to the Landsat data. The computed proportions were subsequently categorized into four classes of  $\leq 25\%$  (6.25 ha), 25-50% (6.25-12.5 ha), 50-75% (12.5-18.75 ha) and  $\geq 75\%$  (18.75 ha) of a MODIS pixel burned according to Landsat TM data. The moderate-resolution burned area products were analysed and compared across each class in order to determine their probability of detection for the different sizes of burned area fractions across the biomes. The probability of detection was computed from Equation (12):

$$Probability\ of\ Detection = \frac{Product_{b,i}}{MODISRef_{b,i}} \quad (12)$$

Where  $b$  represents the total number of the identified burned area proportions, and  $i$  represent any of the four classes stated above. The resulting expression should demonstrate how the probability of burned area identification within a 500 m MODIS pixel increases with sub-MODIS pixel burned area size; thereby suggesting possible detection probabilities upon which the MCD45A1 and BMBAP products can be expected to map the burned areas. Similar analysis has been conducted by Sa, et al. (2007) whereby, Landsat derived burned area proportions were compared with the spectral separability values across 15 x 15 km grid cells. In the analysis reported by Sa, et al. (2007), each quadrant had a Landsat-derived burned area proportion and a spectral separability value (computed from 500m MODIS burn sensitive bands 2, 5 and 6). These values were plotted to examine the relationship between the size distribution of burned areas and their spectral detectability across the 15 x 15 km



quadrants. In this way, the influence of burned area spatial patterns on the spectral detectability of burned areas was assessed.

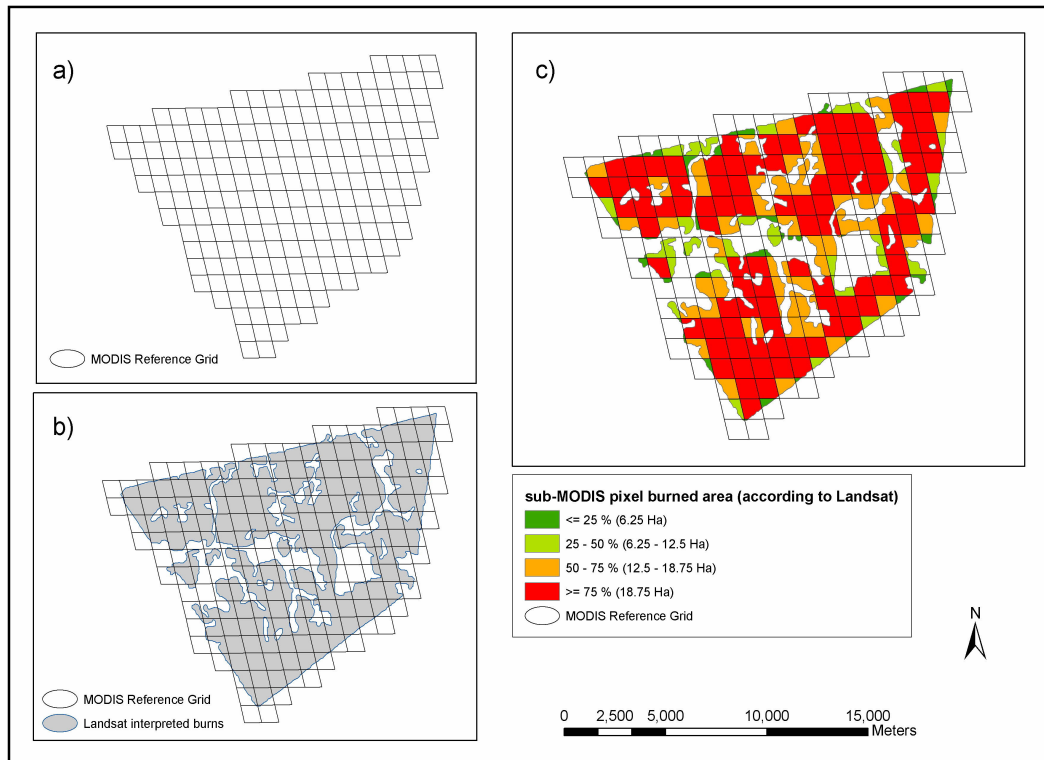


Figure 3.11: The 500 m MODIS reference grids used to compute fractional burned areas corresponding to Landsat TM interpreted burns.

The difference between the present sub-pixel analysis and that reported by Sa, et al. (2007) is that, this study focuses on the analysis of burned area fractions derived within the 500 m MODIS pixels. The purpose of this approach is to depict the kind of the relationship between the proportions of burned area in a 500 m MODIS pixel (derived according to Landsat TM) and their detection probability by the MCD45A1 and BMBAP products. Furthermore, this relationship could reveal patterns that could be used to further understand the extent to which fractional burned area influence the detection accuracy of each burned area product across the different biomes.

#### *3.3.4: Concluding remarks*

This chapter explained three important phases required to determine product accuracy. The first phase described the data used to guide the selection of the validation sites encompassing grassland, savanna, fynbos, and pine forest biomes. The second phase presented the adopted, internationally recognized burned-area validation protocol to produce high-resolution independent reference data for all sites. In the last phase, the three product accuracy reporting procedures were explained including illustrations to indicate their advantages and disadvantages. Furthermore, recent validation results of the MCD45A1 (Roy and Boschetti, 2009) and BMBAP (Giglio, et al., 2009) did not take cognisance of fractional burned area. Therefore, in this study sub-MODIS pixel burned area is considered as an additional analysis to quantify the influence of fractional burned area on the probability of detection by each product.

## CHAPTER 4

### RESULTS AND DISCUSSION

#### 4.1: Introduction

This chapter presents the validation results of the MODIS burned area products. Differences in the computed accuracies of the burned area products are analysed and compared based on biome type, spectral characteristics and the size and spatial distribution of the burned areas. In order to carry out burned area validation analyses using satellite data, an extensive and labour intensive on-screen digitizing was performed to produce high resolution burned area reference data (this included deriving features that could not be interpreted such as clouds and cloud shadows).

#### 4.2: Classification error assessment

Table 4.1 present the per-pixel level accuracy assessment results for the MCD45A1 and BMBAP products across all the six validation sites. The percent area mapped as burned by the Landsat independently-derived reference data and by the MODIS burned area products are presented in the fifth and sixth columns, respectively. Table 4.1 illustrates that the Landsat reference data mapped a greater percent of area burned than the MODIS burned area products for all sites except in Sabie (for the BMBAP product) and in the Free State (for the MCD45A1 product). The depicted exceptions could be attributed to the spatial complexity, size distribution and spectral signatures of burned areas at the sites. This implies that small areas mapped as burned, e.g. <10 ha (which partly cover the extent of a 500 m MODIS pixel), leaves the remaining fraction within the MODIS pixel unmapped, resulting in numerous inclusions of the unburned Landsat 30 m pixels inside a 500 x 500 m block (e.g., see Figure 4.1). In addition, the complexity of the burn shapes (as defined by the reference data) often results in limited unburned gaps in the MODIS pixel which are mapped as burned in the moderate resolution burned area products but not in the reference data.

Table 4.1: Classification error assessment validation results based on the Official MODIS burned area product (MCD45A1) (highlighted in grey to aid interpretation) and the Backup MODIS burned area product (BMBAP) compared with Landsat TM burned area at 30 m resolution.

Biome	Site, Landsat path/row	Landsat dates	Product	Landsat Burned (%)	Product Burned (%)	Unmapped Area (%)	Oe (%)	Ce (%)
Savanna	Southern Kruger 168/077	11/8/07 27/8/07	MCD45A1	3.22	2.8	0	40.38	31.35
			BMBAP		2.33		40.39	17.68
Grassland	Middelburg 169/078	18/8/07 3/9/07	MCD45A1	2.63	1.42	0.38	62.87	31.52
			BMBAP		1.21		65.79	25.64
Fynbos	Western Cape 175/083	17/2/07 6/4/07	MCD45A1	10.28	2.98	2.75	77.25	21.47
			BMBAP		2.21		82.85	18.47
Pine forest	Sabie 169/077	15/6/07 18/8/07	MCD45A1	26.72	13.22	1.93	62.14	23.5
			BMBAP		36.65		14.63	37.76
Grassland	Free State 169/080	18/8/07 3/9/07	MCD45A1	5.18	5.71	0.01	17.45	25.02
			BMBAP		5.09		22.86	21.45
Savanna	Thabazimbi 171/077	15/7/07 16/8/07	MCD45A1	1.38	0.50	0.01	67.25	9.84
			BMBAP		0.50		67.40	10.84

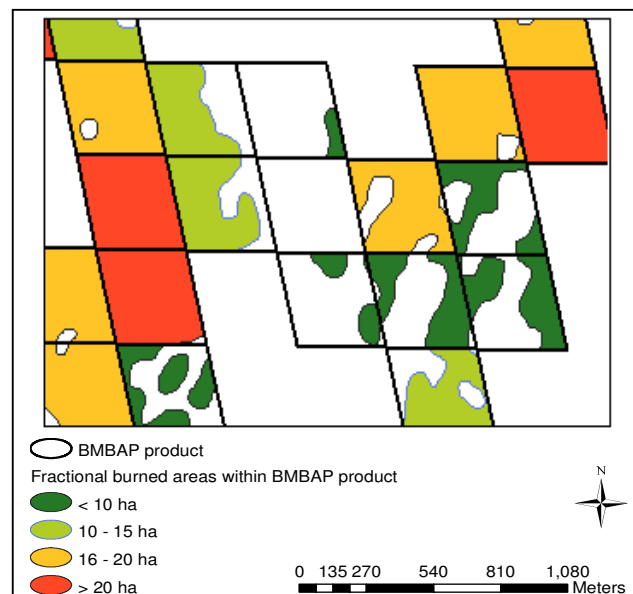


Figure 4.1: Burned areas mapped with Landsat within 500 m MODIS pixels identified as burned by the BMBAP product in the Free State (Grassland biome).

The  $C_e$  and  $O_e$  depicted in the last two columns of Table 4.1 describe the classification error as derived from the burned area products when compared with Landsat TM burned area at 30 m resolution. These results demonstrate that both products had lower  $C_e$  than  $O_e$ , which corroborates with the validation results of the MODIS burned area product reported by Roy and Boschetti (2009) and Loboda and Csiszar (2004). This outcome could generally be explained by the fact that the burned area product producers often assume that preference from the product users will be given to a classified image with lower  $C_e$  than  $O_e$  as, certain product users would wish to avoid greater costs associated with visiting falsely identified burned areas (Boschetti, et al., 2004; Trigg and Roy, 2007; Roy and Boschetti, 2009). Contrary to this view, there could be greater cost associated to  $O_e$  than  $C_e$  for some users of the burned area products. This effect may occur when the product producers apply less stringent reflectance thresholds (Roy, et al., 2005; Giglio, et al., 2009) to detect change, which would potentially minimize  $O_e$  at the cost of maximizing false detections of the true burned areas (Bastarrika, et al., 2011). However, the user's preference to a classified image with lower  $O_e$  than  $C_e$  could be influenced by the 500 m inherent spatial resolution of the MODIS reflective bands which may constrain the detection of small burned areas.

#### *4.2.1: Analysis of the response of $O_e$ to variations in burned area sizes*

In order to assess the relationship between  $O_e$  and burned area sizes, the changes in  $O_e$  relative to the burned area sizes of the MCD45A1 and BMBPA products across the selected biomes in the present study are depicted in Figure 4.2 – 4.5. The logarithmic curves are fitted to the  $O_e$  derived in the products. As depicted in the figures, the  $O_e$  and burned area sizes of the products exhibit a non-linear relationship across some of the selected biomes. In order to measure the sensitivity of  $O_e$  to the variations in burned areas sizes across the MCD45A1 and BMBAP products, a rate of change of  $O_e$  to the burned area size is computed based on the inter-quartile range. In this analysis, the inter-quartile range is selected as a measure of the sensitivity due to the few sample points (a  $1\sigma$  or  $2\sigma$ -level could be a natural choice if the sample sizes were large) as well as ensuring that only the middle 50% of the sample data points are considered (this helps to eliminate data points to the extreme region that

could be biased possibly due to systematic errors). These values are presented in Table 4.2.

Firstly, in order for the products to resolve a burned area in the grassland biome (Free State) at the first-quartile (Q1) threshold (this corresponds to  $O_e$  of 31%/10% for MCD45A1/BMBAP) the burned area size ought to exceed 188 ha/690 ha (Table 4.2). This implies that, in the grassland biome, the MCD45A1 product has the ability to resolve small burned areas compared to the BMBAP. This corroborates with the different  $R^2$  values (Figure 4.2). The intrinsic variability of  $O_e$  due to variations in the burned area sizes in the grassland biome is captured in the sensitivity values of 0.29/0.08 of the MCD45A1/BMBAP products respectively (Table 4.2). This suggests that the  $O_e$  derived from the MCD45A1 product in the grassland biome is more sensitive to variations in the burned area sizes compared to BMBAP product. Similarly, the MCD45A1 product had a higher resolve than the BMBAP product in the savanna (Thabazimbi) and fynbos (Western Cape) biomes i.e. at a Q1 threshold equivalent to  $O_e$  (MCD45A1/BMBAP) of 28%/24% and 38%/27%, would require the minimum burned areas of at least 775 ha/1009 ha (savanna) and 390 ha/750 ha (fynbos) respectively. This corresponds to the MCD45A1/BMBAP sensitivity values of 0.06/0.04 and 0.11/0.06 as reported in Table 4.2. In contrast, the minimum burned area resolvable in the forest biome (Sabie) ought to be at least 2205 ha/1095 ha at a threshold of Q1 (an  $O_e$  of 26%/16% for the MCD45A1/BMBAP). As depicted in Table 4.2, the variability of  $O_e$  of the BMBAP product is more sensitive to variations in the burned area sizes in the forest biome (Sabie) i.e. BMBAP product has a higher sensitivity value of 0.05 compared to the MCD45A1 product (0.02). This is in agreement with the high  $R^2$  value ( $\sim 0.3$ ) of BMBAP relative to the MCD45A1  $R^2$  value of  $\sim 0.1$  (Figure 4.5)

Table 4.2: Inter-quartile range used to measure the sensitivity of  $O_e$  in the products to the variations in burned area sizes. A rate of change of  $O_e$  to the burned area size is computed based on the inter-quartile range.

Site	Quartiles (%)				MCD45A1 (ha)		BMBAP (ha)		Rate of Change $\Delta$	
	Q1_MCD45A1	Q3_MCD45A1	Q1_BMBAP	Q3_BMBAP	Q1_Area	Q3_Area	Q1_Area	Q3_Area	MCD45A1	BMBAP
Thabazimbi	28	72	24	61	775	50	1009	105	0.06	0.04
Free State	31	79	10	61	188	21	690	38	0.29	0.08
Middelburg	22	75	13	42	380	23	770	143	0.15	0.05
Sabie	26	66	16	71	2205	6	1095	4	0.02	0.05
W_Cape	38	77	27	74	390	21	750	22	0.11	0.06

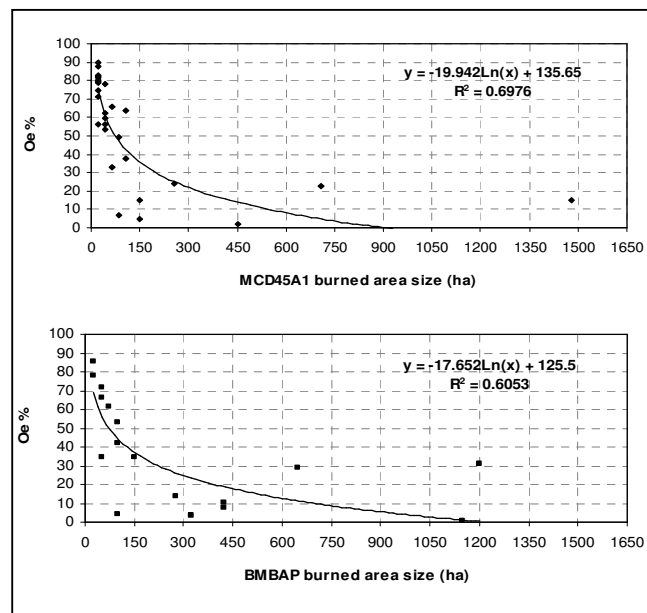


Figure 4.2: Changes in the  $O_e$  relative to the burned area sizes of the MCD45A1 and BMBAP products in Free State (grassland). The  $O_e$  was derived for the MODIS burned areas corresponding to the individual Landsat burned areas).

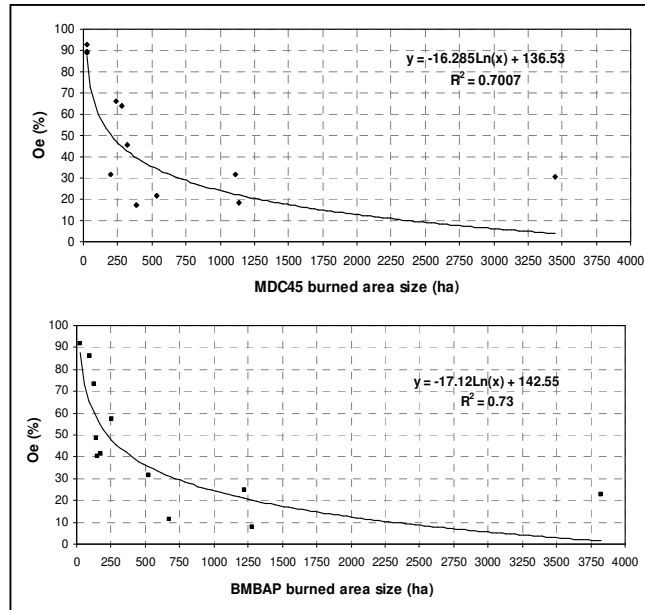


Figure 4.3: Changes in the  $Oe$  relative to the burned area sizes of the MCD45A1 and BMBAP products in Thabazimbi (savanna). The  $Oe$  was derived for the MODIS burned areas corresponding to the individual Landsat burned areas).

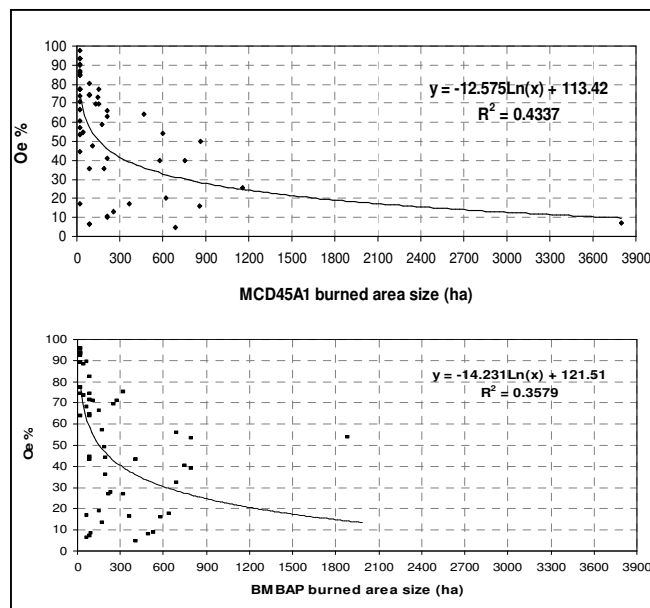


Figure 4.4: Changes in the  $Oe$  relative to the burned area sizes of the MCD45A1 and BMBAP products in Western Cape (fynbos). The  $Oe$  was derived for the MODIS burned areas corresponding to the individual Landsat burned areas).



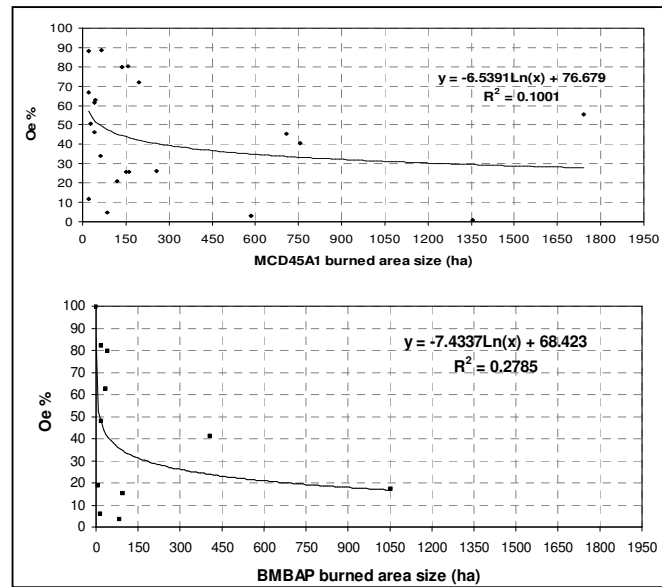


Figure 4.5: Changes in the *Oe* relative to the burned area sizes of the MCD45A1 and BMBAP products in Sabie (pine forest). The *Oe* was derived for the MODIS burned areas corresponding to the individual Landsat burned areas).

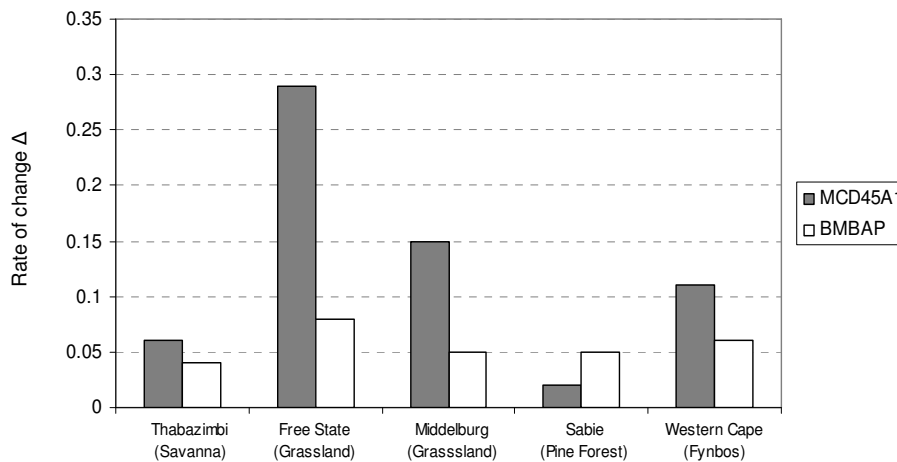


Figure 4.6: A measure of variability of *Oe* due to changes in burned area size for the MCD45A1 and BMBAP product.

A summary of the sensitivity of *Oe* to changes in the burned area sizes across the selected biomes considered in the present analysis is illustrated in Figure 4.6. The *Oe* computed from the MCD45A1 product is more sensitive and therefore could be

highly influenced by changes in the burned area sizes across the selected biomes, except in the pine forest biome. The Kruger (savanna - not shown) and Middelburg (grassland) biomes are not described here because; the products perform similarly to the selected-corresponding biomes. Additionally, the pattern revealed by the products (Figure 4.6) corroborates with the derived  $O_e$  values (shown in Table 4.1) affirming that the MCD45A1 product has lower  $O_e$  than BMBAP product, notwithstanding the pine forest biome. Furthermore, these discrepancies in product performance across the biomes are discussed in subsequent sections of this chapter.

#### *4.2.2: Comparison of product performance*

In this subsection, a spatial view and product comparison of the burned area products across all the validation sites is presented. The entire subsection comprises of supporting maps for the derived accuracy metrics presented in Table 4.1, and show the overall mapping and comparison of the products, in terms of  $C_e$  and  $O_e$ .

##### *4.2.2.1: Savanna*

Fire is a crucial factor in the savanna biome partly as a result of its dominant grassy layer coupled with a mixture of shrubs and woodland, and the mean annual rainfall variation of approximately 458.15 - 858.48 mm, which leads to the accumulation of sufficient biomass fuel to produce large fires (Scholes, et al., 1996; Korontzi, et al., 2003). Consequently, these fires give rise to spectrally distinct, transient burned areas spanning small, medium and largely sized burns (0.36 - 120 ha and 120 -  $\geq$ 1000 ha); thereby exhibiting favourable conditions for detection in the burned area products.

Figure 4.7 show the burned area mapping performance of the products in the savanna biome over southern Kruger. The products performed relatively similar by mapping 59.62% and 59.61% (for MCD45A1 and BMBAP respectively) of area burned from the total Landsat burned area of 4098.55 ha (assumed to be ground truth). This means ~60% of the true burned area was detected as burned in the products (i.e. describes the producer's accuracy). In southern Kruger, neither product showed marked differences in  $O_e$  (Table 4.1).

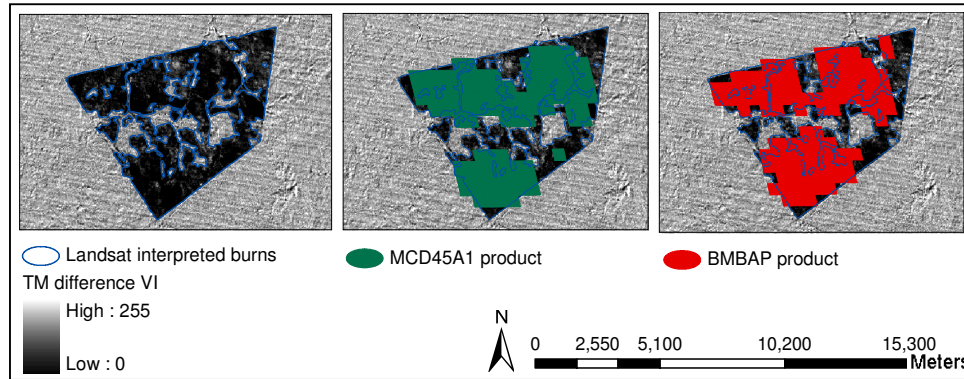


Figure 4.7: Illustration of the burned areas in southern Kruger reveals strong spectral contrast (i.e. appear dark) and complex shapes.

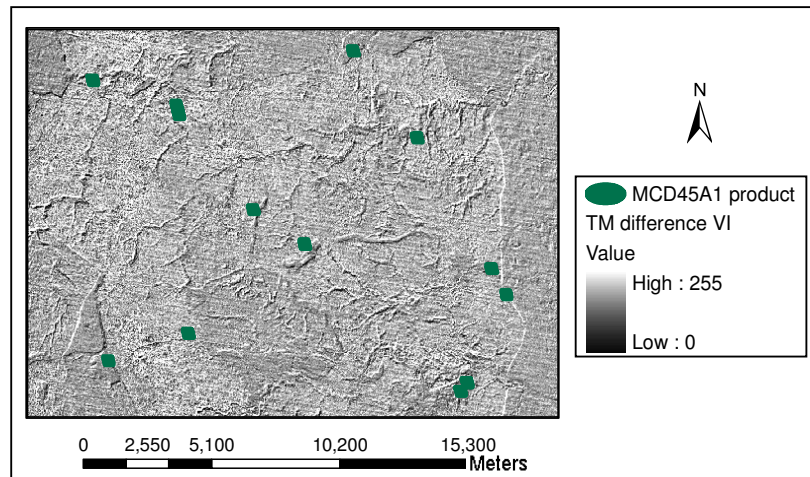


Figure 4.8: *C<sub>e</sub>* in the MCD45A1 product over southern Kruger National Park in the absence of any burns.

The MCD45A1 product appears to classify a higher proportion (~2.8% which corresponds to 3558.42 ha) of the savanna area as burned than the BMBAP product (~2.33% which corresponds to 2966.58 ha). For example, when analysing the results by burned area size in southern Kruger, the MCD45A1 product revealed a higher detection (~19%) in the case of small burned area sizes <50 ha than the BMBAP product (~13%). Whereas, for burned area sizes from 50-100 ha and >100 ha both

MODIS products reported slightly higher burned area detection of 66.7% and 80% accordingly.

The observed differences in *Oe* could be attributed to the presence of tree cover and the spectral mixture of the burned-unburned area signal, which may have presented different reflectance circumstances for the burned area mapping approaches used to define the products (Roy, et al., 2005a; Giglio, et al., 2009). More alarming are the differences in *Ce* (~14%) between the products particularly in the southern Kruger site. Figure 4.8 illustrates the falsely identified burned areas in the MCD45A1 product that constitutes 438.87 ha (12.3% of the total area mapped by MCD45A1) over southern Kruger National park (even though the TM difference VI image did not highlight any presence of area burned). This could be ascribed to the potentially confusing spectral changes in the area arising from, for example, the underlying reflective bright and dark soil that reduces the reflectance in the wavelengths used to detect the burned areas (Roy, et al., 2005a). Another contributing factor in *Ce* revealed in both products could be from the occurrence of small unburned areas located inside large burns and the little unburned gaps between the interpreted burned areas (characterized by complex shapes) that appeared to be classified as burned in the products (e.g., Figure 4.7, Figure 4.9 and Figure 4.10). In particular, the BMBAP gave the highest user's accuracy (lowest *Ce* of 17.68%) for the burned savanna in southern Kruger whereas, the MCD45A1 revealed the highest user's accuracy (lowest *Ce* of 9.84%) in Thabazimbi characterized by the same biome.

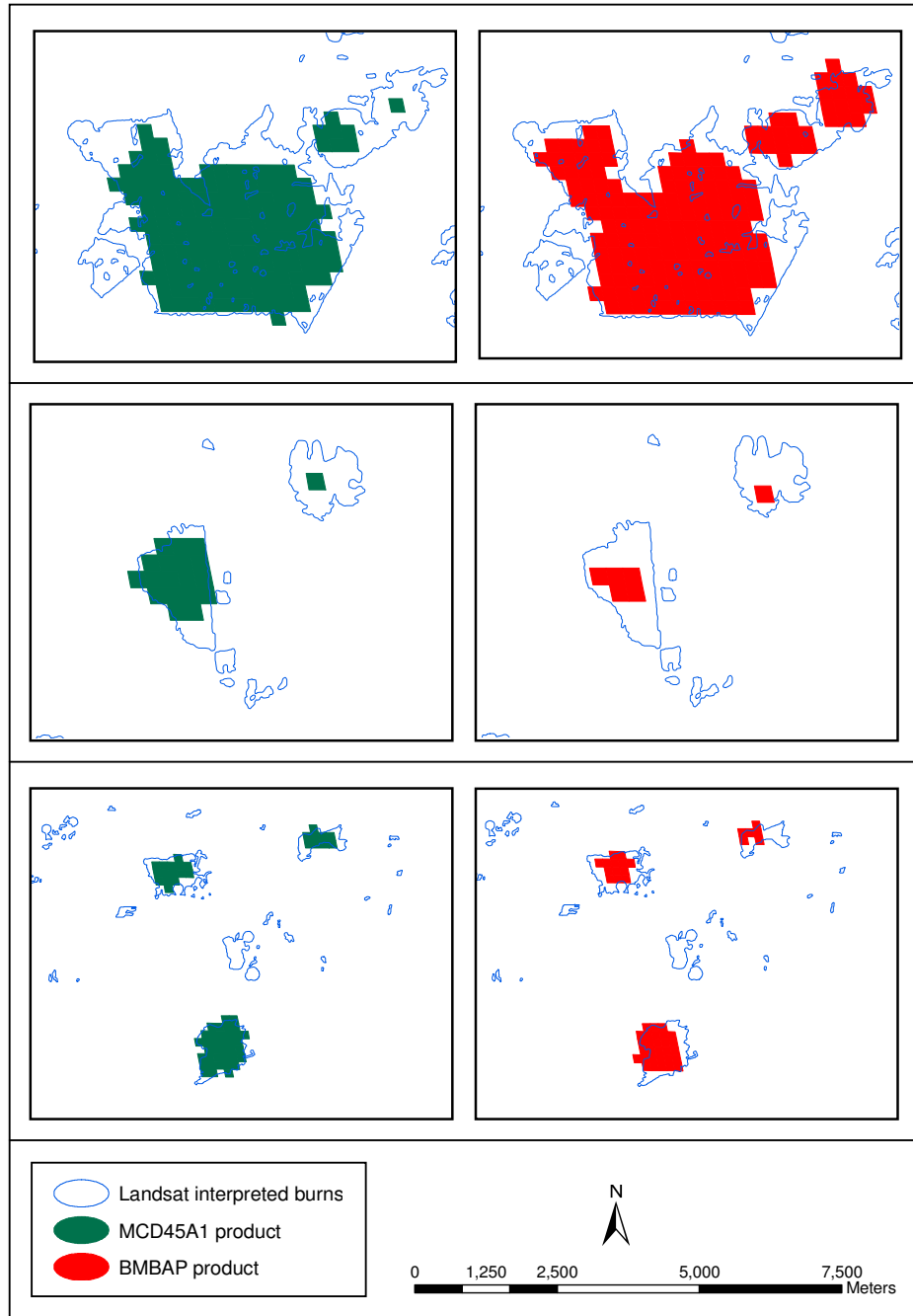


Figure 4.9: Illustration of the mapping performance of the products in Thabazimbi reveals similar performance by corresponding to most of the Landsat burned areas.

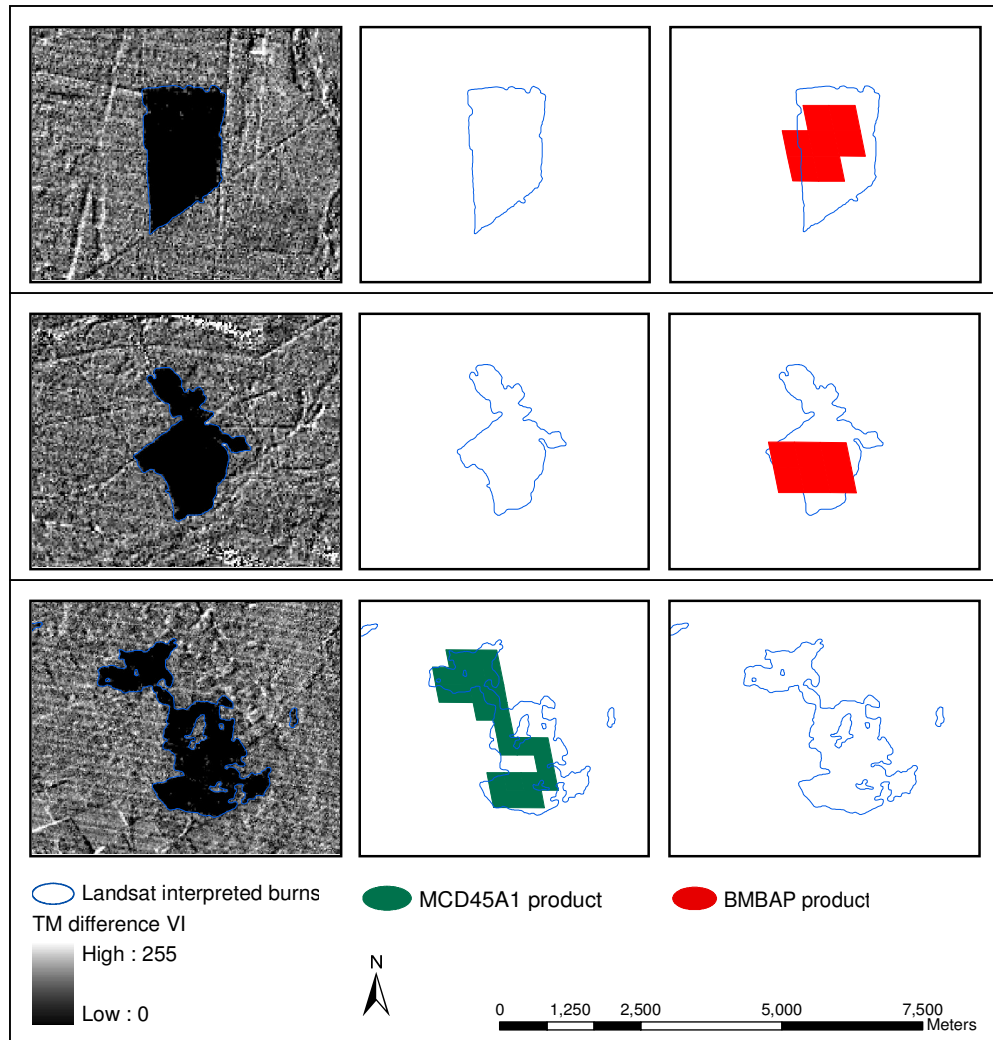


Figure 4.10: Illustration of *O<sub>e</sub>* in the MODIS products over spectrally distinct burned areas in Thabazimbi.

4.2.2.2: Grassland

Figure 4.11 and Figure 4.12 show selected scenes of the burned area performance of the products across the grassland biome in Middelburg and Free State sites, respectively.

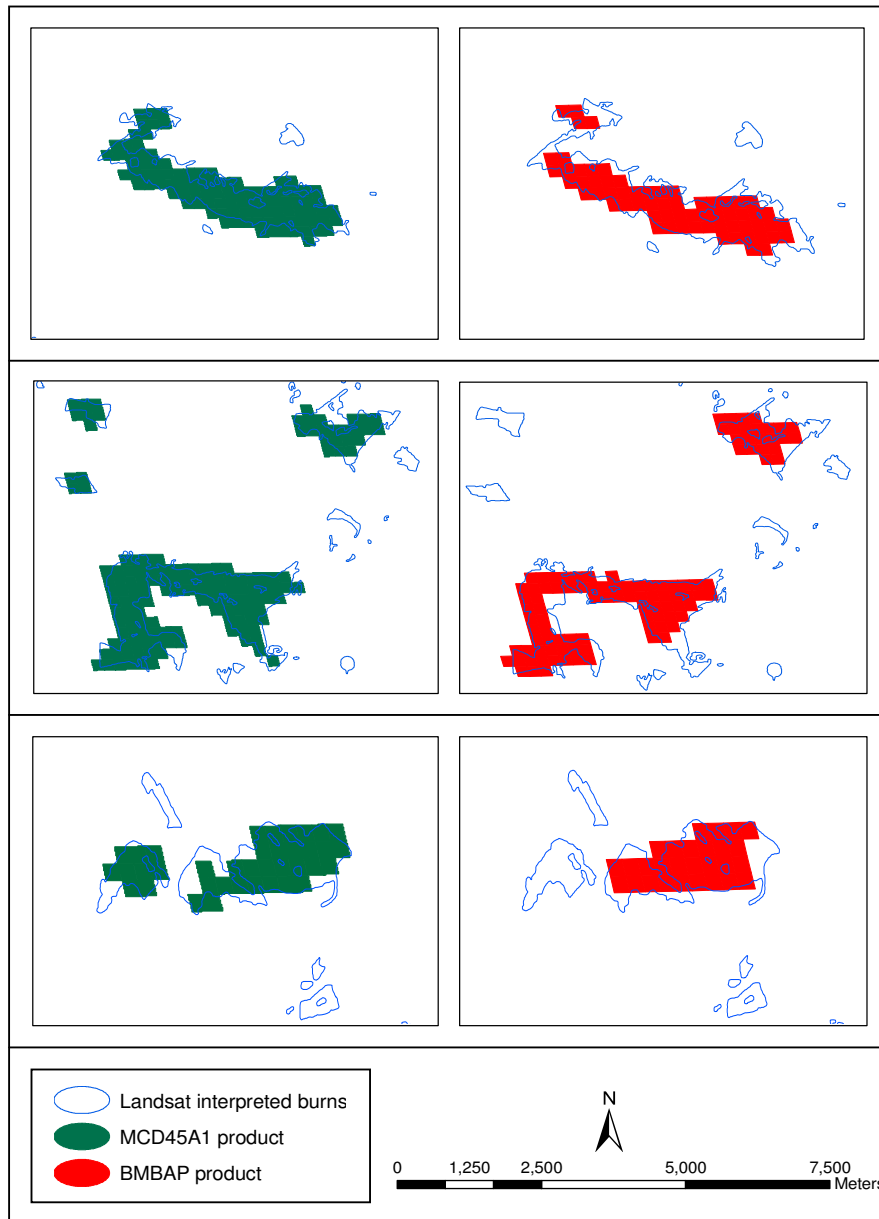


Figure 4.11: MODIS-based burned area mapping in Middelburg with the MCD45A1 product showing higher burned area classification relative to the BMBAP product.

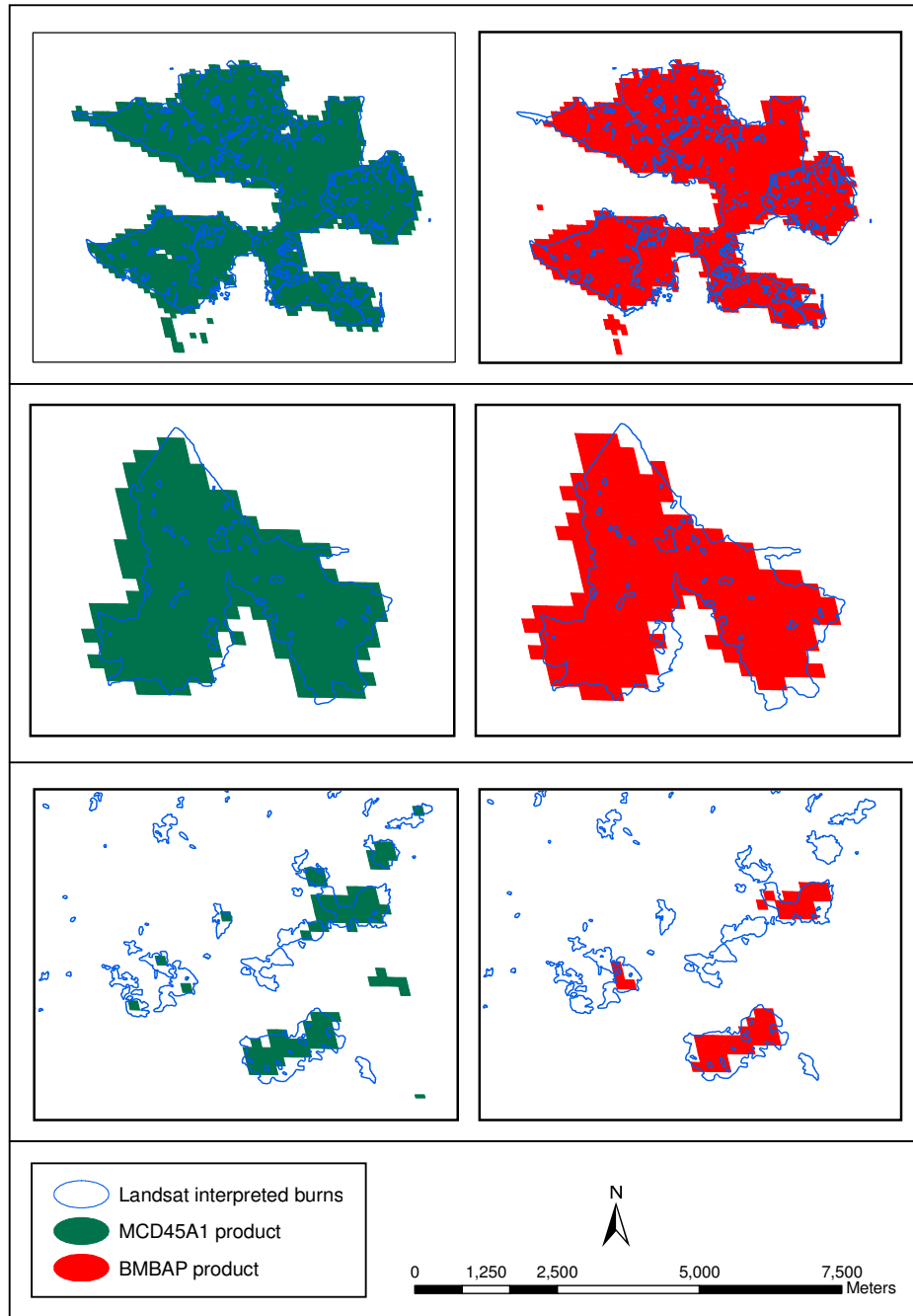


Figure 4.12: The burned area mapping performance of the MODIS products in the Free State.



These sites are marked by a contiguous terrain (~1000-3000 m in the Free State and ~1100-2000 m in Middelburg above sea level) that is covered by a single layer of grasses (with very few trees precluded by for example, frequent fire and grazing) (Rutherford, et al., 1997; Mucina and Rutherford, 2006) spanning the mean annual rainfall of approximately 608.52 - 974.81 mm. The *Oe* in the two burned area products across Middelburg revealed subtle differences of ~2.92% whereby, the BMBAP product under-mapped true burned area at an *Oe* of 65.79% relative to the MCD45A1 product (which had an *Oe* of 62.87%) (Table 4.1; Figure 4.11). Furthermore, in the Free State (Figure 4.12) the BMBAP product demonstrated slightly lower burned area classification accuracy (22.25% *Oe*) relative to the MCD45A1 product (17.45% *Oe*) (Table 4.1). Nonetheless, in the grassland biome both products correctly classified 34.21%/37.13% (Middelburg) and 77.75%/82.55% (Free State) for BMBAP/MCD45A1 of the Landsat burned area as burned. This suggests that the MCD45A1 product appears to have higher burned area classification than the BMBAP product; though a significant fraction (dominated by small-medium sized burns from ~0.36 - 120 ha) remain undetected in either product. Consequently, ameliorations in their approaches particularly in the capturing of small burned areas may be indispensable. In particular, the MCD45A1 product appeared to classify a higher fraction of the unburned surface as burned (especially along the edges of the Landsat interpreted burned areas (Figure 4.12)) than the BMBAP product; and this could have largely contributed to the slightly higher *Ce* (Table 4.1). The derived *Ce* in both products had minor differences of 3.57% (in Free State) and 5.88% (in Middelburg), and hence suggested the BMBAP product may be expected to provide the highest user's accuracies of 78.55% and 74.36% in the grassland biome, respectively.

#### 4.2.2.3: *Pine Forest*

Forest fire is one of the major natural disturbances in the Sabie region, which results in significant changes of the forest ecosystem functioning and financial losses. The region is characterized by forest mountain ranges and expansive valleys, spanning the mean annual rainfall of approximately 568.67 - 810.11 mm. Consequently, the region's climate and topography provide more chances of ignition and wind drive

flames particularly, in the dry periods from late autumn to spring (<http://www.komatilandforests.co.za>). The MODIS burned area products revealed significant differences in their burned area mapping accuracies over the pine forest (primarily utilized for commercial purposes in the Sabie region) (Table 4.1). A total burned area proportion of ~26.72% (which corresponds to 18259.58 ha) was estimated in the independent reference data within the mapped region. The MODIS pixels identified in the MCD45A1 product only classified as burned a lower proportion of 13.22% whereas, the BMBAP product had classified an increasingly higher burned area proportion of 36.65% relative to Landsat interpretations. Figure 4.13 illustrates the MCD45A1 product missed a significant portion of area burned in the pine forest (~62.14% *Oe*) and thus, did not reveal adequate burned area mapping in this region. The variable post-fire reflectance changes on account of the (partially burned and/ or unburned) high tree canopy could have compromised the performance of MCD45A1 product in this region. This finding closely corroborates with comparison results of the MCD45A1 product with 1 km active fire data across low and high forest cover in South America by Roy, et al. (2005a), who reported higher burned area mapping classifications in the MCD45A1 product over low forest cover, which is contrasted to the high forest cover results where much of the area burned was classified by the active fire data. The explanation of this outcome may be because; background characterization of the mapped burned areas within the 500 m MODIS pixel dimension is more eminent than that provided at 1 km spatial resolution. As a result, the active fire data may overestimate the actual burned area if the fires are smaller relative to the 1 km pixel dimension (Roy, et al., 2005a). Nonetheless, a few of the available MODIS pixels classified as burned in the MCD45A1 product appeared to correspond with the Landsat interpreted burned area, which was expressed by *Ce* of 23.5% than that of the BMBAP product of 37.76% (Table 4.1). Conversely, the BMBAP product captured most of the burned forest in the Sabie region with remarkably lower *Oe* (which could be due to the exploitation of active fire data in its approach to calibrate the search for burned areas (Giglio, et al., 2009)), but appeared to have more false burned area classifications than the MCD45A1 product (Figure 4.13).

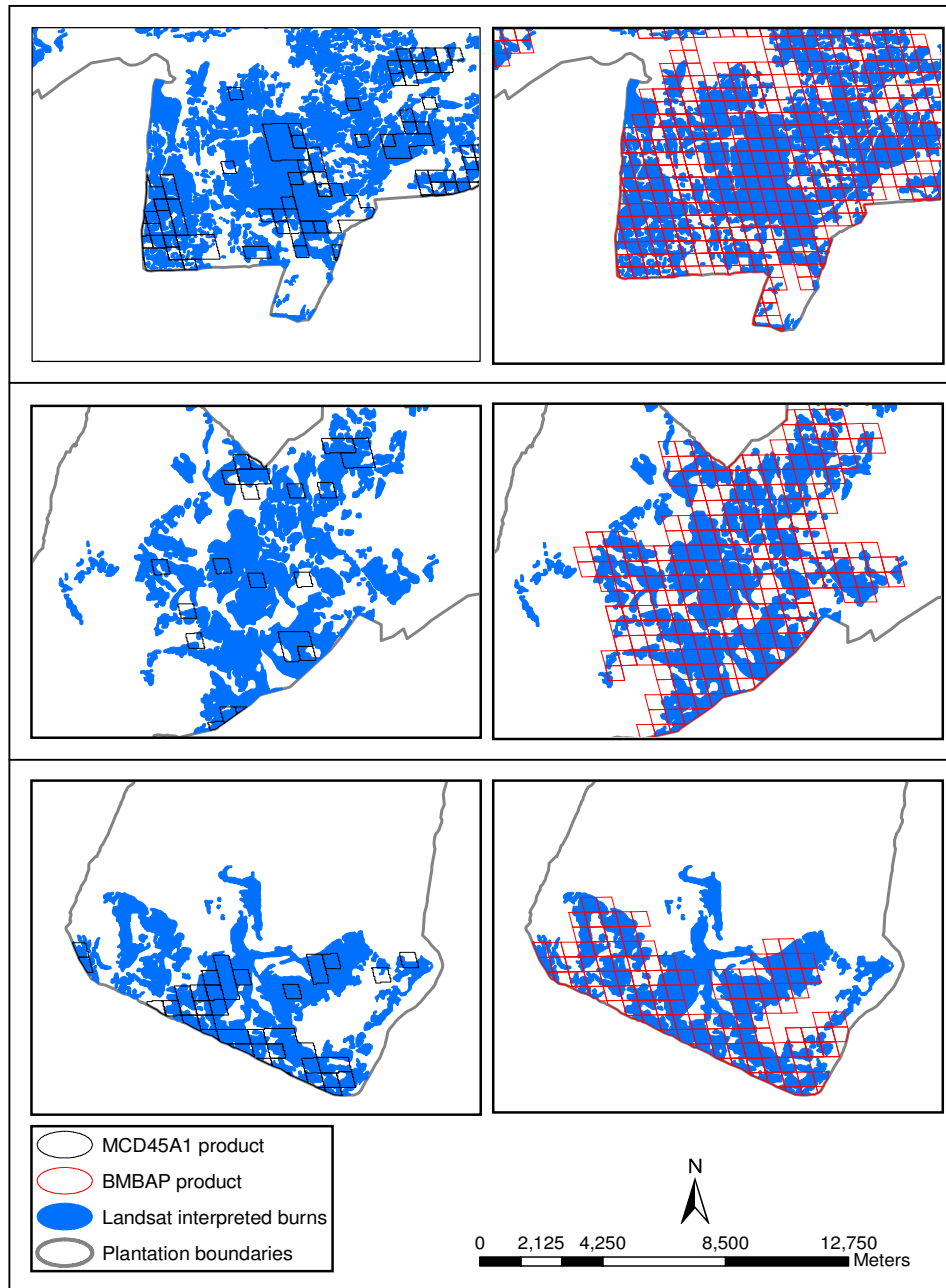


Figure 4.13: A spatial representation of the burned area mapping performance of the products in the Sabie region, which depicts effective performance of the BMBAP product than the MCD45A1 product.

Most of the burned area shapes in the pine forest appeared spatially complex, and when mapped by the products resulted in unburned fractions within the MODIS pixels labelled as burned by the products. This could have inflated  $C_e$  in both products (particularly in the BMBAP product). Additionally, the predominant narrow and/ or fragmented burned areas relative to the MODIS 500 m resolution may remain undetected, thereby contributing toward  $O_e$  in the products. This site presented burned areas that were the most difficult and time consuming to interpret and digitize, coupled with the unmapped areas (clouds and clouds shadows), which highlighted spectral changes that required careful interpretation not to be confused with the actual burned areas (Figure 4.14). Figure 4.14 depicts the multi-temporal Landsat TM data acquired 15 June (first row) and 18 August (second row), 2007, in the Sabie region (near the Blyde plantations located north of the mapped region). Clouds and cloud shadows evident on image 2 (second row) were digitized and tagged as unmapped areas (third row) to avoid spectral confusion of their signature with the actual burned areas highlighted on the TM difference VI image during the interpretation process.

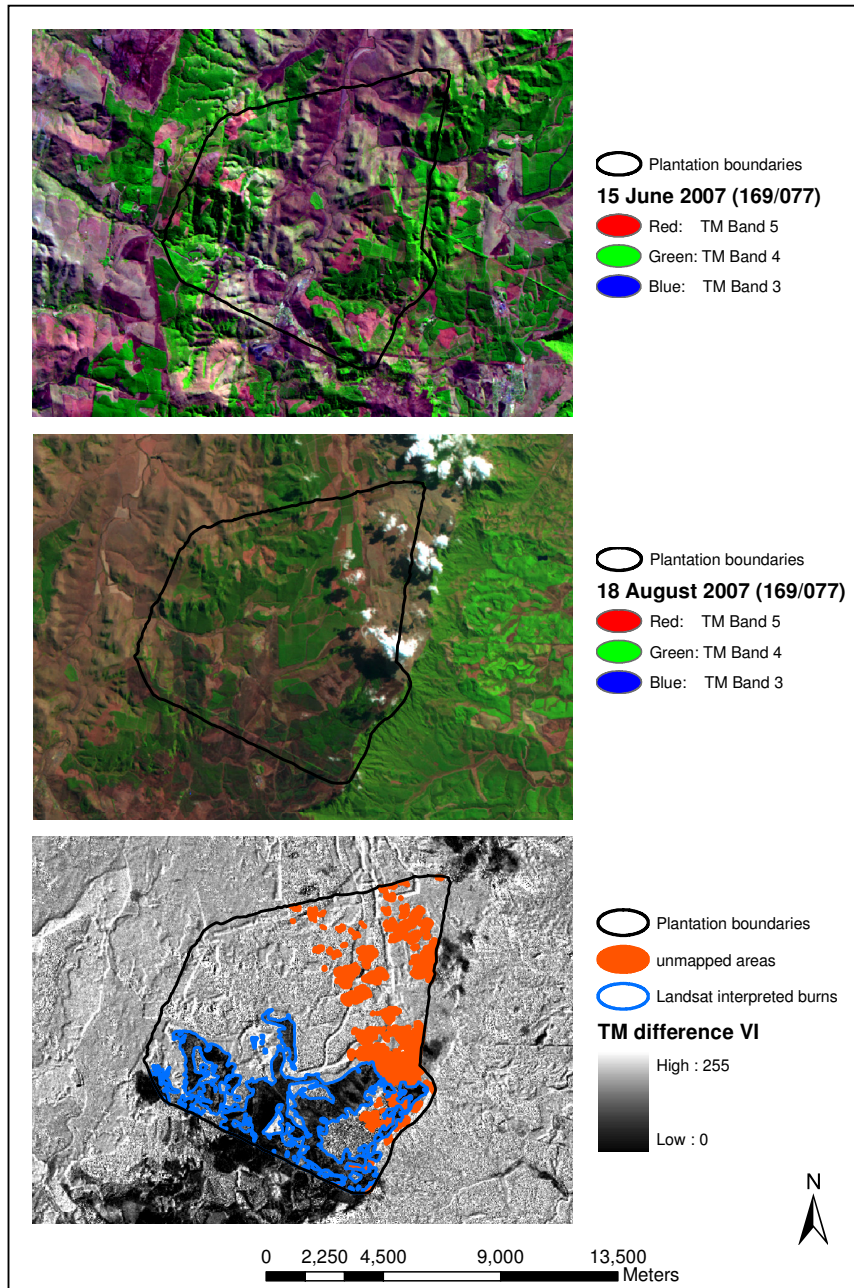


Figure 4.14: Landsat TM data acquired 15 June (first row) and 18 August (second row), 2007, in the Sabie region along with unmapped areas (third row) showing the interpretation process.

#### 4.2.2.4: Fynbos

The Western Cape site encompasses the fynbos biome (found exclusively in the south-western region of South Africa) that includes a mixture of fine-leaved low shrubs and a small grassy layer, experiencing mean annual rainfall in the margin of approximately 259.89 - 503.50 mm.

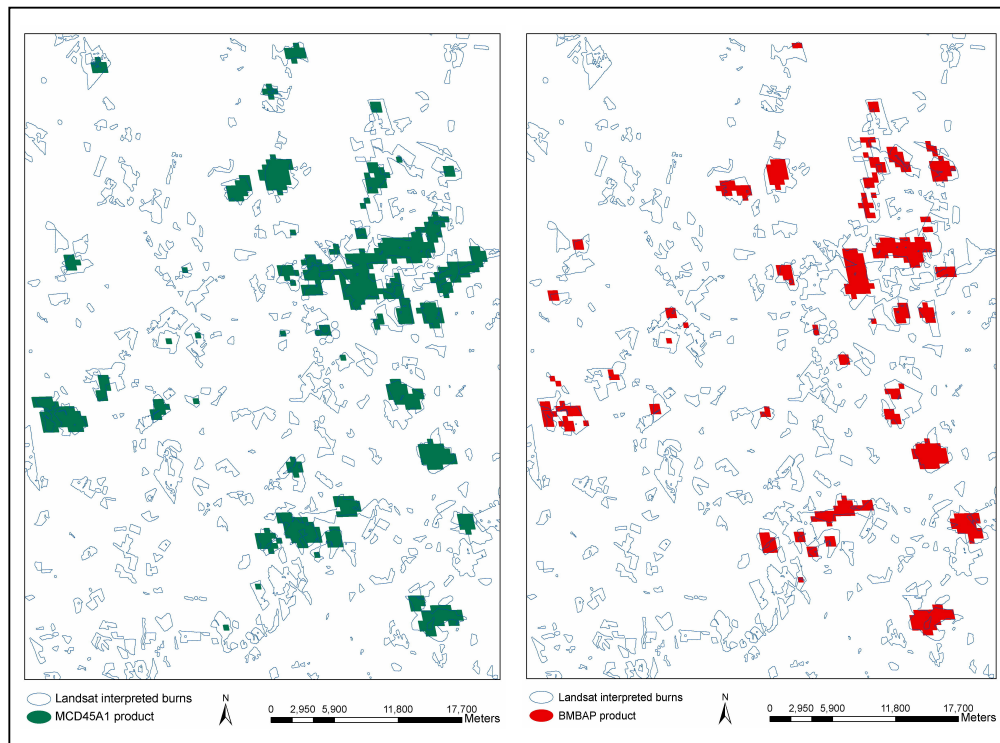


Figure 4.15: A spatial representation of the burned area products in the Western Cape showing their overall mapping performance.

Fynbos is considered as one of the main fire prone biomes in South Africa (owing to the presence of the available flammable biomass fuel) and is marked by winter rainfall (Kraaij, et al., 2010) and a summer season of burning (generally, December - April). Figure 4.15 depicts a selected area within the Western Cape validation site, which provides a wide spatial view of the overall mapping performance of the burned area products. The predominant burned area sizes were in the range of 0.36 –

1000 ha (and a few exceptional burns >1000 ha) characterized by simple homogenous shapes. In particular, the MCD45A1 product labelled a greater proportion of area as burned (i.e., ~77% *Oe*) compared to the BMBAP product (i.e., ~88% *Oe*).

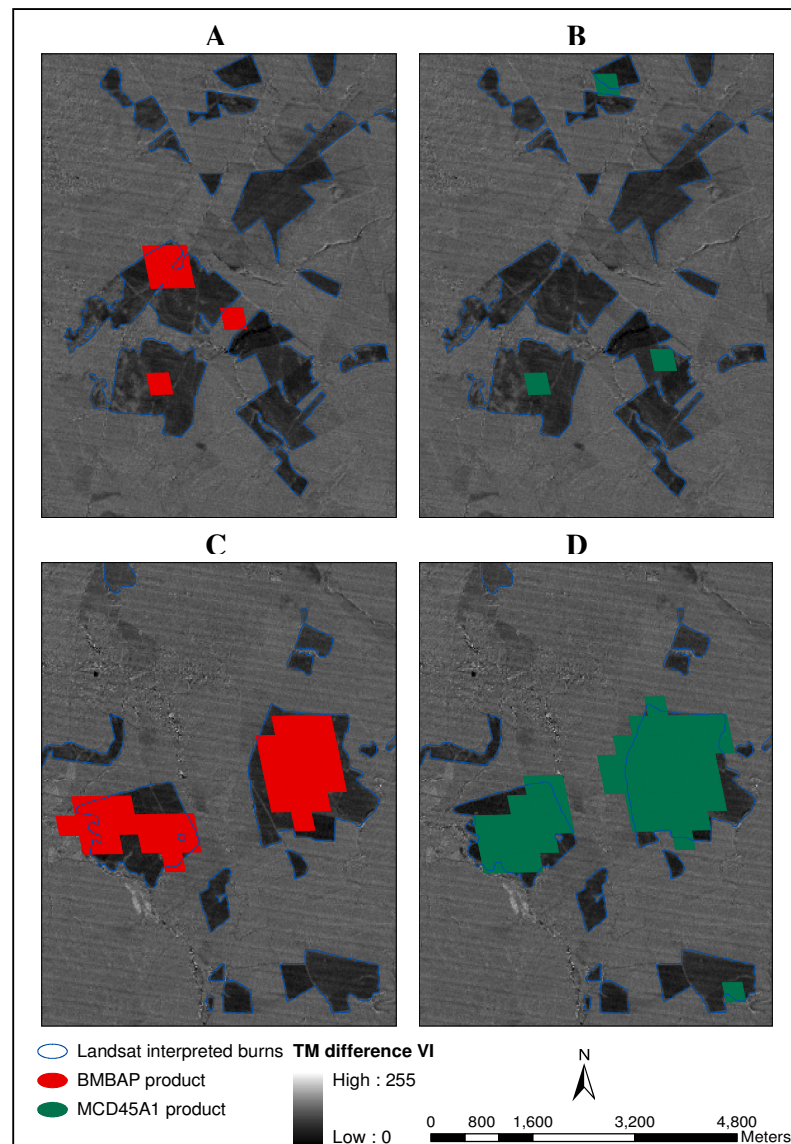


Figure 4.16: Illustrations of Landsat burned areas (A – D) superimposed on the TM difference VI image not identified by the burned area products in Western Cape.

The derived errors for both products suggest that a significant portion of the burned areas remained undetected in both products. Figure 4.16 show examples of Landsat interpreted burned areas superimposed on the TM difference VI image, which have been omitted in the MCD45A1 and BMBAP products. A visual analysis of enhanced burned area changes on the Landsat data show a rather weak reflectance change, which could have not been sufficient for detection by the MODIS products and thereby, influenced the detection accuracy of the products across the fynbos biome. Furthermore, the MCD45A1 product can be expected to capture more of the burned fynbos biome across the selected site but at a cost of higher  $Ce$  (evident particularly along the edges of the Landsat interpreted burned areas) (Figure 4.16). Conversely, the BMBAP product can be expected to provide the highest user's accuracy (lower  $Ce$ ) over the burned fynbos, but at a cost of higher  $Oe$  than the MCD45A1 product (Figure 4.16; Table 4.1).

### **4.3: Influence of fractional burned area on detection accuracy**

The classification error assessment conducted by Roy and Boschetti, (2009) and given in this study (in terms of the confusion matrices; Table 4.1), assesses the entire 500 m MODIS pixels at 30 m resolution as either burned or unburned and does not consider fractional burned area. For example, even where only 20% or less of a MODIS pixel has been burned (based on Landsat interpreted burned area) the assessment expects the MODIS product to detect it as burned, although assigning the burned classification to all 30 m pixels inside the 500 x 500 m area naturally leads to large  $Ce$ . In this way, there is a possibility of inherently overestimating the error during assessment of the burned area products, simply due to the difference in resolution of Landsat and MODIS, i.e. 30 m vs. 500 m. As a consequence, Table 4.3 presents the classification accuracy assessment results of the MODIS burned area products based on 500 m MODIS pixels that are  $\geq 50\%$  and  $\geq 75\%$  burned (according to Landsat), respectively. The first part of Table 4.3 shows the  $Oe$  and  $Ce$  including their counterparts (i.e. producer's and user's accuracy) derived for the products by counting the number of MODIS pixels that were flagged as burned (i.e.  $\geq 50\%$  of a MODIS pixel burned) and/or unburned (i.e.  $< 50\%$  of a MODIS pixel burned) in the product. When only MODIS pixels that correspond to at least 50%



(~13 ha) of fractional burned area are considered, the overall  $C_e$  in the MCD45A1 product decreased by ~6.2% and for the BMBAP product by ~2.3% (differences in  $C_e$  between the initial matrix in Table 4.1 and the matrix based on 50% fractional burned area threshold in Table 4.3). Similarly, the overall  $O_e$  in the MCD45A1 product decreased by ~7% and for the BMBAP product by ~8.5% (differences in  $O_e$  between Table 4.1 and Table 4.3 based on 50% fractional burned area threshold).

Table 4.3: Classification accuracy assessment of the Official MODIS burned area product (MCD45A1) and the Backup MODIS burned area product (BMBAP) based on 500 m MODIS pixels which are  $\geq 50\%$  and  $\geq 75\%$  burned according to Landsat.

Site, Landsat path/row	Landsat dates	Product	MODIS pixels $\geq 50\%$ burned				MODIS pixels $\geq 75\%$ burned			
			Prod (%)	User (%)	$O_e$ (%)	$C_e$ (%)	Prod (%)	User (%)	$O_e$ (%)	$C_e$ (%)
Southern Kruger 168/077	11/8/07 27/8/07	MCD45A1	64.86	57.60	35.14	42.40	73.17	56.27	26.83	43.73
		BMBAP	67.03	68.20	32.97	31.80	74.80	63.80	25.20	36.20
Middelburg 169/078	18/8/07 3/9/07	MCD45A1	51.96	89.62	48.04	10.38	64.17	85.68	35.83	14.32
		BMBAP	46.55	94.10	53.45	5.90	61.87	91.66	38.13	8.34
Western Cape 175/083	17/2/07 6/4/07	MCD45A1	26.86	95.38	73.14	4.62	35.93	94.01	64.07	5.99
		BMBAP	20.94	94.78	79.06	5.22	28.31	94.10	71.69	5.90
Sabie 169/077	15/6/07 18/8/07	MCD45A1	35.79	87.72	64.21	12.28	41.40	85.06	58.60	14.94
		BMBAP	85.86	44.49	14.14	55.51	92.14	40.83	7.86	59.17
Free State 169/080	18/8/07 3/9/07	MCD45A1	90.19	68.01	9.81	31.99	95.31	61.69	4.69	38.31
		BMBAP	86.27	81.88	13.73	18.12	93.26	75.21	6.74	24.79
Thabazimbi 171/077	15/7/07 16/8/07	MCD45A1	44.84	96.26	55.16	3.74	59.30	95.65	40.70	4.35
		BMBAP	50.29	98.60	49.71	1.40	65.45	97.51	34.55	2.49

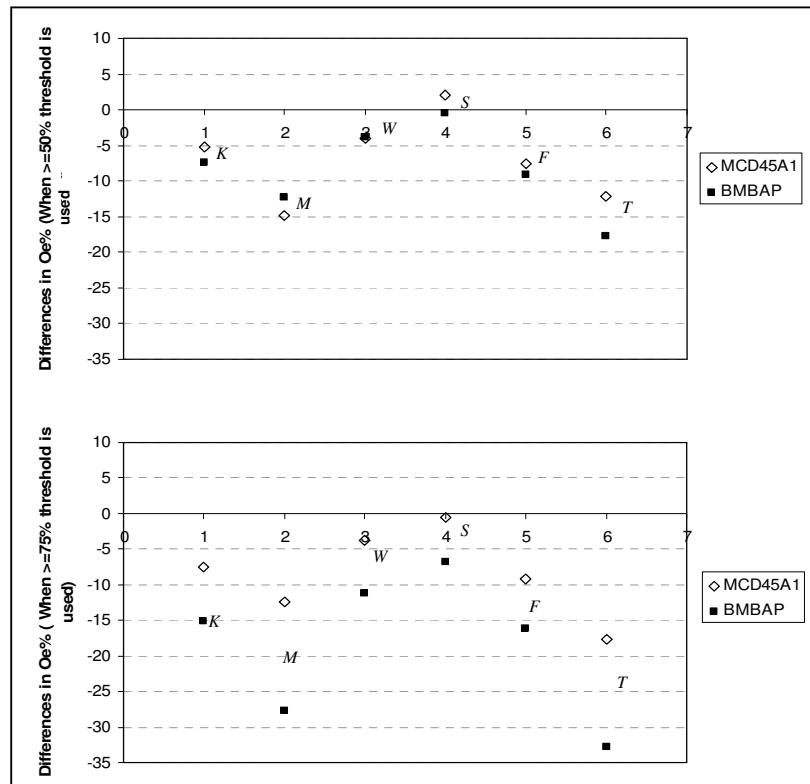


Figure 4.17: Differences in the  $Oe$  and  $Ce$  (before and after  $\geq 50\%$  fractional burned area threshold) for the burned area products. The symbols F, S, K, M, T and W represents the Free State, Sabie, Kruger, Middelburg, Thabazimbi and Western Cape sites respectively.

This implies when the moderate resolution pixel is only partially burned, the classification accuracy of the burned area products will be compromised (based on the confusion matrix). In order to assess the influence of fractional burned area on the  $Oe$  and  $Ce$  (as computed from the products) across all the biomes, the differences between  $Oe/Ce$  before (based on Landsat 30 m pixels, see Table 4.1) and after fractional burned areas (based on MODIS pixels, see Table 4.3) are calculated and plotted in Figure 4.17 and Figure 4.18. The upper panel of Figure 4.17 and Figure 4.18 illustrate the differences in  $Oe$  and  $Ce$  that are at a threshold of  $\geq 50\%$  burned areas.

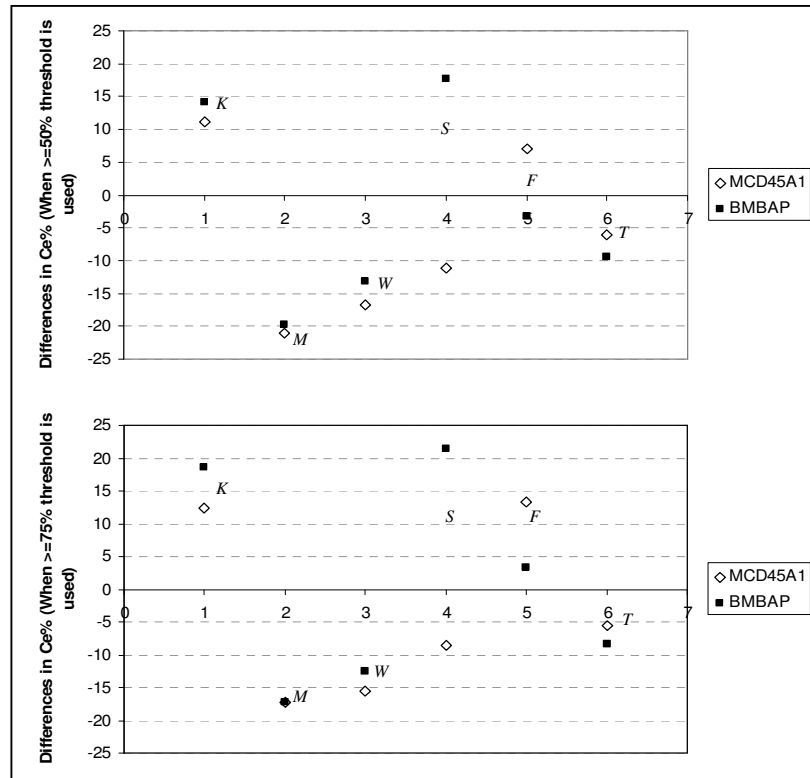


Figure 4.18: Differences in the *Oe* and *Ce* (before and after  $\geq 75\%$  fractional burned area threshold for the burned area products. The symbols F, S, K, M, T and W represents the Free State, Sabie, Kruger, Middelburg, Thabazimbi and Western Cape sites respectively.

Generally, at the  $\geq 50\%$  threshold, considering the fractional burned areas in the analysis, decreases the *Oe/Ce* (across all the biomes) i.e., majority of the points are below the zero *Oe/Ce* line. This outcome could be explained by the increasing number of burned MODIS pixels below the specified threshold (i.e.  $< 50\%$ ) that were incorrectly classified as burned in the product. This implies that a MODIS pixel is considered as burned only if  $\geq 50\%$  of the pixel is burned. For instance, the MCD45A1 product in Free State classified a slightly higher proportion of unburned pixels as burned (i.e.  $\frac{729}{2279}$  where the numerator represents the number of MODIS pixels incorrectly classified as burned in the product, and the denominator represents

the total number of unburned MODIS pixels i.e. <50%) thereby, increasing  $C_e$  (Figure 4.18). Furthermore, the BMBAP product revealed similar changes in  $C_e$  by incorrectly classifying 877 MODIS pixels as burned from a total of 1580 unburned MODIS pixels.

The second part of Table 4.3 shows  $O_e$  and  $C_e$  computed based on MODIS pixels that are  $\geq 75\%$  burned (according to Landsat interpreted burned area). The differences in  $O_e/C_e$  (before and after considering fractional burned areas in the analysis) are plotted in Figure 4.17 and Figure 4.18 (bottom panel). As illustrated in Figure 4.17 and Figure 4.18 (bottom panel), the 75% threshold decreases the  $O_e/C_e$ . In particular, there is a noticeable influence especially in  $O_e$  for both products (large negative values). To explain the observed influence, when only MODIS pixels that correspond to at least 75% (~18.75 ha) of fractional burned area are considered, the overall  $O_e$  in the MCD45A1 product decreased by 16.1% and for the BMBAP product by 18.3% (differences in  $O_e$  between the initial matrix in Table 4.1 and the matrix based on 75% fractional burned area threshold in Table 4.3). Whereas, the overall  $C_e$  in the MCD45A1 product decreased by ~3.5% (differences in  $C_e$  between Table 4.1 and Table 4.3) and, slightly increased by ~1% for the BMBAP product. There appears to be a trade-off between  $C_e$  and  $O_e$  when the thresholds are applied (Boschetti, et al., 2004) and as result,  $O_e$  decreases at the cost of increasing the  $C_e$  (this can be observed in the general shift of the  $C_e$  differences towards the zero line, Figure 4.18 (bottom panel)). As expected, a higher proportion of truly burned pixels (i.e. MODIS pixels  $\geq 75\%$  burned) were correctly classified as burned in the products while, a lower proportion of truly unburned pixels (i.e. MODIS pixels <75% burned) were classified correctly as unburned. However,  $C_e$  slightly increases for both products in all sites (Figure 4.18 (bottom panel)) when the 75% threshold is applied. This means there was a higher proportion of unburned pixels (i.e. MODIS pixels <75% burned) which were classified as burned in the products. The differences in  $O_e$  and  $C_e$  (plotted in Figure 4.17 and Figure 4.18) show that the sensitivity of the products becomes much higher over burned areas corresponding to  $\geq 75\%$  of a MODIS pixel burned. Consequently,  $O_e$  in both products lessens significantly, meaning there could be a threshold above which these moderate-resolution products can be expected to reliably detect the burned areas.

#### 4.4: Analysis of burned area estimations

Results depicting the relationship between estimated burned area by the two MODIS products and Landsat independent reference data are summarized in Table 4.4 in terms of the coefficient of determination and regression coefficients (the total surface area burned per site is also presented). Additionally, the relationship between MCD45A1 and BMBAP products (in terms of scatter plots) is illustrated in Figure 4.19 – 4.24. The coefficient of determination ( $R^2$ ) shown in Table 4.4 depict a spread in spatial variance between 2.5 km grid cells. The variance quantified by the  $R^2$  and the near-zero standard error values indicated a significant level of agreement between the Landsat independent reference data and the MODIS burned area products (e.g., in the grassland ( $R^2 = 0.7377$  to  $0.908$ ) and savanna ( $R^2 = 0.8052$  to  $0.8848$ ) biomes). Weaker correlation measures were observed in the fynbos ( $R^2 = 0.4704$  to  $0.4981$ ) biome, while in the pine forest the  $R^2$  values range from  $0.3815$  to  $0.8601$  between the products.

Table 4.4: Coefficient of determination and regression coefficients of the comparison between the burned area proportions derived from the two MODIS products and multi-temporal Landsat interpreted burned area in 2.5 x 2.5 km grid cells.

MODIS Product	$R^2$	Standard Error	Slope	Intercept	Total area (Ha)
<b>Southern Kruger (savanna)</b>					
MCD45A1	0.863	0.0830	0.8334	0.0029	3558.42
BMBAP	0.8848	0.0813	0.8973	-0.0296	2966.58
<b>Thabazimbi (savanna)</b>					
MCD45A1	0.8056	0.1264	0.927	-0.076	8498.49
BMBAP	0.8052	0.1160	0.868	-0.053	8554.50
<b>Western Cape (fynbos)</b>					
MCD45A1	0.4704	0.1481	0.7515	-0.0609	18123.12
BMBAP	0.4981	0.1121	0.5655	-0.0233	13464.19
<b>Middelburg (grassland)</b>					
MCD45A1	0.7377	0.0988	0.922	-0.0163	14492.18
BMBAP	0.8414	0.0773	0.9328	-0.0188	12297.80
<b>Free State (grassland)</b>					
MCD45A1	0.908	0.1143	1.104	0.019	60189.14
BMBAP	0.904	0.1146	1.068	0.009	54269.46
<b>Sabie (pine forest)</b>					
MCD45A1	0.3815	0.1051	0.4899	0.0129	7397.40
BMBAP	0.8601	0.0818	1.2884	0.0228	22346.05

The observed variation in the level of agreement between the MODIS products and Landsat estimates of area burned could be attributed to the spatial, spectral and temporal characteristics of the burned areas across different validation sites encompassed by our analysis, including the algorithm classification procedures (Roy and Boschetti, (2009)). Conversely, the two burned area products depict similar pattern in the regression coefficients and  $R^2$  values across the biomes (Table 4.4). The slope and intercept values shown in Table 4.4 measure the extent of area burned that the product estimates relative to the Landsat independent reference data. A unit slope could be interpreted as the product estimating the same extent of area burned as the Landsat independent reference data. The product underestimates the area burned when the value of the slope is less than one, and overestimates area burned when the slope value exceeds one (Boschetti, et al., 2006; Roy and Boschetti, 2009). The regression results (shown in Table 4.4) suggests that the BMBAP product underestimated the burned area (i.e., the slope values  $< 1$ ) in southern Kruger, Thabazimbi, Western Cape and Middelburg, but slightly overestimated burned area (slope values  $> 1$ ) in the Free State and Sabie regions, respectively. On the other hand, the MCD45A1 product underestimated burned area in all the validation sites, except in the Free State. Therefore, most accurate burned area estimates for the BMBAP product (in ascending order were) 93%, 90%, 87% and 57% corresponding to Middelburg, southern Kruger, Thabazimbi and Western Cape respectively. Meanwhile, the MCD45A1 product obtained 93%, 92%, 83%, 75% and 49% of the estimated true area burned in Thabazimbi, Middelburg, southern Kruger, Western Cape and Sabie, respectively.

### Western Cape (fynbos)

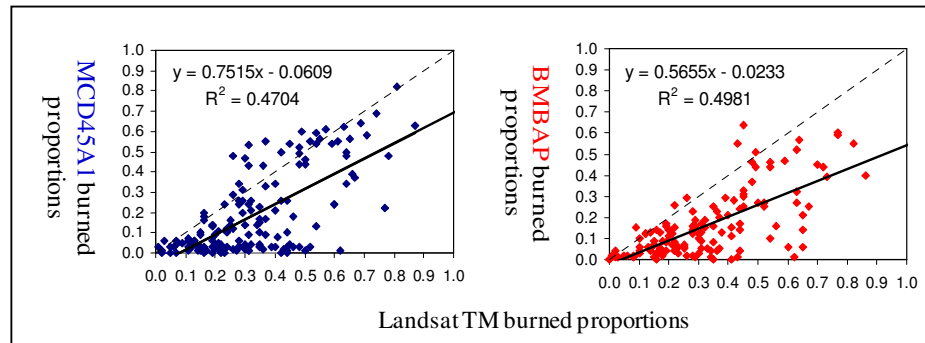


Figure 4.19: Scatter plots of the burned area proportions derived from the two MODIS burned area products (y-axis) and multitemporal Landsat data (x-axis) across the 2.5 x 2.5 km grid cells for the Western Cape encompassing the fynbos biome. Only grid cells containing proportions tagged as burned in the Landsat and the MODIS burned area products were considered.

### Sabie (pine forest)

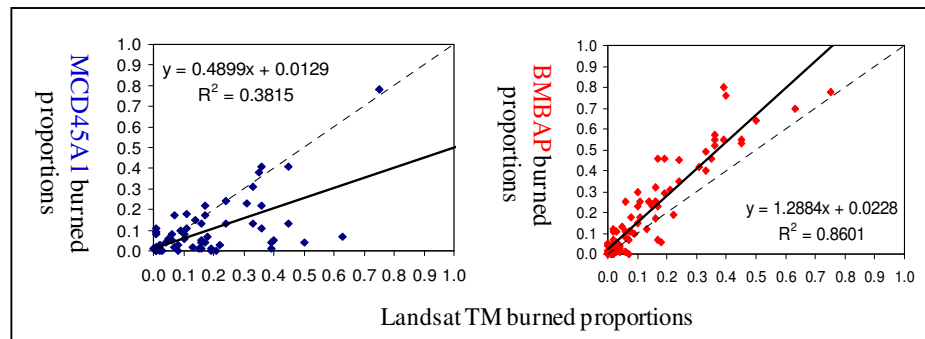


Figure 4.20: Scatter plots of the burned area proportions derived from the two MODIS burned area products (y-axis) and multitemporal Landsat data (x-axis) across the 2.5 x 2.5 km grid cells for Sabie. Only grid cells containing proportions tagged as burned in the Landsat and MODIS burned area products were considered.

Huge differences of burned area estimation were observed for the Western Cape (fynbos) and Sabie (pine forest) sites. Majority of the burned areas in Western Cape ranged from medium (50 – 120 ha) to large (>120 ha) and had fairly simple homogenous shapes (Figure 4.19 and Figure 4.20). However, the correlation of

burned-area proportion estimates over the Western Cape was rather weak between Landsat and the MODIS burned area products resulting in low  $R^2$  values. In particular, both products underestimated true area burned such that the BMBAP product underestimated ~43% and the MCD45A1 product underestimated ~25% of true area burned, respectively. For example, visual image analysis of the enhanced burned areas on the TM temporal difference VI image of the spectral indices ( $VI_{date2} - VI_{date1}$ ) revealed little change in the post-fire spectral reflectance of the burned areas in the Western Cape. Additionally, the acquired multitemporal TM scenes had a 48-day acquisition difference which may have been sufficiently longer than the persistence of the burned area spectral signal (Roy, et al., 2005b). Hence, this could have largely contributed to the reported low estimates of area burned by the MODIS products in the Western Cape. On the contrary, at Sabie approximately 85% of the burned areas are small (< 50 ha) and spatially fragmented, and only few spatially extensive burned areas (120 – 1000 ha; > 1000 ha) appear to dominate the landscape (Figure 4.26).

#### Free State (grassland)

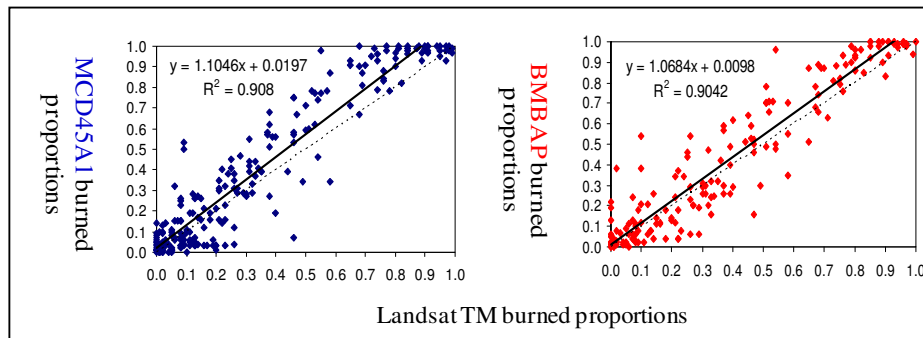


Figure 4.21: Scatter plots of the burned area proportions derived from the two MODIS burned area products (y-axis) and multitemporal Landsat data (x-axis) across the 2.5 x 2.5 km grid cells for the Free State encompassing the grassland biome. Only grid cells containing proportions tagged as burned in the Landsat and MODIS burned area products were considered.



### Middelburg (grassland)

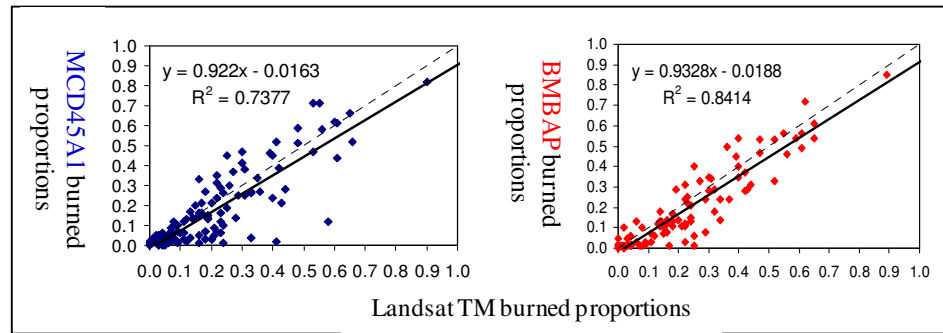


Figure 4.22: Scatter plots of the burned area proportions derived from the two MODIS burned area products (y-axis) and multitemporal Landsat data (x-axis) across the 2.5 x 2.5 km grid cells for Middelburg encompassing the grassland biome. Only grid cells containing proportions tagged as burned in the Landsat and MODIS burned area products were considered.

Additionally, the enhanced spectral contrast of the burned areas on the TM temporal difference VI image appeared relatively dark and the shapes of the burned areas had complex structures. Over most forest ecosystems, fires burn large fuel loads to leave spectrally distinct burned areas (Eva and Lambin, 2000) but again humid conditions and vegetation structure could lead to small and scattered burned areas (Bucini and Lambin, 2002; van Wilgen and Scholes, 1997). Consequently, the coefficient of determination revealed a good linear relationship (high  $R^2$  value) of the burned area proportion estimates between Landsat and the BMBAP product whereas, the derived slope coefficient was moderately higher than one. Therefore, the BMBAP product overestimated (~29%) the burned area in the pine forest. Such an alarming overestimation by the BMBAP product could have largely been as a result of spectral uncertainties between the burned forest patches and the recently clear-felled forest trees, which result in a mixture of spectral signatures that cause confusion for the various algorithm parameters (Giglio, et al., 2009).

On the other hand, a very low  $R^2$  value was described for the MCD45A1 product in Sabie and this revealed a relatively weak linear relationship with the Landsat burned area proportions. Additionally, the MCD45A1 product had less

accurate estimates of area burned (low slope value) in Sabie, and therefore obtained the largest underestimation (~51%) of area burned in the pine forest. The algorithm (used to define the MCD45A1 product) assumes that post-fire reflectance change of MODIS band 6 will drop following a forest fire (Roy, et al., 2005a) which may not be the case across all forest regions. This was revealed in recent findings on the MODIS Global burned area validation and product status (<http://modis.gsfc.nasa.gov>) and consequently, minor updates were made to the algorithm to accommodate the various post-fire reflectance changes over the different forest regions (Boschetti, et al., 2010).

Markedly similar performance of the MCD45A1 and BMBAP products was observed in the Free State (grassland) biome. The linear regression fitted to the Free State biome (Figure 4.21) revealed the best (highest  $R^2$  values) agreement between the burned area proportion estimates derived from Landsat and the MODIS products. More concerning, was the derived slope coefficients higher than one across the site. Visual image analysis suggests that large burns of sizes 120 – 1000 ha and >1000 ha (Figure 4.25) constituted most of the total burned surface and therefore, some overestimation is likely to occur at 500 m spatial resolution. This is largely due to the inclusion of small unburned areas located inside the large burns. As a consequence, the MCD45A1 product overestimated true burned area (by ~10%) whereas the BMBAP product overestimated true area burned (by ~7%) in the Free State, which generally encompasses the grassland biome. This is followed by more accurate estimates of area burned (high  $R^2$  and slope coefficients close to 1) for Middelburg, Thabazimbi and southern Kruger sites (Figure 4.22, Figure 4.23 and Figure 4.24) (which corresponds to the grassland and savanna biomes). Usually, fires burn large hectares of land in the grassland and savanna biomes (Scholes, et al., 2002; Roy, et al., 2005b), particularly in the late dry season. These fires spread readily and produce larger and more contiguous, spectrally distinct burned areas. Therefore, these results suggests that the MCD45A1 and BMBAP products provides adequate regional information regarding the extent of area burned especially, over the burning grassland and savanna systems where the effect of spatial resolution and spectral differences in the accuracy of burned area estimates are minimized.

### Thabazimbi (savanna)

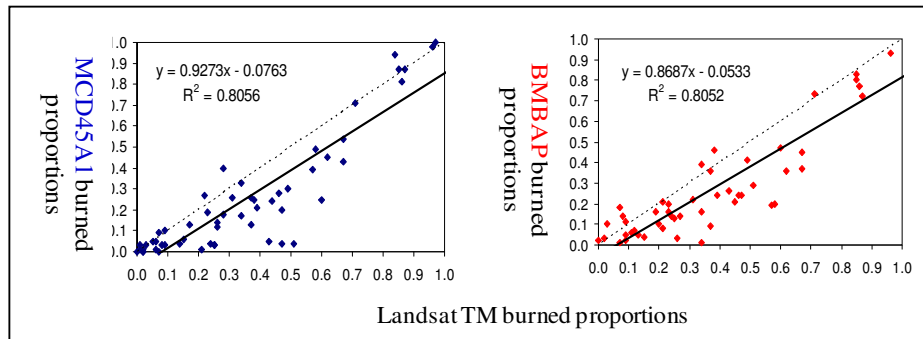


Figure 4.23: Scatter plots of the burned area proportions derived from the two MODIS burned area products (y-axis) and multitemporal Landsat data (x-axis) across the 2.5 x 2.5 km grid cells for Thabazimbi encompassing the savanna biome. Only grid cells containing proportions tagged as burned in the Landsat and the MODIS burned area products were considered.

### Southern Kruger (savanna)

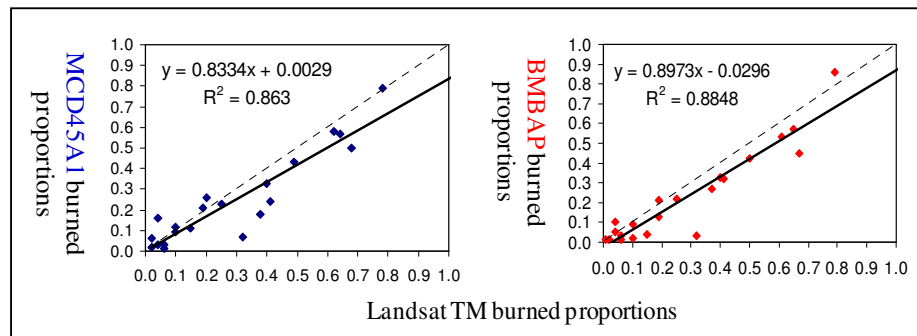


Figure 4.24: Scatter plots of the burned area proportions derived from the two MODIS burned area products (y-axis) and multitemporal Landsat data (x-axis) across the 2.5 x 2.5 km grid cells for southern Kruger encompassing the savanna biome. Only grid cells containing proportions tagged as burned in the Landsat and the MODIS burned area products were considered.

a) Thabazimbi: Savanna

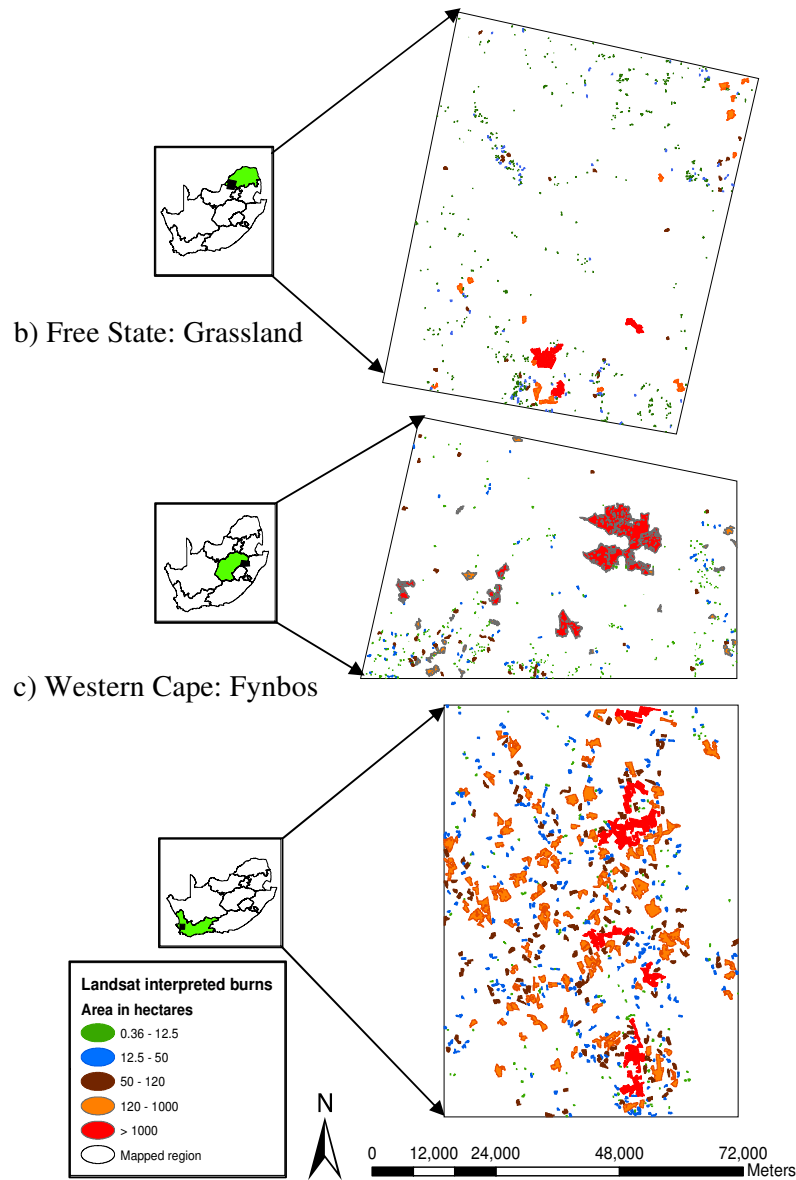
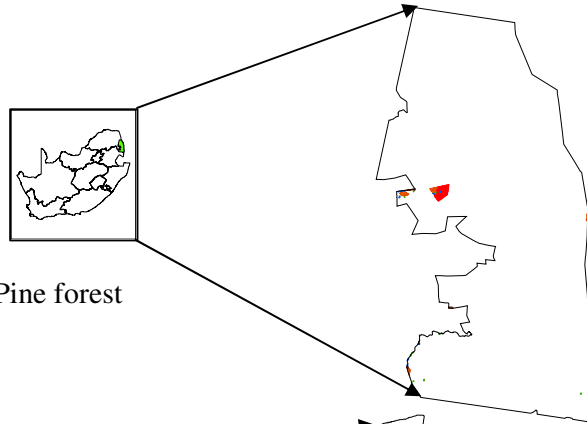
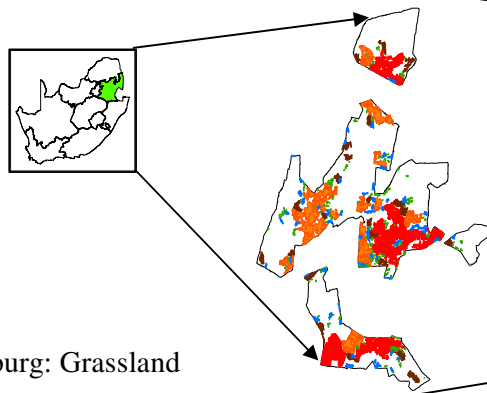


Figure 4.25: Spatial coherence of the burned area patterns interpreted and produced from multitemporal Landsat TM data over the three validation sites.

d) Kruger: Savanna



e) Sabie: Pine forest



f) Middelburg: Grassland

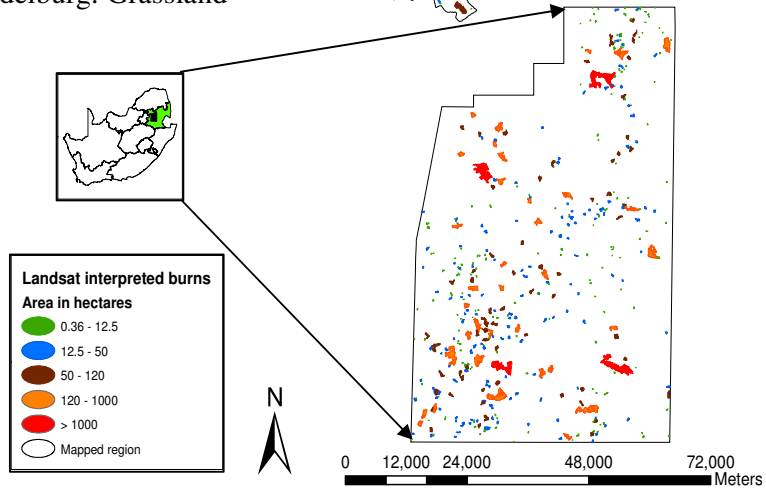


Figure 4.26: Spatial coherence of the burned area patterns interpreted and produced from multitemporal Landsat TM data over the three validation sites.

#### **4.5: Analysis of sub-MODIS pixel burned area**

A quantitative analysis of the influence of sub-MODIS pixel burned area on the probability of detection by the MCD45A1 and BMBAP products was performed. The MODIS reference grids were simply used to compute proportions of burned area within each 500 m grid cell corresponding to the Landsat TM independent reference data. The number of MODIS pixels with burned area proportions of 25%, 50% and 75% area burned according to Landsat TM is indicated in Figure 4.27 and Figure 4.28. The results illustrate the influence of fractional burned area on the accuracy of the moderate resolution MCD45A1 and BMBAP products, notably how the probability of burned area identification within a 500 m MODIS pixel increases with sub-MODIS pixel burned area size.

It is evident from Figure 4.27 and Figure 4.28 that both burned area products have a positive linear trend between the proportion of a burned MODIS pixel and the probability of being detected by MODIS across all validation sites. These observations demonstrate the inherent error in the burned area products due to the limitations arising from the moderate spatial resolution of the MODIS instrument. The detection probabilities of the MODIS products can be inferred by the fractional area of the MODIS pixels burned. These results suggest that a burned area has to be at least 13 ha in size, corresponding to half of a MODIS pixel, in order for the products to detect it with a mean probability of ~34-39% (for MCD45A1 and BMBAP correspondingly) (Figure 4.27 and Figure 4.28). These findings corroborate previous conclusions that a burned area proportion of approximately 50% can be considered an appropriate threshold for medium resolution burned area detection (e.g., Eva and Lambin, 1998b; Boschetti, et al., 2004; Sa, et al., 2007; Miettinen, 2007, Giglio, et al., 2009). However, this could vary depending on the spectral contrast between burned and unburned areas across the different vegetation types (Eva and Lambin, 1998b).

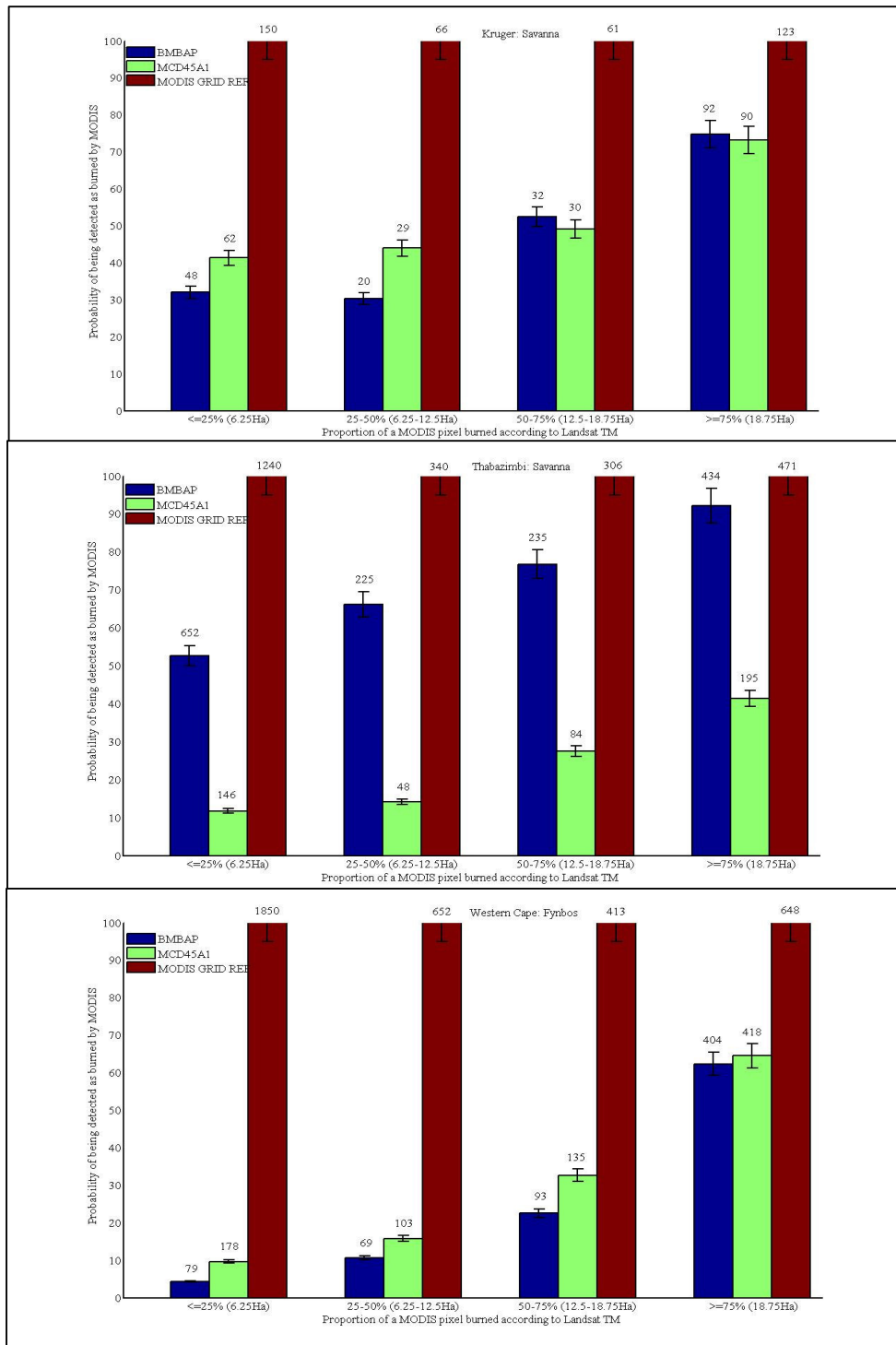


Figure 4.27: Histograms of sub-MODIS pixel burned area analysis used to depict the relationship between burned area proportions according to Landsat and the probability of detection by the products in Kruger, Thabazimbi and Western Cape.

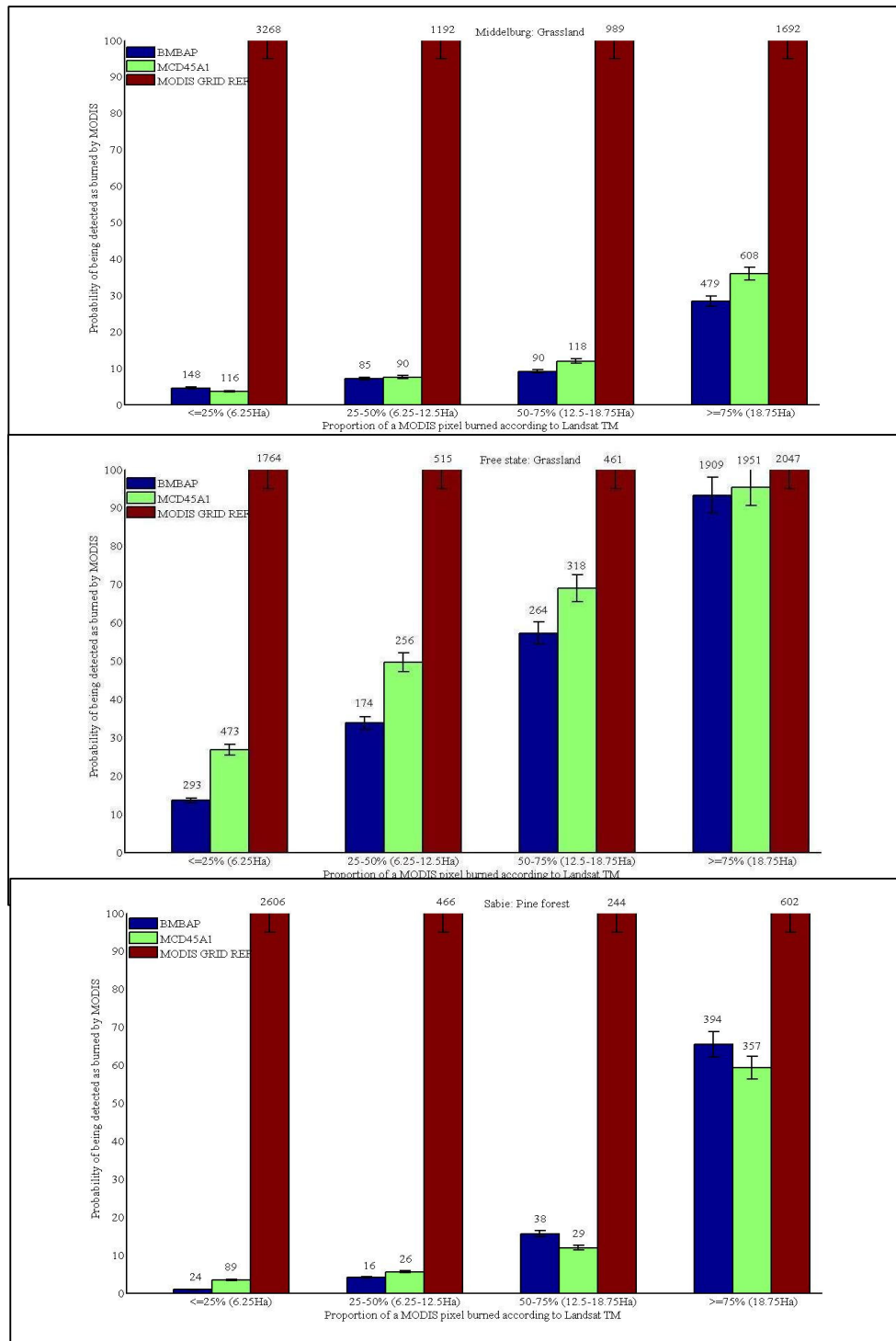


Figure 4.28: Histograms of sub-MODIS pixel burned area analysis used to depict the relationship between burned area proportions according to Landsat TM and the probability of detection by the products in Middelburg, Free State and Sabie.



For instance, even burned area fractions that correspond to approximately 25% (6.25 ha) of a MODIS pixel could be detected with a probability of ~53% by BMBAP in the Thabazimbi area (e.g., Figure 4.27). The MCD45A1 product attained high (49.7%) burned area detection probability relative to the BMBAP product (33.8%) for fractional burns below 50% of a MODIS pixel in all sites (Figure 4.27 and Figure 4.28) except for Thabazimbi. The MCD45A1 product showed inadequate performance in Thabazimbi reaching maximum detection of 14.1% than the BMBAP product at 66.2% for the preceding fractional burned areas (Figure 4.27). Conversely, the BMBAP product showed a comparatively steady increase in the probability of detection for burned area proportions more than half of a MODIS pixel, particularly in southern Kruger, Thabazimbi and Sabie, respectively.

The lowest values of burned area detection probability in BMBAP (0.9 - 4.5%) and MCD45A1 (3.4 - 9.6%) products were found in the Sabie (pine forest), Middelburg (grassland) and Western Cape (fynbos) sites, respectively. In general, these sites had the highest density (1437) of individual burns derived using Landsat interpreted burned area maps. The markedly similar performance of the products across the above-mentioned sites (particularly over burned area proportions of  $\leq 25\%$ ;  $50\%$  and  $< 75\%$ ) could be attributed to the mosaic of small (0.36 – 50 ha) burned areas and the mixture of burned-unburned spectral signatures of the burns (e.g. Sa, et al., 2003; Sa, et al., 2007). For example, according to Giglio, et al. (2009), the algorithm used to define the BMBAP product can be reasonably assumed to detect burns that correspond to at least 50% (~13 ha) of a MODIS pixel; and this is evident in other sites such as, Thabazimbi and Free State. Nonetheless, the products revealed a high detection probability at sub-MODIS pixel burned areas  $\geq 75\%$  (Figure 4.27 and Figure 4.28). In addition, the BMBAP product attained the highest burned area detection probability (~65.4%) in Sabie, followed by the MCD45A1 product in the Western Cape (~64.5%) and Middelburg (~40%) sites, respectively. A significant improvement over the afore-mentioned sites in the probability of burned area detection by both MODIS products was observed at the Free State, southern Kruger and Thabazimbi sites (Figure 4.27 and Figure 4.28). The spatial coherence of the burned area patterns over these sites demonstrated a diversity of burned shapes, from narrow and/ or fragmented (0.36; 12.5; 50 ha), to large and compact ( $> 1000$

ha) (Figure 4.25 and Figure 4.26). Interestingly, when compared to the Sabie, Middelburg and Western Cape sites, both products at the respective sites reached maximum detection of 52.6% in Thabazimbi (BMBAP), and 41.3% in southern Kruger (MCD45A1) for the burned area proportions corresponding to  $\leq 25\%$  (6.25 ha) of a MODIS pixel. These observations indicated that, in contrast to product performance in the Sabie, Middelburg and Western Cape sites, even small burns between 20 – 30% of a 500 m MODIS pixel or less could reasonably be detected as burned (e.g. Eva and Lambin, 1998b).

Figure 4.27 and Figure 4.28 reveal the products could be expected to give the highest detection probability for burned area proportions that correspond to at least 75% ( $\geq 18.75$  ha) of a MODIS pixel as evident in the Free State and Thabazimbi sites, respectively. As a result, the MCD45A1 product achieved the highest detection probability in the Free State (grassland), which is equivalent to 95.3% whereas; the BMBAP product reached the highest detection probability of 92.14% in Thabazimbi (savanna). Huge differences can be seen over Thabazimbi where the MCD45A1 product revealed a significantly lower detection probability relative to BMBAP. As a result, the presence of tree cover or overstorey vegetation in Thabazimbi, could have led to a significant decrease in the spectral detectability of the burned areas in the MCD45A1 product. Similarly, both products appeared to be inconsistent (i.e. in their detection probability) with the grassland biome in the Free State and Middelburg sites (Figure 4.28). The reason for this discrepancy could be attributed to the substantial differences of burned areas at the respective sites (Figure 4.25 and Figure 4.26).

#### **4.6: Concluding remarks**

This study has presented validation results of the MCD45A1 and BMBAP products across the main fire prone biomes (encompassing savanna, grassland, fynbos and pine forest) in South Africa. The accuracy assessment methods, based on the confusion matrix, linear regression and sub-MODIS pixel burned area analysis, have been used to compare the 500 m burned area products with independent reference data obtained by interpreting multi-temporal 30 m Landsat TM scenes. The initial accuracy indices presented in this study, by means of the confusion matrix (Table

4.1) indicate that both products had lower  $C_e$  than  $O_e$ . Additionally, the MCD45A1 product had lower  $O_e$  than the BMBAP product in all study sites (excluding Sabie) when fractional burned area are not considered (Table 4.1). Conversely, the BMBAP product provided lower  $O_e$  for three of the six study sites (spanning the pine forest and savanna biomes) when 50%/75% fractional burned area are considered (Table 4.3). While this non-linear relationship between the  $C_e$  and  $O_e$  could be largely inferred on the relationship between the user's preference and the detection criteria enforced by product producers (Roy and Boschetti, 2009; Giglio, et al., 2009; Roy, et al., 2008; Giglio, et al., 2006; Roy, et al., 2005a); this study showed that the MCD45A1 product has the ability to resolve small burned areas compared to the BMBAP product. Therefore, the  $O_e$  derived from the MCD45A1 product is more sensitive to variations in burned area sizes relative to the BMBAP product (shown in Table 4.2 and Figure 4.6) particularly in grassland, fynbos and savanna biomes. Whereas, the variability of  $O_e$  of the BMBAP product reveal high sensitivity to burned area sizes in the pine forest biome.

We acknowledge that the accuracy assessment presented in Table 4.1 (in terms of the confusion matrix) does not take cognisance of fractional burned area and as a result, inherently overestimated error in the products (similar to Roy and Boschetti, et al., 2009). Supplementary to this issue, this study has presented a classification accuracy assessment of the products based on 500 m MODIS pixels that are  $\geq 50\%/75\%$  burned according to Landsat (Table 4.3). This analysis suggests an overall reduction in  $C_e$  of  $\sim 6.2\%/2.3\%$  for the MCD45A1/BMBAP product followed by  $\sim 7\%/8.5\%$  reduction in  $O_e$  for the respective products based on a 50% fractional burned area threshold (Table 4.3). Furthermore, the overall  $O_e$  in the MCD45A1/BMBAP product decreased by  $\sim 16.1\%/18.3\%$  when a 75% burned area threshold are applied to the MODIS pixels. These findings are in corroboration with the sub-MODIS pixel burned area analysis (presented in Figure 4.27 and Figure 4.28) that show evidence of the influence of fractional burned area in the detection accuracy of the products. In particular, the probability of identifying a burned area within a 500 m MODIS pixel is directly related to the proportion of the MODIS pixel burned. Thus, the initial classification accuracy results (shown in Table 4.1) based on

Landsat pixels do not provide a reasonable measure of classification errors in the MODIS burned area products.

Coefficient of determination and regression coefficients are estimated in order to compare burned area proportions derived from the two MODIS products and the multi-temporal Landsat interpreted burned area in 2.5 x 2.5 km grid cells. The regional regression results presented in the current study only included grid cells containing proportions tagged as burned in both the Landsat data and the MODIS burned area products. We acknowledge the exclusion of grid cells with unburned proportions in the analysis may influence product accuracy quantification results since; a location with no detected burned area does not necessarily guarantee absolute absence of fires at that particular location (Giglio, et al., 2009). However, the impact of their exclusion was not measured in this study but, was tested by Roy and Boschetti, (2009) who reported that excluding grid cells with unburned proportions in Landsat data and the burned area products does not alter regional regression results.

The adopted threshold (minimum mapping unit of 240 m) during the production of high-resolution burned area reference maps (Roy, et al., 2005b) would have led to the capture of an increased number of small burned areas (which can be spatially viewed on Figure 4.25 and Figure 4.26) that were largely undetected by the MODIS burned area products and thus, contributed to the inflated errors of in the products (Table 4.1). The limitations arising from the adopted threshold has also been highlighted in previous studies (e.g., Roy, et al., 2005b; Roy and Boschetti, 2009). In addition, given that the burned area signal is short-lived; a longer temporal difference between the reference data (i.e. Landsat) acquisition dates, may result in some of the affected areas on the second image not being clearly identified to produce rigorous independent reference data (e.g., Eva and Lambin, 1998a; Boschetti, et al., 2006; Roy and Boschetti, 2009). However, this varies across the different biomes, as for burned forests may remain detectable for longer periods in contrast to savanna and grassland systems where burned areas may last up to a few weeks mainly as a result of dissipation of char and mineral ash by, for example, wind, precipitation and rapid vegetation regrowth (Roy, et al., 1999).

The derived accuracy results of the MODIS burned area products in this study are based on a validation exercise carried over a single dry season. Consequently, product validation over longer periods is emphasized across more sites including the acquisition of additional high resolution imagery to capture more variation and error that the burned area products encompass. Overall, our analysis indicates that the MCD45A1 product provides the highest burned area mapping accuracy over the fynbos and grassland biomes. In comparison, the BMBAP product possibly provides the highest burned area mapping accuracy across the pine forest and savanna biomes. However, the MCD45A1 product appears to be better at mapping small burned areas (with proportions  $\leq 50\%$  of a MODIS pixel) while, the BMBAP product seems more reliable at detecting large burned areas (corresponding to proportions  $> 50\%$  of a MODIS pixel). Furthermore, according to Roy, et al. (2008) we can expect the MCD45A1 product to provide much higher burned area detection than the BMBAP product across homogeneous landscapes with low percent tree cover. On the other hand, the BMBAP product appears to map the burned areas more reliably than the MCD45A1 in regions characterized by high percent tree cover. The differences in the derived accuracy measures revealed by the two products can, to a great extent be attributed to the different approaches adopted during their production; this has been reported in Roy, et al., (2005a) and Giglio, et al., (2009). This is an important area of future research.

## CHAPTER 5

### CONCLUSION

#### 5.1: Conclusions

Previous research that has been undertaken to validate the MODIS global burned area products namely, the MCD45A1 (Roy and Boschetti, 2009) and BMBAP (Giglio, et al., 2009) in South Africa used ETM+ scenes located around the southern Kruger National Park (KNP), which encompassed the savanna biome. The present study has extended validation of the MODIS global burned area products in South Africa during the 2007 dry season across six validation sites, which are characterized by different biomes (this include fynbos, pine forest, grassland and savanna), mean annual rainfall variability, and high fire activity.

The independent reference data used in this study to validate the burned area products were produced and standardized following the internationally recognized burned-area validation protocol described by Roy, et al. (2005b). The protocol required acquisition of multirate high-resolution data for each site, coupled with visual interpretation and on-screen digitizing of the computed post-fire reflectance changes highlighted between the TM acquisition dates. Based on the independent reference data within the mapped regions at 6 sites; accuracy information of the products was derived following three main analysis procedures.

Firstly, the commission and omission errors in the burned area products were quantitatively expressed by use of a confusion matrix for pixel-level accuracy assessment. From this assessment, it can be concluded that the MCD45A1 product had lower omission errors than the BMBAP product whereas, the BMBAP product presented lower commission errors than the MCD45A1 product (not withstanding the pine forest biome). Secondly, a quantitative analysis which demonstrates the influence of sub-MODIS pixel burned area on the probability of detection by each product was performed. This analysis suggested that the MCD45A1 product appears to be better at mapping small burned areas (this is characterized by burned area

fractions  $\leq 50\%$  of a MODIS pixel) while, the BMBAP product seems more reliable at detecting large burned areas (marked by burned area fractions  $> 50\%$  of a MODIS pixel). This analysis was not considered during previous validation of global MODIS burned area products (Roy and Boschetti, 2009; Giglio, et al., 2009), and thus serves as an additional analysis that takes cognisance of the biases present in the product accuracy measures derived by use of a confusion matrix. It has been widely reported that the accuracy measures obtained by use of a confusion matrix are often biased, as a result of the inherent difference in the spatial resolution of the moderate-resolution products and the high-resolution independent reference data during validation (e.g., Foody, 1996; Binaghi, 1999; Boschetti, et al., 2004). Therefore, the classification error assessment conducted by Roy and Boschetti (2009) and Giglio, et al. (2009) and given in this study (in terms of the confusion matrices), overestimated the error, simply due to the inherent differences in the spatial resolution of Landsat and MODIS, i.e. 30 m vs 500 m. Thirdly, simple linear regression was used to assess the relationship between burned area proportion estimates derived from the MODIS burned area products and Landsat interpreted burned area data across the 2.5 x 2.5 km grids. It can be concluded that the MCD45A1 and BMBAP products provided adequate regional information regarding the extent of area burned. This was evident particularly, over the burning grassland and savanna biomes where the effect of spatial resolution and spectral differences in the accuracy of burned area estimates are minimized.

In this study, the differences in the derived accuracy measures of the burned area products are reasoned to be influenced by the type of vegetation, spectral contrast, size and spatial distribution of the burned areas. These findings support previous studies that describe the physical characteristics influencing burned area product accuracy, and suggest that the MODIS burned area products be integrated to improve their areas of weakness.

The minimum mapping unit of 240 m (adopted to reduce the mapping effort) during the production of high-resolution burned area reference maps (Roy, et al., 2005b) has resulted to the acquisition of an increased number of small burned areas (some below the 500 m MODIS pixel), which remained largely undetected by the burned area products and thus, contributed to the inflated errors of omission in the

products (Roy and Boschetti, 2009). The Western Cape and Sabie sites presented burned areas that were the most difficult and time consuming to interpret and digitize, due to the presence of clouds and cloud shadows. Likewise, unknown features which could not be confirmed subject to the absence of fieldwork appeared spectrally similar to the actual burned areas and thus, required careful interpretation to avoid confusion. This and the longer time intervals between the acquisition dates (e.g., 48 days in the Western Cape and 64 days in Sabie) may have influenced the reliability of the mapped burned areas using multitemporal TM data.

The classification procedures (which were beyond the scope this research) utilized in computing the MCD45A1 and BMBAP products have important differences which also might have contributed to their nonequivalent burned area mapping performances across the biomes. Among these are the following: i) the MCD45A1 product approach does not exploit any active fire information, whereas the BMBAP makes use of active fire data in its approach; ii) the MCD45A1 product primarily relies on a reflectance-only approach whereas, the BMBAP product approach hinges on a burn-sensitive vegetation index as a primary indicator to discover the burned areas (Roy et al., 2002; Roy et al., 2005a; Giglio et al., 2009; Giglio et al., 2010a).

This study has presented an accuracy assessment of the MODIS global burned area products across the different biomes in South Africa. In the fynbos and grassland biomes, the MCD45A1 product provided the highest burned area mapping accuracy, while in the pine forest and savanna biomes, the BMBAP product gave the highest burned area mapping accuracies than the MCD45A1 product. These findings have significant implications for fire monitoring in southern Africa and could be expected to contribute toward the information needs of policy-makers, ecologists, natural resource managers and the remote sensing community. Furthermore, this research study has demonstrated that the probability of identifying a burned area within a 500 m MODIS pixel is directly related to the fraction of the MODIS pixel burned. This also corroborates with previous research work that accentuated the relevance of fractional burned area when assessing the accuracy of lower resolution remotely-sensed burned area products using data from high resolution sensors, such



as ASTER or Landsat (Eva and Lambin, 1998a; Sa et al., 2003; Boschetti et al., 2004; Roy and Landmann, 2005c; Sa et al., 2007).

## **5.2: Recommendations and future work**

It would be valuable to expand this assessment over numerous sites with the use of more high resolution reference data to capture more variation and error that the burned area products encompass; thereby improving the statistical significance of this study. Additional information acquired by means of fieldwork is emphasized to ameliorate the mapping reliability of burned areas, particularly over features that could not be interpreted and the burned areas that may have been obscured by unburned high tree canopy. Moreover, the development of accuracy reporting methods to appropriately evaluate the remotely-sensed satellite products is an attractive feature that necessitates further research (Boschetti; et al., 2004; Roy et al., 2005b; Foody, 2008; Eckmann, et al., 2010) so that useful burned area product accuracy information can be obtained that intends to address the information needs of various users in southern Africa.

## REFERENCES

- Acocks, J.P.H., 1988. *Veld Types of South Africa*. 3rd ed. South Africa: Botanical Research Institute.
- Andreae, M. O., 1991. Biomass burning. Its history, use, and distribution and its impact on environmental quality and global climate. In: J.S. Levine, ed. *Global Biomass Burning: Atmospheric, Climatic, and Biospheric Implications*. Cambridge, Massachusetts: MIT Press, pp. 3-21.
- Andreae, M. O., 1997. Emissions of trace gases and aerosols from southern African savanna fires. In: B.W. van Wilgen, M.O. Andreae, J.G. Goldammer and J.A. Lindesay, eds. *Fire in Southern African Savannas*. South Africa: Witwatersrand University Press, pp. 161–184.
- Andreae, M. O. and Merlet, P., 2001. Emission of trace gases and aerosols from biomass burning. *Global Biogeochemical Cycles*, 15, pp.955-966.
- Anon. 1993. Annex A. The land cover map of Great Britain. Land cover classes: a description. *Institute of Terrestrial Ecology*, pp.1-17.
- Archibald, S., Scholes, R.J., Roy, D.P., Roberts, G. and Boschetti, L., 2010. Southern Africa fire regimes as revealed by remote sensing. *International Journal of Wildland Fire*, 19, pp.861-878.
- Arino, O. and Rosaz, J., 1999. 1997 and 1998 world ATSR Fire atlas using ERS-2 ATSR-2 data. In: *Proceedings of the joint fire science conference*. Boise, Idaho, USA, 15–17 June 1999. University of Idaho: International Association of Wildland Fire.
- Barbosa, P. M., Grégoire, J.-M. and Pereira, J. M. C., 1999. An algorithm for extracting burned areas from time series of AVHRR GAC data applied at a continental scale. *Remote Sensing of Environment*, 69, pp.253– 263.
- Bastarrika, A., Chuvieco, E. and Martín, M.P., 2011. Mapping burned areas from Landsat TM/ETM+ data with a two-phase algorithm: Balancing omission and commission errors. *Remote Sensing of Environment*, 115, pp. 1003-1012.
- Besag, J. E., 1986. On the statistical analysis of dirty pictures. *Journal of the Royal Statistical Society, Series B*, 48, pp.259–302.

- Binaghi, E., Brivio, P. A., Ghezzi, P. and Rampini, A., 1999. A fuzzy set based accuracy assessment of soft classifications. *Pattern Recognition Letters*, 20, pp.935–948.
- Bird, M.I. and Cali, J.A., 1998. A million year record of fire in sub-Saharan Africa. *Nature*, 394, pp.767–769.
- Bond, W. J., 1997. Fire. In: R. M. Cowling, D. M. Richardson and S. M. Pierce, eds. *Vegetation of southern Africa*. Cambridge: Cambridge University Press, pp.421–446.
- Boschetti, L., Flasse, S. and Brivio, P.A., 2004. Analysis of the conflict between omission and commission in low spatial resolution thematic products: the Pareto Boundary. *Remote Sensing of Environment*, 91, pp.280-292.
- Boschetti, L., Brivio, P.A., Eva, H.D., Gallego, J., Baraldi, A. and Gregoire, J.M., 2006. A sampling method for the retrospective validation of Global Burned Area products. *IEEE Transactions on Geoscience and Remote Sensing*, 44, pp.1765-1773.
- Boschetti, L., Roy, D. and Justice C., 2010. *MODIS Global Burned Area Validation and product Status*. [online] University of Maryland: NASA. Available at: <[http://modis.gsfc.nasa.gov/sci\\_team/meetings/201001/presentations/land/boschetti.pdf](http://modis.gsfc.nasa.gov/sci_team/meetings/201001/presentations/land/boschetti.pdf)> [Accessed 6 May 2010].
- Bucini, G. and Lambin, E. F., 2002. Fire impacts on vegetation in Central Africa: A remote-sensing-based statistical analysis. *Applied Geography*, 22, pp.27– 48.
- Chuvieco, E., Rianño, D., Aguado, I. and Cocero, D., 2002. Estimation of fuel moisture content from multitemporal analysis of Landsat Thematic Mapper reflectance data: Applications in fire danger assessment. *International Journal of Remote Sensing*, 23, pp.2145–2162.
- Congalton, R. G., Oderwald, R. G. and Mead, R. A., 1983. Assessing Landsat classification accuracy using discrete multivariate analysis statistical techniques. *Photogrammetric Engineering and Remote Sensing*, 49, pp.1671– 1678.
- Congalton, R. G., 1991. A review of assessing the accuracy of classifications of remotely sensed data. *Remote Sensing of Environment*, 37, pp.35– 46.
- Crutzen, P.J. and Goldammer, J.G. eds., 1993. *Fire in the Environment: the Ecological, Atmospheric and Climatic Importance of Vegetation Fires*. Dahlem

- Workshop Reports, Environmental Sciences Research Report, 13, Chichester, UK: Wiley.
- Delmas, R. A., Loudjani, P., Podaire, A. and Menaut, J. C., 1991. Biomass burning in Africa: An assessment of annually burned biomass. In: J. S. Levine, ed. *Global Biomass Burning: Atmospheric, Climatic, and Biospheric Implications*. Cambridge: MIT Press, pp.126–132.
- Dozier, J., 1981. A method for satellite identification of surface temperature fields of sub-pixel resolution. *Remote Sensing of Environment*, 11, pp.221–229.
- Dwyer, E., Pinnock, S., Grégoire, J.M. and Pereira, J.M.C., 2000. Global spatial and temporal distribution of vegetation fire as determined from satellite observations. *International Journal of Remote Sensing*, 21, pp.1289–1302.
- Eckmann, T.C., Still, C.J., Roberts, D.A. and Michaelsen, J.C., 2010. Variations in subpixel fire properties with season and land cover in Southern Africa. *Earth Interactions*, 14, DOI: 10.1175/2010EI328.1.
- Edward, D., 1983. A broad-purpose structural classification of vegetation for practical purposes. *Bothalia*, 14, pp.705–712.
- Ellicott, V., Vermote, E., Giglio, L. and Roberts, G., 2009. Estimating biomass consumed from fire using MODIS FRE. *Geophysical Research Letters*, 36, p.L13401 10.1029/2009GL038581.
- Elvidge, C. D., Kroehl, H. W., Kihn, E. A., Baugh, K. E., Davis, E. R. and Hao, W.–M., 1996. Algorithm for the retrieval of fire pixels from DMSP operational linescan system data. In: J. S. Levine, ed. *Biomass burning and global change: Remote sensing, modeling and inventory development, and biomass burning in Africa*. Cambridge: MIT Press, pp. 73–85.
- Ershov, D.V., Efrmov, V.Yu., Ilyin, V.O., Krasheninnikova, Yu.S., Loupian, E.A., Mazurov, A.A., Proshin, A.A. and Flitman E.V., 2004. Operational Data Use within the Information System for Remote Sensing of Forest Fires. In: Northern Eurasian GOF/GOLD Fire Network Workshop, *Satellite-based fire monitoring network in Northern Eurasia: Methods, Data Products, Applications*. Space Research Institute, Moscow, 17 November 2004.
- Eva, H. and Lambin, E. F., 1998a. Burnt area mapping in central Africa using ATSR data. *International Journal of Remote Sensing*, 19, pp.3473–3497.

- Eva, H. and Lambin, E. F., 1998b. Remote sensing of biomass burning in tropical regions: sampling issues and multisensor approach. *Remote Sensing of Environment*, 64, pp.292-315.
- Eva, H. and Lambin, E. F., 2000. Fires and land-cover change in the tropics: A remote sensing analysis at the landscape scale. *Journal of Biogeography*, 27, pp.765–776.
- Fairbanks, D.H.K., Thompson, M.W., Vink, E.R., Newby, T.S., van den Berg, H.M. and Everard, D.A., 2000. The South African Land-Cover Characteristics Database: a synopsis of the landscape. *South African Journal of Science*, 96, pp.69–82.
- Ferna´ndez, A., Illera, P. and Casanova, J.L., 1997. Automatic mapping of surfaces affected by forest fires in Spain using AVHRR NDVI composite image data. *Remote Sensing of Environment*, 60, pp.153–162.
- Fire Information For Resource Management System*. [online] Available at <<http://maps.geog.umd.edu/firms>> [Accessed 12 June 2009].
- Foody, G. M., 1996. Approaches for the production and evaluation of fuzzy land cover classification from remotely sensed data. *International Journal of Remote Sensing*, 17, pp.1317–1340.
- Foody, G.M., 2008. Harshness in image classification accuracy assessment. *International Journal of Remote Sensing*, 29, pp. 3137-3158.
- Fraser, R. H., Li, Z. and Cihlar, J., 2000. Hotspot and NDVI differencing synergy (HANDS): A new technique for burned area mapping over boreal forest. *Remote Sensing of Environment*, 74, pp.362– 376.
- Frost, P.G.H., 1999. Fire in southern African woodlands: origins, impacts, effects, and control. In: *Proceedings of an FAO Meeting on Public Policies Affecting Forest Fires*, FAO Forestry Paper 138, pp. 181–205.
- Giglio, L., Kendall, J. D. and Justice, C. O., 1999. Evaluation of global fire detection algorithms using simulated AVHRR infrared data. *International Journal of Remote Sensing*, 20, pp.1947– 1985.
- Giglio, L., Kendall, J. D. and Tucker, C. J., 2000. Remote sensing of fires with the TRMM VIRS. *International Journal of Remote Sensing*, 21, pp.203–207.

- Giglio, L. and Justice, C. O., 2003. Effect of wavelength selection on characterization of fire size and temperature. *International Journal of Remote Sensing*, 24, pp.3515–3520.
- Giglio, L., van der Werf, G. R., Randerson, J. T., Collatz, G. J. and Kasibhatla, P. S., 2006. Global estimation of burned area using MODIS active fire observations. *Atmospheric Chemistry and Physics*, 6, pp.957–974.
- Giglio, L., 2007. Characterization of the tropical diurnal fire cycle using VIRS and MODIS observations. *Remote Sensing of Environment*, 108, pp.407–421.
- Giglio, L., Loboda, T., Roy, D.P., Quayle, B. and Justice, C.O., 2009. An active-fire based burned area mapping algorithm for the MODIS sensor. *Remote Sensing of Environment*, 113, pp.408-420.
- Giglio, L., Randerson, J.T., van der Werf, G.R., Kasibhatla, P.S., Collatz, G.J., Morton, D.C. and DeFries, R.S., 2010a. Assessing variability and long-term trends in burned area by merging multiple satellite fire products. *Biogeosciences*, 7, pp.1171-1186.
- Giglio, L., 2010b. *MODIS Collection 5 Active Fire Product User's Guide*. [online] University of Maryland. Available at: <[http://modisfire.umd.edu/documents/MODIS\\_Fire\\_Users\\_Guide\\_2.4.pdf](http://modisfire.umd.edu/documents/MODIS_Fire_Users_Guide_2.4.pdf)> [Accessed 6 September 2010].
- Greenberg, J. P., Zimmerman, P.R, Heidt, L. and Pollock, W., 1984. Hydrocarbon and carbon monoxide emissions from biomass burning in Brazil. *Journal of Geophysical Research*, 89, 1350-4.
- Hao, W.M., Liu, M.H. and Crutzen, P.J., 1990. Estimates of annual and regional releases of CO<sub>2</sub> and other trace gases to the atmosphere from fires in the tropics, based on the FAO Statistics for the period 1975-1980. In: J.C. Goldammer, ed. *Fire in the Tropical Biota*. pp.440-462.
- Huffman, G.J., Adler, R.F., Rudolph, B., Schneider, U. and P. Keehn., 1995. Global precipitation estimates based on a technique for combining satellite-based estimates, rain gauge analysis, and NWP model precipitation information. *Journal of Climate*, 8, pp.1284–1295.

- Jensen, J.R., Cowen, D., Narumalani, S., Weatherbee, O. and Althausen, J., 1993. Evaluation of CoastWatch Change Detection Protocol in South Carolina. *Photogrammetric Engineering and Remote Sensing*, 59, pp.1039-1046.
- Jensen, J.R., 1996. *Introductory Digital Image Processing: A Remote Sensing Perspective*. 2nd ed. New Jersey: Prentice Hall.
- Justice, C. O., Giglio, L., Korontzi, S., Owens, J., Alleaume, S., Morisette, J. T., Roy, D. P., Petitecolin, F., Descloitres, J. and Kaufman, Y., 2002a. Global fire products from MODIS. *Remote Sensing of Environment*, 83, pp.245–263 (this issue).
- Justice, C. O., Giglio, L., Korontzi, S., Owens, J., Morisette, J., Roy, D. P., Descloitres, J., Alleaume, S., Petitcolin, F. and Kaufman, Y., 2002b. The MODIS fire products. *Remote Sensing of Environment*, 83, pp.244–262.
- Justice, C., Townshend, J., Vermote, E., Masuoka, E., Wolfe, R., Saleous, N., Roy, D. P. and Morisette, J. T., 2002c. An overview of MODIS Land data processing and product status. *Remote Sensing of Environment*, 83, pp.3–15.
- Justice, C.O., Smith, R., Gill, A.M. Csiszar, I., 2003. A review of current space-based fire monitoring in Australia and the GOF/GOLD program for international coordination. *International Journal of Wildland Fire*, 12, pp.247–258.
- Justice, C., Giglio, L., Boschetti, L., Roy, D., Csiszar, I., Morisette, J. and Kaufman, Y., 2006. *Modis Fire Products*. [online] MODIS Science Team: NASA. Available at: [http://modis.gsfc.nasa.gov/data/atbd/atbd\\_mod14.pdf](http://modis.gsfc.nasa.gov/data/atbd/atbd_mod14.pdf) [Accessed 6 September 2009].
- Karkanias, P., Shahack-Gross, R., Ayalon, A., Bar-Matthews, M., Barkai, R., Frumkin, A., Gopher, A. and Stiner, M., 2007. Evidence for habitual use of fire at the end of the lower Paleolithic: site-formation processes at Qesem Cave, Israel. *Journal of Human Evolution*, 53, pp.197-212.
- Kaufman, Y.J. and Remer, L.A., 1994. Detection of forests using MID-IR reflectance, an application for aerosol studies. *IEEE Transactions on Geoscience and Remote Sensing*, 32, pp.672–683.
- Kaufman, Y.J., Justice, C.O., Flynn, L.P., Kendall, J.D., Prins, E., Giglio, L., Ward, D.E., Menzel, WP. and Setzer, AW., 1998. Potential global fire monitoring from

- EOS MODIS. *Journal of Geophysical Research-Atmospheres*, 103, pp.32215–32238.
- Kasischke, E.S. and Bruhwiler, L.P., 2003. Emissions of carbon dioxide, carbon monoxide, and methane from boreal forest fires in 1998. *Journal of Geophysical Research*, 108, 8146 (D1).
- Kraaij, T., 2010. Changing the fire management regime in the renosterveld and lowland fynbos of the Bontebok National Park. *South African Journal of Botany*, 76, pp.550-557.
- Komatiland Forests*. [online] Available at < <http://www.komatilandforests.co.za/>> [Accessed 10 July 2009].
- Korontzi, S., Justice, C.O. and Scholes R.J., 2003. The influence of timing and spatial extent of vegetation fires in southern Africa on atmospheric emissions. *Journal of Arid Environments*, 54, pp.395–404.
- Kummerow, C., Barnes, W., Kozu, T., Shiue, J. and Simpson, J., 1998. The Tropical Rainfall Measuring Mission (TRMM) Sensor Package. *Journal of Atmospheric and Oceanic Technology*, 15, pp.809–817.
- Kummerow, C., Simpson, J., Thiele, O., Barnes, W., Chang, A., Stocker, E., Adler, R., Hou, A., Kakar, R., Wentz, F., Ashcroft, P., Kozu, T., Hong, Y., Okamoto, K., Iguchi, T., Kuroiwa, H., Im, E., Haddad, Z., Huffman, G., Ferrier, B., Olson, W., Zipser, E., Smith, E., Wilheit, T., North, G., Krishnamurti, T. and Nakamura, K., 2000. The status of the Tropical Rainfall Measuring Mission (TRMM) after two years in orbit. *Journal of Applied Meteorology*, 15, pp.1965–1982.
- Landmann, T., 2003. *A case study for Skukuza: Estimating biophysical properties of fires using EOS-MODIS satellite data*. Ph.D. University of Göttingen.
- Levine, J.S. ed., 1996. *Biomass Burning and Global Change*. Cambridge, MA: MIT Press.
- Lindgren, D.T., 1985. Land use/land cover: inventory and change. In: M. Nijhoff, eds. *Land Use Planning and Remote Sensing*, Boston: Publishers, pp.101-115.
- Loboda, T.V. and Csiszar, I.A. (2004). Estimating burned area from AVHRR and MODIS: validation results and sources of error. In: *Proceedings of the 2nd Open All-Russia Conference: Current Aspects of Remote Sensing of Earth from Space*.



- Moscow, Russia, 16-18 November 2004. Space Research Institute of the Russian Academy of Sciences: Publishing House GRANP.
- Lucht, W. and Lewis, P. E., 2000. Theoretical noise sensitivity of BRDF and albedo retrieval from the EOS-MODIS and MISR sensors with respect to angular sampling. *International Journal of Remote Sensing*, 21, pp.81– 98.
- Matson, M. and Dozier, J., 1981. Identification of sub resolution high temperature sources using a thermal IR sensor. *Photogrammetric Engineering and Remote Sensing*, 47, pp.1311-1318.
- Miettinen, J., 2007. Burnt area mapping in insular Southeast Asia using medium resolution satellite imagery. Ph.D. University of Helsinki, Finland.
- Montgomery, D.C. and Runger, G.C., 2007. *Applied statistics and probability for engineers*. 4th ed. New York,USA: Wiley.
- Morissette, J. T., Privette, J. L. and Justice, C. O., 2002. A framework for the validation of MODIS Land products. *Remote Sensing of Environment*, 83, pp.77– 96.
- Morissette, J.T., Baret, F. and Liang, S., 2006. Special issue on global land product validation. *IEEE Transactions on Geoscience and Remote Sensing*, 44, pp.1695– 1697.
- Mucina, L. and Rutherford, M. C. eds., 2006. *The Vegetation of South Africa, Lesotho and Swaziland. Strelitzia 19*. Pretoria, South Africa: South African National Biodiversity Institute.
- Openshaw, S., 1984. *The modifiable areal unit problem Concepts and Techniques in Modern Geography*. Norwich, U.K:Geo Books.
- Pereira, J. M. C., Chuvieco, E., Beaudoin, A. and Desbols, N., 1997. Remote sensing of burned areas. In: E. Chuvieco, ed. *A review of remote sensing methods for the study of large wildland fires*. Alcalá de Henares, Spain: Universidad de Alcalá, pp. 127-183.
- Pereira, J.M.C., Sa´, A.C.L., Sousa, A.M.O., Silva, J.M.N., Santos, T.N. and Carreiras, J.M.B., 1999. Spectral characterisation and discrimination of burnt areas. In: E. Chuvieco, ed. *Remote Sensing of Large Wildfires in the European Mediterranean Basin*.Berlin: Springer, pp.123–138.

- Phinn, S.R. and Rowland, T., 2001. Quantifying and visualising geometric misregistration from Landsat Thematic Mapper imagery and its effects on change-detection in a rapidly urbanising catchment. *Asian-Pacific Remote Sensing and GIS Journal*, 14, pp.41–54.
- Piccolini, I., 1998. Development and validation of an adaptive algorithm for burn scar detection using ERS/ATSR-2 data. Ph.D. Sapienza University of Rome, Italy.
- Prins, E. M. and Menzel, W. P., 1992. Geostationary satellite detection of biomass burning in South America. *International Journal of Remote Sensing*, 13, pp.2783–2799.
- Razafimpanilo, H., Frouin, R., Iacobellis, S.F. and Somerville, R.C.J., 1995. Methodology for estimating burned area from AVHRR reflectance data. *Remote Sensing of Environment*, 54, pp.273-289.
- Roberts, G., Wooster, M.J., Perry, G. L.W., Drake, N., Rebelo, L.-M. and Dipotso, F., 2005. Retrieval of biomass combustion rates and totals from fire radiative power observations: Application to southern Africa using geostationary SEVIRI imagery. *Journal of Geophysical Research Atmospheres*, 110, D21111, doi: 10.1029/2005JD006018.
- Robinson, J., 1991. Fire from space – global fire evaluation using infrared remote sensing. *International Journal of Remote Sensing*, 12, pp.3–24.
- Roujean, J.-L., Leroy, M. and Deschamps, P. Y., 1992. A bi-directional reflectance model of the Earth's surface for the correction of remote sensing data. *Journal of Geophysical Research*, 97, pp.20255–20468.
- Roy, D. P., Giglio, L., Kendall, J. D. and Justice, C. O., 1999. Multitemporal active-fire based burn scar detection algorithm. *International Journal of Remote Sensing*, 20, pp.1031–1038.
- Roy, D.P., 2000. The impact of misregistration upon composited wide field of view satellite data and implications for change detection. *IEEE Transactions on Geoscience and Remote Sensing*, 38, pp.2017–2032.
- Roy, D. P., Lewis, P. E. and Justice, C. O., 2002. Burned area mapping using multi-temporal moderate spatial resolution data—A bi-directional reflectance model-based expectation approach. *Remote Sensing of Environment*, 83, pp.263– 286.

- Roy, D.P., Jin, Y., Lewis, P.E. and Justice, C.O., 2005a. Prototyping a global algorithm for systematic fire-affected area mapping using MODIS time series data. *Remote sensing of Environment*, 97, pp.137 – 162.
- Roy, D. P., Frost, P., Justice, C. O., Landmann, T., Roux, J. L. and Gumbo, K., Makungwa, S., Dunham, K., Du Toit, R., Mhwandagara, K., Zacarias, A., Tacheba, B., Dube, O., Pereira, J., Mushove, P., Morisette, J., Santhana S., Vannan, and Davies, D., 2005b. The Southern Africa Fire Network (SAFNet) regional burned area product validation protocol. *International Journal of Remote Sensing*, 26, pp.4265–4292.
- Roy, D. P. and Landmann, T., 2005c. Characterizing the surface heterogeneity of fire effects using multi-temporal reflective wavelength data. *International Journal of Remote Sensing*, 26, pp.4197–4218.
- Roy, D. P., Trigg, S. N., Bhima, R., Brockett, B., Dube, O., Frost, P., Govender, N., Landmann, T., Le Roux, J., Lepono, T., Macuacua, J., Mbow, C., Mhwandagara, K., Mosepele, B., Mutanga, O., Neo-Mahupeleng, G., Norman, M. and S. Virgilo., 2006. The utility of satellite fire product accuracy information—Perspectives and recommendations from the Southern Africa fire network. *IEEE Transactions on Geoscience and Remote Sensing*, 44, pp.1928–1930.
- Roy, D. P., Boschetti, L., Justice, C. O. and Ju, J., 2008. The Collection 5 MODIS burned area product—Global evaluation by comparison with the MODIS active fire product. *Remote Sensing of Environment*, 112, pp.3690–3707.
- Roy, D.P. and Boschetti, L., 2009. Southern Africa Validation of the MODIS, L3JRC, and GlobCarbon Burned-Area Products. *IEEE Transactions on Geoscience and Remote Sensing*, 47, pp.1032-1044.
- Rutherford, M.C., 1997. Categorization of biomes. In: R.M. Cowling, D.M. Richardson and S.M. Pierce, eds. *Vegetation of Southern Africa*, Cambridge: Cambridge University Press, pp.91–98.
- Sá, A.C.L., Pereira, J.M.C., Vasconcelos, M.J.P., Silva, J.M.N., Ribeiro, N. and Awasse, A., 2003. Assessing the feasibility of sub-pixel burned area mapping in

- miombo woodlands of northern Mozambique using MODIS imagery. *International Journal of Remote Sensing*, 24, pp.1783–1796.
- Sá, A.C.L., Pereira, J.M.C. and Gardner, R.H., 2007. Analysis of the relationship between spatial pattern and spectral detectability of areas burned in southern Africa using satellite data. *International Journal of Remote Sensing*, 28, pp.3583–3601.
- Scholes, R. J., Kendall, J. D. and Justice, C. O., 1996. The quantity of biomass burned in southern Africa. *Journal of Geophysical Research*, 101, pp.667–676.
- Scholes, R.J., Dowty, P.R., Caylor, K., Parsons, D.A.B., Frost, P.G.H. and Shugart, H.H., 2002. Trends in savanna structure and composition along an aridity gradient in the Kalahari. *Journal of Vegetation Science*, 13, pp.419–428.
- Silva, J. M. N., Sá, A. C. L. and Pereira, J. M. C., 2005. Comparison of burned area estimates derived from SPOT-VEGETATION and Landsat ETM+ data in Africa: Influence of spatial pattern and vegetation type. *Remote Sensing of Environment*, 96, pp.188–201.
- Simon, M., Plummer, S., Fierens, F., Hoelzemann, J.J. and Arino, O., 2004. *Burnt area detection at global scale using ATSR-2: The GLOBSCAR products and their qualification*. *Journal of Geophysical Research Atmospheres*, 109, D14S02, doi:10.1029/2003JD003622.
- Simpson, J., Robert, F.A., Gerald, R.N., 1988. A Proposed Tropical Rainfall Measuring Mission (TRMM) Satellite. *Bulletin of the American Meteorological Society*, 69, pp. 278–278.
- Smith, J.H., Stehman, S.V., Wickham, J.D. and L. Yang., 2003. Effects of landscape characteristics on land-cover class accuracy. *Remote Sensing of Environment*, 84, pp.342–349.
- Smith, R., Adams, M., Maier, S., Craig, R., Kristina, A. and Maling, I., 2007. Estimating the area of stubble burning from the number of active fires detected by satellite. *Remote Sensing of Environment*, 109, pp.95– 106.
- Stehman, S. V., 1997. Selecting and interpreting measures of thematic classification accuracy. *Remote Sensing of Environment*, 62, pp.77– 89.
- Strahler, A., Boschetti, L., Foody, G., Friedl, M., Hansen, M., Harold, M., Mayaux, P., Morisette, J., Stehman, S. and Wodcock, C., 2006. *Global land cover*

- validation: Recommendations for evaluation and accuracy assessment of global land cover maps*. Luxembourg: Belgium, European Commission EUR 22156, pp.58
- Tansey, K., 2002. *Implementation of the regional burnt area algorithms for the GBA-2000 initiative*. Brussels, Belgium: European Commission EUR 20532, pp.159.
- Tansey, K., Grégoire, J. M., Stroppiana, D., Sousa, A., Silva, J. M. N. and Pereira, J. M. C., 2004. Vegetation burning in the year 2000: Global burned area estimates from SPOT VEGETATION data. *Journal of Geophysical Research*, 109, D14S03. doi:10.1029/2003JD003598.
- Tansey, K., Beston, J., Hoscilo, A., Page, S.E. and Hernández C.U.P., 2008. Relationship between MODIS fire hot spot count and burned area in a degraded tropical peat swamp forest in Central Kalimantan, Indonesia. *Journal of Geophysical Research*, 113, D23112, doi: 10.1029/2008JD010717.
- Thompson, M.W., 1996. A standard land-cover classification scheme for remote sensing applications in South Africa. *South African Journal of Science*, 92, pp.34–42.
- Trigg S. N. and Roy D. P., 2007. A focus group study of factors that promote and constrain the use of satellite derived fire products by resource managers in Southern Africa. *Journal of Environmental Management*, 82, pp.95-110.
- Townshend, J.R.G., Justice, C.O., Gurney, C. and McManus, J., 1992. The impact of misregistration on change detection. *IEEE Transactions on Geoscience and Remote Sensing*, 30(5), pp.1054-1060.
- United States Geological Survey (USGS) - Landsat*. [online] Available at <[http://landsat.usgs.gov/about\\_landsat5.php](http://landsat.usgs.gov/about_landsat5.php)> [Accessed 20 July 2009].
- Van der Merwe, J. H. and Van Niekerk, A., 2007. Vegetation Map of South Africa, Lesotho and Swaziland (edition 2), 1:1 000 000 scale sheet maps. In: L. Mucina, M. C. Rutherford and L. W. Powrie, eds. *Vegetation Map of South Africa, Lesotho and Swaziland*. Pretoria, South Africa: South African National Biodiversity Institute.
- Van Wilgen, B. and Scholes, R., 1997. The vegetation and fire regimes of Southern Hemisphere Africa. In: B. Van Wilgen, M. Andreae, J. Goldammer and J.A.

- Lindesay, eds. *Fire in Southern African Savannas*. Johannesburg: Witwatersrand University Press, pp.27–46.
- Vafeidis, A.T. and Drake, N.A., 2005. A two-step method for estimating the extent of burned areas with the use of coarse-resolution data. *International Journal of Remote Sensing*, 26, pp.2441–2459.
- Vermote, E. F., El Saleous, N. Z. and Justice, C. O., 2002. Operational atmospheric correction of the MODIS data in the visible to middle infrared: First results. *Remote Sensing of Environment*, 83, pp.97–111.
- Walford, N., 1995. *Geographical data analysis*. Chichester, UK: Wiley.
- Warehouse Inventory Search Tool*. [online] Available at <<http://wist.echo.nasa.gov>> [Accessed 20 August 2009].
- Wedderburn-Bisshop, G., Walls, J., Senerath, U.G. and Stewart, A.J., 2002. A methodology for mapping change in woody landcover in Queensland from 1999 to 2001 using Landsat ETM+. In: *Proceedings of the 11th Australasian Remote Sensing and Photogrammetry Conference*. Brisbane, Australia, 2-6 September 2002. Surveying and Spatial Sciences Institute.
- White, F., 1983. The vegetation of Africa: A descriptive memoir to accompany the UNESCO/AETFAT/UNSO vegetation map of Africa. *Natural Resources Research*, 20, Paris: UNESCO.